THE UNIVERSITY
of ADELAIDE

FACULTY OF SCIENCES
SCHOOL OF PHYSICAL SCIENCES

Advanced Radiation Sensing Techniques

Jarrah Lionel Herbert Mik

Supervisors:
Prof. David OTTAWAY
Prof. Nigel SPOONER
Dr. Christopher KALNINS

To my dearest Gerrit and Lionel.

Statement of Originality

I certify that this work contains no material which has been accepted for the award of any other degree or diploma in my name, in any university or other tertiary institution and, to the best of my knowledge and belief, contains no material previously published or written by another person, except where due reference has been made in the text. In addition, I certify that no part of this work will, in the future, be used in a submission in my name, for any other degree or diploma in any university or other tertiary institution without the prior approval of the University of Adelaide and where applicable, any partner institution responsible for the joint-award of this degree. I give permission for the digital version of my thesis to be made available on the web, via the University's digital research repository, the Library Search and also through web search engines, unless permission has been granted by the University to restrict access for a period of time. I acknowledge the support I have received for my research through the provision of an Australian Government Research Training Program Scholarship.

- Jarrah Lionel Herbert Mik
  25 August 2020

Abstract

Real-time monitoring of alpha and beta emitting radionuclides in the environment and in mineral-processing has always proved elusive. The short path lengths, low target activities and harsh environments mean a quite specialised sensor is required. Two sensors have been constructed and tested with the sensitivity to measure gross alpha and beta particles below the activity level of 1 Bq/ml using optical fibres made of scintillating polymers. Scintillation allows for direct, real-time, semi-continuous measurements that are not available with current techniques. These polymers are suitable for withstanding the low pH solutions at elevated temperatures in abrasive mineral-processing environments. The new devices were found to be more sensitive by a factor related to the increase in their surface area and the new detection limit is now below 0.1 Bq/ml for the beta sensor and 0.15 for the alpha sensor. The feasibility of a novel sensing technique to specifically detect polonium-210 (Po-210) is also investigated. The envisioned device would allow in-line sensing of Po-210 specifically by selective uptake onto a coated scintillator.

Acknowledgements

I would like to thank my family, both immediate and extended for their continued support with my studies. Thank you, for being patient with my terrible attendance rates at important dates, and my general absent mindedness. But common, who knew I'd remember more than two birthdays last year? Especially one of those being mine! I mustn't have been working hard enough. Here's hoping I'll be a bit more attentive over the next few more years, or, your patience doesn't waver.

Thanks again, and hey, at least I can't ask you to proofread this one!

Next, I'd like to acknowledge the tireless efforts of my supervisors over the past few years, David Ottaway, Nigel Spooner and Chris Kalnins. Whether it was hands on teaching in the laboratory, interpretation of curious measurements, or general life advice and the telling of fascinating tales. They always gave their time, focus and most critical their honesty. The latter being a quality underappreciated by some students, but these moments were when I learnt the most. I sincerely look forward to continued research with them, and hopefully a few drinks and laughs (I'll bring the port).

Continuing the theme of supervision. I'd like to give a special acknowledgement to the efforts of Danielle Questiaux and Mick Stuckings. Together they provided many recommending readings, enlightening explanations, contagious laughter, and the simple reminder to relax and breath. Between these two stellar individuals, I learnt the complexities of radiation determination and more, and had a great time whilst doing so. Thank you both.

Over the past year, I learnt the meaning of the phrase: It takes a village to raise a child. The environment and people one cohabits with moulds them for better or for worse. So, I'd like to blame my current mental derangement on the residents of Floor 2, Room 78 of the Braggs building. All jokes aside, someone needs to round this bunch up, separate them, then monitor them in separate rooms. If we can harness their creative whit, encouragement and optimism everyone could get through a HDR degree.

I truly appreciate the efforts of the University of Adelaide support staff, in particular, Bob Chivell. Now, sadly in a greener pasture. Wow. That sounded grim. I mean, a pasture where he is appreciated for the extent of his expertise and more importantly his good-hearted nature. Thank you, Bob.

I'd like to thank the support of the members of the Australian Research Council Australian Copper-Uranium Transformation Research Hub for their support and encouragement throughout my time as a part of the research hub. Particular thanks to Mark Rollog and Rahul Ram for their efforts at educating a physicist in chemistry and geology. A truly haunting prospect.

To the experts at OptoFab (and who could forget Alistair) I'd like to express my gratitude for the many jigs made, holes drilled, pipette tips used, and I believe a go on a hacksaw at one point. Keep on keeping on and thanks again.

And thank you to anyone I've forgotten...

This research was conducted by the Australian Research Council Australian Copper-Uranium Transformation Research Hub (project number IH130200033) and funded by the Australian Government. The authors acknowledge funding from the Commonwealth of Australia Defence Science and Technology Group.

This work was performed in part at the OptoFab node of the Australian National Fabrication Facility utilizing Commonwealth and SA State Government funding.

The author also acknowledges the funding of the Operators' Radiation Committee (ORC) and the Australasian Radiation Protection Society (ARPS) for the attendance of a conference in 2019.

Contents

List of Figures

List of Tables

List of Acronyms

RN RadioNuclide
IOCG-U Iron Oxide Copper Gold Uranium
LSC Liquid Scintillation Counting
RL RadioLuminescence
PMT PhotoMultiplier Tube
CCD Charge-Coupled Device
PMMA PolyMethyl MethAcrylate
CSDA Continuous Slowing Down Approximation

MCA Multi-Channel Analyser
HV High Voltage
PHS Pulse Height Spectrum
SEP Single Electron Peak
NIST National Institute of Standards and Technology
DI DeIonised
RF Radio Frequency
SDS Safety Data Sheet

Chapter 1

Introduction

This thesis presents research towards the development of radionuclide detection techniques for in-situ monitoring of radionuclides (RNs) in mineral processing liquids. We specifically focus on liquids used in the processing of Iron Oxide Copper Gold Uranium (IOCG-U) ore deposits in Australia, but these sensors could be deployed in any application where the RN content of a liquid needs to be determined. The RN content is ascertained by the detection of alpha and beta particle emissions with optical fibre based sensors. The feasibility of using electrochemical techniques to specifically detect polonium-210 (Po-210) is also investigated.

1.1 Research Motivation

1.1.1 Mining Application

The extraction of valuable metals from IOCG-U ore deposits in Australia is both time consuming and expensive with ores requiring many stages of mineral processing to remove varying levels of RNs, and there is an ongoing requirement to reduce the radioactivity in the concentrates so they increase in value. Improvements to the current techniques require an understanding of how contaminant materials, such as uranium-238 (U-238) and it's daughters, and the radioactivity that they cause is distributed during each stage. These distributions are variable in each mineral and usually in each section of the IOCG-U deposit. Many of these RNs have short half-lives meaning that very low concentrations cause pertinent radiation levels.

Uranium-238 Decay Chain

Uranium is naturally occurring and is commonly found throughout the earth's crust. The most common isotope of uranium is U-238, making up 92.284% of uranium and U-235 around 0.7%. Hence, we don't specifically target U-235 and it's daughters in this project due to their low abundance. The U-238 decay chain is shown in Figure 1.1.

Over time U and it's daughters can reach a state called secular equilibrium. Secular equilibrium is reached when the rate of production of an isotope is equal to it's decay

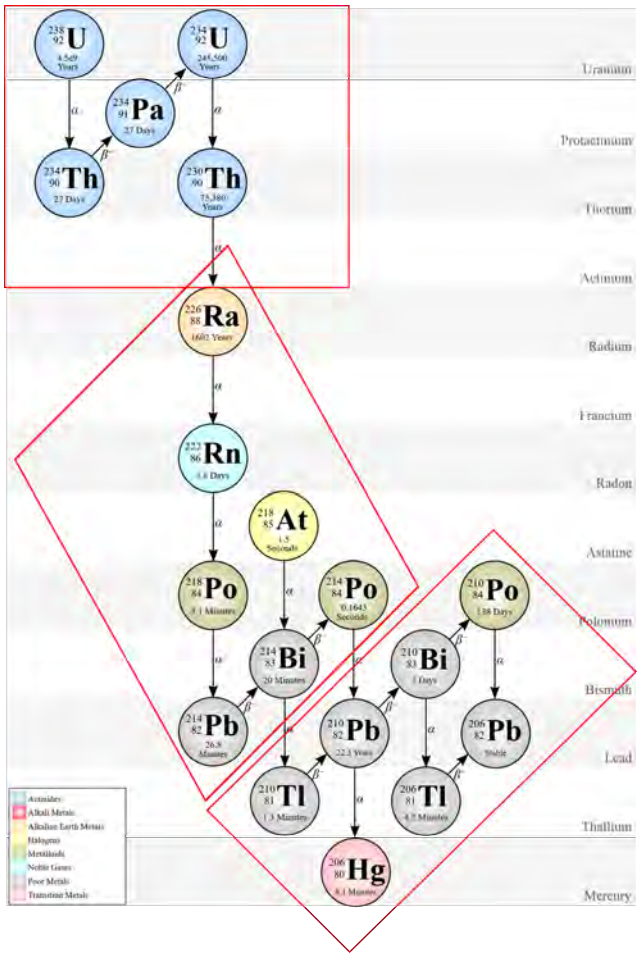

Figure 1.1: U-238 decay chain. α and β denote the type of emission. Each red box represents RNs removed/disrupted in different mineral processing stages.

rate, causing the mass ratios to remain constant. The U-238 decay chain starts with an alpha emission from U-238, followed by the sequential emission of 7 alpha decays and 6 beta decays (Figure 1.1). However, throughout mineral processing this system is disturbed from equilibrium since different RNs are present and mobilised chemically during each processing stage (red boxes in Figure 1.1). Therefore, the actual alpha and beta emissions are variable requiring detection throughout or between mineral processing stages to facilitate removal.

RN Analysis Techniques

The concentrations of U-238 and it's daughters are currently determined using lab based techniques.

The energy spectra of beta particles form a distribution rather than a characteristic peak since it originates from a three body nuclear decay. In this case a neutron becoming a proton, a neutrino and a high speed electron. The energy of this decay is distributed between these decay products, hence, the energy spectra of beta particles

forms a distribution. This limits the use of beta spectroscopy in samples containing multiple emitters as these distributions tend to overlap. However, a characteristic gamma ray is emitted from each of the beta emitters. Thus, the concentrations of beta emitters can be reliably determined through gamma ray spectroscopy.

A germanium detector is used to determine the count rates of gamma rays [2]. A spectrum is formed from these count rates with peaks corresponding to the gamma ray emitters present in the radioactive sample.However, samples with low RN concentrations require long acquisition times, limiting this techniques use for in-situ monitoring in this environment.

All of the alpha emitters also emit a characteristic gamma ray that can be used to determine their concentration. However, the gamma ray emission from Po-210 is too weak to be used practically in this technique. Therefore, alpha spectroscopy is used to determine the concentration of Po-210.

Alpha particle spectroscopy is used to determine the concentration of alpha emitting RNs. To find the concentration accurately often requires lengthy chemical separation or similarly complex techniques. The concentration is determined similarly to the previous technique and also requires specialised software and equipment to account for further complexities. Again, this process limits the techniques use for in-situ monitoring in this environment.

The variations in the contaminants and their low abundances limit the already time consuming off-site analysis as a tool to understand these distributions. Real time in-situ monitoring can provide an understanding of these distributions throughout each processing stage. This will allow for the development of high quality concentrates of valuable metals for export that comply with modern trade regulations regarding RN concentrations.

1.1.2 Research Scope

This work focuses on developing alpha and beta particle sensors utilising highly sensitive optical fibres. These sensors are an extension of the work by C. Whittaker [3]. New, more sensitive, prototypes are constructed, characterised and tested in their intended sensing environment. Methods of removing surface contaminants to improve longevity are identified. A systematic investigation into identifying the source of these devices background signal is undertaken to understand sensitivity limitations. This investigation includes proposals for field deployable devices. The current generation fo devices have already achieved their sensitivity goal of 1 Bq/ml set by the industry sponsor to enable compliance with modern trade regulations set by the IAEA [4]. The improvements in each sensor facilitated more reliable real-time monitoring at low radioactivity levels and allows the future pursuit of applications with even higher sensitivity requirements, such as real-time environmental monitor-

ing.

The feasibility of detecting polonium specificity in solution through electrochemical processes is also explored. The envisioned device would allow in-line sensing of Po-210 specifically by selective uptake onto a coated scintillator. The selectivity of Po-210 uptake onto various metals was tested, the most efficient was then repeated to determine the performance in mineral processing liquids. The coating of a readily available scintillating screen was performed to evaluate a candidate for the interchangeable sensor unit.

1.1.3 Radiation Detection

Radiation dosimetry is the detection and quantification of ionising radiation. This field spans from environmental radiation monitoring to dose determination in radiation therapy. There are numerous methods of detecting radiation all of which have differing characteristics. Common ways of detecting ionising radiation include; liquid scintillation counting (LSC), semiconductor devices and the use of scintillating materials. The efficiency and effectiveness of these detection methods differs depending on the properties of the radiation to be detected. The design of a detector for a given application is then of high importance. A discussion of these methods and their applicability to this application is provided below.

The devices developed in this thesis rely on the interactions of ionising radiation with scintillating materials. During these interactions atoms and molecules within the material are ionised and excited due to dose deposition by the ionising particle (alpha or beta particle). A fraction of this energy is converted into photons as these atoms or molecules de-excite. This mechanism is referred to as scintillation, or radioluminescence (RL) and the scintillation can be measured using a photo-detector such as a photomultiplier tube (PMT). The following detection techniques utilise this phenomena for detection of ionising radiation.

LSC is the process of dissolving samples containing RNs into a liquid that produces scintillation [5]. This method can be used to count both alpha and beta particle emitting isotopes in a solution [6], but is most commonly applied to low energy beta radiation [7–9]. A PMT (or two) is used to measure the light pulses produced by the scintillator liquid [5]. This technique can be used to discriminate between particles in mixed samples as alpha particles are more heavily ionising than beta particles [10]. The scintillators used in the alpha and beta sensors also take advantage of this property.

The main limitation in LSC is self-absorption of the emitted light by materials within the sample [11] where emitted light has a spectral overlap with the absorption spectrum of the liquid. This can be corrected by considering the specific energy loss within a material, using the theory outlined in Birks [12, 13]. However, this

added complexity and LSC's lab-based nature makes it unsuitable for this application.

Another technique utilises semiconductor devices. When ionising radiation is incident on the semiconductor it creates a signal proportional to the energy deposited by the incoming radiation.

Advantages of semiconductor devices are: (1) they can be used to detect ionising radiation effectively at room temperature and (2) the short penetration depths of ionising radiation in silicon allow use in situations where space is limited. Semiconductor devices have been shown to have high energy resolution [14, 15]. Unfortunately, semiconductor devices have low counting efficiencies and are not used to analyse low activity samples, as such they are not viable for this application.

In-situ sensing requires a real-time response to ionising radiation. A method that provides this is using scintillating plastics or crystals and appropriate photo-detectors. Optical fibres drawn from these materials are often employed to take advantage of these materials sensitivity in a robust manner. Early examples of such a device used in liquids is presented by Steinberg [16, 17]. This method was developed to get around the limitations found in LSC and designed for particle-tracking experiments. The method employed 'cylindrical filaments' of a scintillator material placed in a solution of sodium carbonate (C-14), a beta particle emitter. The light produced was interpreted with a PMT.

Optical fibres are employed in two variants, one where the photons produced by a scintillator material are guided along a coupled optical fibre (extrinsic), or the scintillator material is extruded into a fibre allowing the fibre to produce and transport the photons (intrinsic). Each method is situationally advantageous.

One example of an extrinsic sensor is found in [18]: where a sensing probe made of polystyrene (organic scintillating material) is used to detect low energy alpha particles. The ionising radiation interacts with the probe and the light produced is guided along an optical fibre to a PMT. Another example is the Radline detector discussed by Jackson et.al [19]. This device utilises a zinc tungstate ($ZnWO_4$) scintillating crystal connected to a fibre optic cable which transmits light to a CCD camera. In each case the accumulated dose measured by these detectors is linear with increasing dose so this form of a detector is suitable for real-time measurements of varying dose concentrations. The extrinsic nature of these sensors means each detector is not compact, however, they can be operated remotely. Depending on the losses the signal may also be diminished before interpretation. This issue is reduced significantly by the signal being produced within the fibre (intrinsically), like the sensors discussed in this thesis.

The detectors developed in this document take advantage of the large surface area to volume ratio of an optical fibre that allow more possible interactions with incoming ionising radiation, but with a much smaller volume. This enables for multiple fibres to be used in a small volume, forming a compact sensor that is highly sensitive to the short path length ionising radiation in mineral processing liquids. The intrinsic nature also allows for the tailoring of fibre geometries to increase sensitivity and allow sensing of specific radiation types.

Examples of intrinsic sensors typically employ scintillating plastic optical fibres, typically polystyrene with a PMMA cladding, or core materials doped with scintillating materials [20–25]. Each of these designs explored the fibre geometry to enable an efficient response to radiation. A combination of these designs has been used in the sensors explored in this thesis.

The sensors investigated in this thesis are an extension of the investigation of polystyrene fibre bundles by C.Whittaker [3, 26–28]. The fibre bundles required an appropriate choice of fibre that had,

- The best response to alpha and beta particle radiation
- An optimised transmission
- Light emitted from the scintillator at an appropriate wavelength
- An optimised fibre spacing to maximise the sensing volume

The research presented in this thesis includes the development of new, more sensitive prototypes utilising these results with larger total volumes. Also included are investigations into sensor decontamination and sensitivity limitations including proposals for future field deployable designs.

The amount of light produced within the scintillator from incoming radiation is critical for real-time monitoring. The commercially available polystyrene optical fibres were tested in [3, 26, 27] resulted in the selection of different fibre geometries to maximise the light yield from alpha or beta particles. In both cases the transmission was maximum with a PMMA cladding. Claddings of different thicknesses were used to discriminate between alpha and beta particles. The emission wavelength was chosen to lie within the 400-500 nm region to efficiently couple to the photodetector. This wavelength also possessed lower reabsorption of the light produced within the scintillator [3].

With the optimal fibres chosen the sensors were then designed: multiple fibres were used to form each sensor unit, as the sensitivity of the sensor increases with the amount of fibres due to the increase in the detector volume. However, it was found in [26] that for the beta particle sensor the best sensitivity (strongest signal) was

found by spacing the fibres apart by 2-5 mm. This spacing reflects the distance travelled by beta particles present in mineral processing liquids. In contrast the alpha particle sensor gave the best sensitivity by close-spacing the fibres together ("paint brush"). The next section will describe the relevant theory to detail the reasoning behind each sensor geometry.

1.2 Alpha and Beta Particle Sensors

The beta and alpha particle sensors are formed by grouping optical fibres made of scintillating polymers. Scintillators drawn into optical fibres are practical as radiation sensors since their geometries allow for a large interaction volume for their size, allowing for many interactions with ionising radiation. Each type of ionising particle interacts with matter differently and this difference allows for sensors specifically tailored to the type of radiation to be detected. The efforts surrounding these prototypes is to focus on further improving the sensitivity limit by an order of magnitude.

1.2.1 Beta Particle Sensor

The design of this sensor is based on the interaction mechanisms of electrons with matter. These mechanisms directly affect the range of these particles which dictates the fibre spacing and diameter used for this device.

Beta Particles

"Beta particles" is the term that includes electrons (e^-) and positrons (e^+). These particles dissipate energy in excitation and ionisation. Bremsstrahlung (braking) radiation is also produced but this effect is more apparent at higher energies and for materials with higher Z numbers (Z = atomic number of absorber) as the effect is proportional to Z^2 [29].

Energy Loss Mechanism

Beta particles interact with matter via Coulombic forces with atomic electrons. They transfer energy by ionising and exciting atoms and/or molecules within a material. For a given energy, beta particles travel faster than other charged particles so the Coulombic forces has less time to act. Therefore, beta particles will lose energy at a slower rate giving the effect of the particle gradually slowing down through many collisions. Each collision results in a deviation in the direction of travel resulting in a transverse spread in energy as the particle travels.

The possible interactions for beta particles with matter are (Figure 1.2):

- **Elastic Scattering:** Interaction between an electron and atom. The kinetic energy of the scattered electron is conserved during this interaction.

- **Inelastic Scattering:** Interaction between electron and atom where some of the electron's kinetic energy is transferred to the atom. Depending on the amount transferred, this can either cause electronic excitations or ionisation. This is the main interaction for medium and low energy particles, of the type studied in this thesis.
- **Bremsstrahlung (braking radiation):** Deceleration of an electron near an atom due to the electrostatic force. The electron radiates energy as it decelerates in the form of X-rays (photons). The energy of the X-rays are equal to the amount of energy lost during deceleration.
- **Positron Annihilation:** When a positron and an electron collide they can undergo electron-positron annihilation. The energy of this interaction is then converted into high energy photons. The momentum of the positron dictates the scattering angles of the emitted photons.

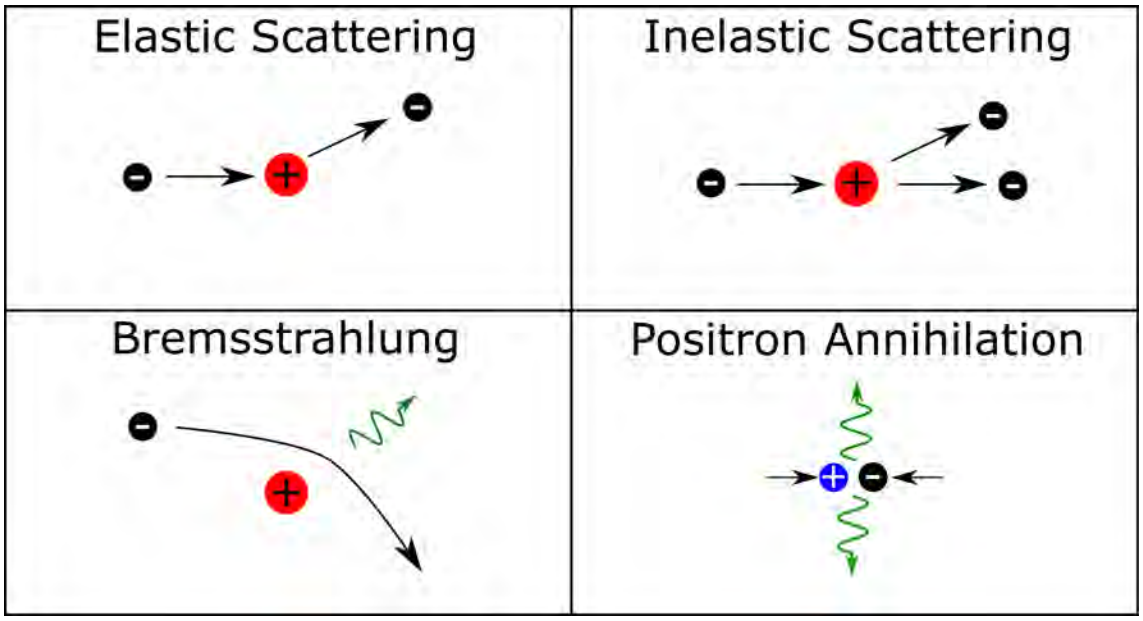

Figure 1.2: Pictorial representations of the possible interactions for beta particles.

Stopping Power

The stopping power describes the rate of energy loss of a charged particle as it travels through a material. For relativistic particles (beta particles) this is described by the modified Bethe-Bloch formula (Equation 1.1 [30]).

$$-\left(\frac{dE}{dx}\right) = \frac{z^2 e^4}{4\pi\epsilon_0^2 m_e v^2} NZ\left[ln\frac{2m_e v^2}{I} - ln(1-(v^2/c^2)) - \frac{v^2}{c^2}\right] \tag{1.1}$$

where, z is the charge of the projectile, e is the charge of an electron, m_e is the rest mass of electron, v is the speed of the incoming particle, N is the number density

of electrons in the target material, Z is the atomic number of the target material, I is the mean excitation energy of the medium and c is the speed of light. This equation includes relativistic corrections due to the mass of an electron and additional terms when compared to the Bethe-Bloch formula (1.5) to correct for the energy losses caused by Bremsstrahlung. The stopping power of polystyrene for increasing energies of beta particles is shown in Figure 1.3.

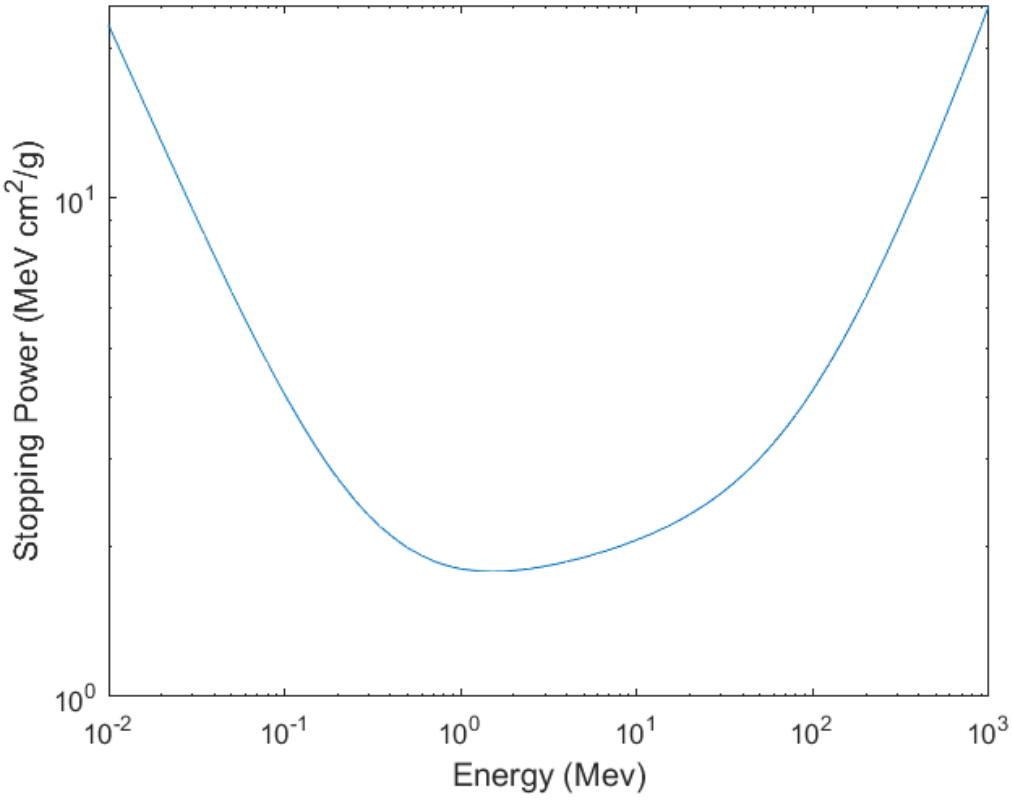

Figure 1.3: Stopping power of polystyrene for increasing energies of beta particles [1].

The total stopping power for beta particles includes the energy lost through radiative interactions (Bremsstrahlung) in addition to energy lost through collisional processes (Equation 1.1).

$$\left(\frac{dE}{dx}\right) = \left(\frac{dE}{dx}\right)_{collisional} + \left(\frac{dE}{dx}\right)_{radiative} \tag{1.2}$$

The radiative component of the stopping power describes the energy loss due to Bremsstrahlung [30],

$$\left(\frac{dE}{dx}\right) = NEZ^2 f(Z, E) \tag{1.3}$$

where, N is the number density of electrons in the target material, E is the total energy of the incoming particle, Z is the atomic number of the target material, and $f(Z, E)$ is a slowly varying function of Z and E [30].

More energy is lost as the number of interactions increases, so this formula is heavily dependent on the atomic number of the target material, Z, as this increases the number of electrons per unit volume. The stopping power can be used to find the range of a charged particle.

Range

The path length of a beta particle is considered differently than for heavy charged particles due to multiple collisions along its path. The path length is dependent of the Z value and density of the absorber since this is proportional to the amount of collisions occur [29].

For charged particles, the concept of range, rather than corresponding to a path length, corresponds to the thickness of a material needed to stop it at a given energy. The CSDA Range (Continuous Slowing Down Approximation) describes this quantity for a charged particle with a kinetic energy, T,

$$R(T) = \int_0^T \left(-\frac{dE}{dx}\right)^{-1} dE \tag{1.4}$$

and considers the total stopping power. However, the range of an electron for a given energy varies from this value due to it's variable path.

The CSDA range then dictates the maximum separation and the thickness of the scintillators (fibres) used in these sensors. The beta particles in the intended sensing environment travel on the mm scale. Therefore the separation between and thickness of each scintillator is also on the mm scale [3, 26].

1.2.2 Alpha Particle Sensor

The design of this sensor is based on the interaction mechanisms of alpha particles with matter. These mechanisms directly affect the geometry of the fibres used and allows discrimination between alpha and beta particles.

Alpha Particles

Alpha particles are heavy charged particles that also interact with matter via Coulombic forces but their higher mass and charge of alpha particles gives much greater ionisation 'power' [31]. This causes many more collisions with atomic electrons [29], hindering their ability to penetrate far through matter. This has implications then for the geometry of this sensor and the previous.

Energy Loss Mechanism

The possible interactions of alpha particles with matter include (Figure 1.4):

- **Inelastic Scattering:** Alpha particle collisions with atomic electrons. During these inelastic collisions, there is a maximum amount of energy an alpha particle can transfer to an electron. This effect is governed by the laws of conservation of energy and momentum. The maximum energy transferred (E_{max}) can be found by considering these laws during an inelastic collision between a 'stationary' electron and an incoming alpha particle. $E_{max} = 4Em_e/m$ [32], where E is the initial kinetic energy of the alpha particle, m_e is the electron mass and m is the mass of the alpha particle, or any charged particle. From this formula it is obvious that only a small amount of E can be transferred per collision. Thus, the deflection of an alpha particle along its path is minimal and many collisions are required before the alpha particle is stopped.

- **Nuclear Collisions:** Either an elastic or inelastic collision between an alpha particle and a nucleus. These collisions are much rarer than collisions with electrons. In the elastic case (Rutherford Scattering) there is no particle or nuclear excitation. The charged particle is deviated from its path by the Coulombic force. For inelastic collisions the atom is left in an excited state after the collision.

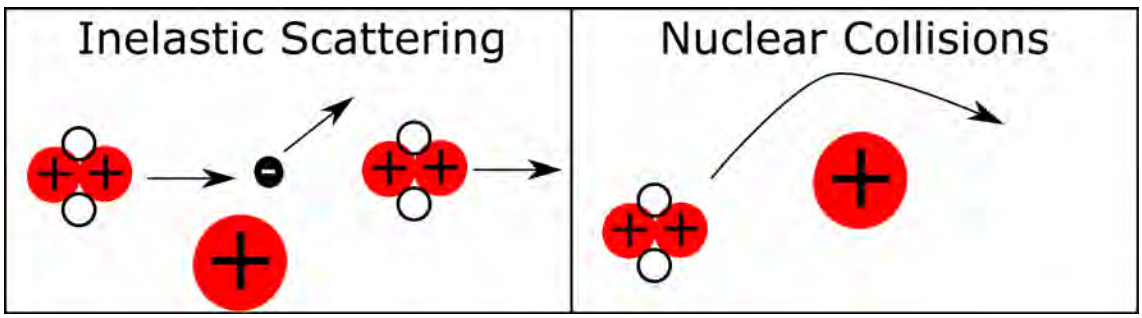

Figure 1.4: Pictorial representations of the possible interactions for alpha particles.

Stopping Power

The stopping power of a heavily charged particle is determined using the Bethe-Bloch formula (Equation 1.5 [30]).

$$-\left(\frac{dE}{dx}\right) = \frac{z^2e^4}{4\pi\epsilon_0^2 m_e v^2} NZln\left(\frac{2m_e v^2}{I}\right) \tag{1.5}$$

where each of these parameters are the same as in Equation 1.1. This equation is significantly simpler than Equation 1.1 because the last two terms in Equation 1.1 describe relativistic effects. The stopping power of polystyrene for increasing

energies of alpha particles is shown in Figure 1.5.

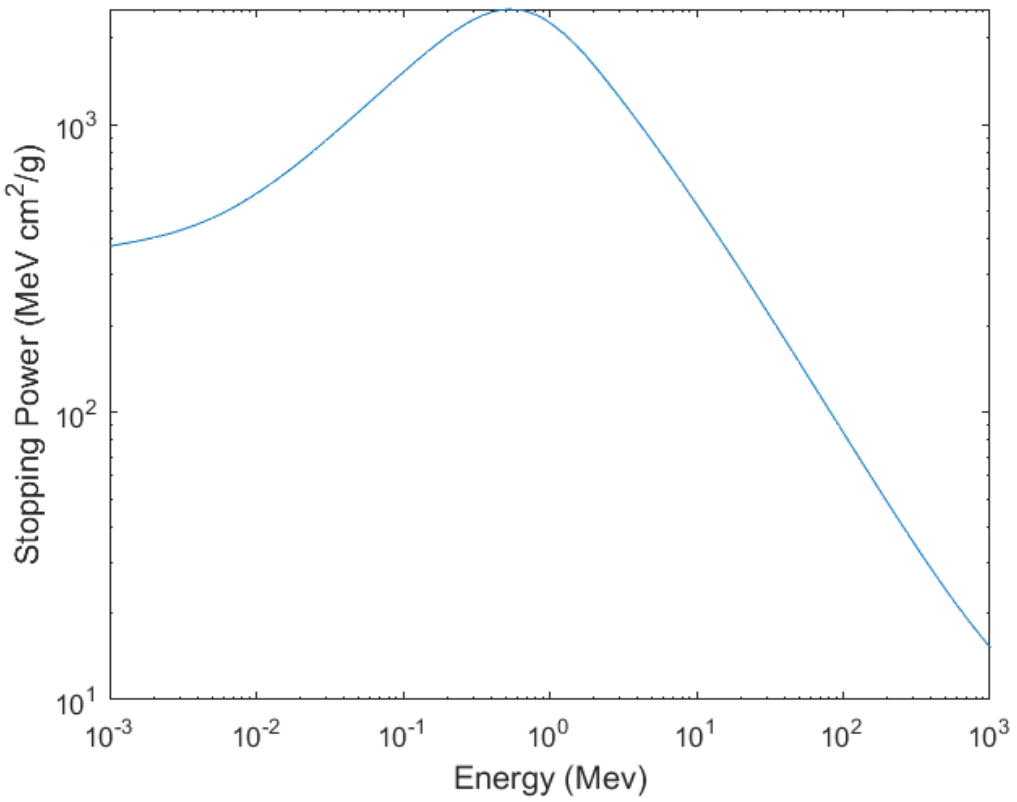

Figure 1.5: Stopping power of polystyrene for increasing energies of alpha particles [1].

The formula shows that particles of higher charge will transfer energy at a higher rate ($-\frac{dE}{dx} \propto z$). Equation 1.5 also shows that the alpha particle losses energy and therefore as $\nu \to 0$, $-\frac{dE}{dx}$ will increase causing a maximum energy loss due to ion pair formation at the end of the particles track. This causes a peak in the stopping power known as the Bragg peak (Figure 1.6). This feature is not seen for beta particles due to their erratic path. After the Bragg peak the energy of the alpha particle will approach zero. The represents the particle coming to rest since it will acquire two available electrons through Coulombic attraction and become a helium atom [31].

This effect indicates that minimising the cladding thickness of the scintillating fibres is critical since the maximum dose deposition occurs at the end of the alpha particles path. The thickness is then required to be much less than the path length to maximise dose deposition into the fibre's core. In contrast to the beta particle

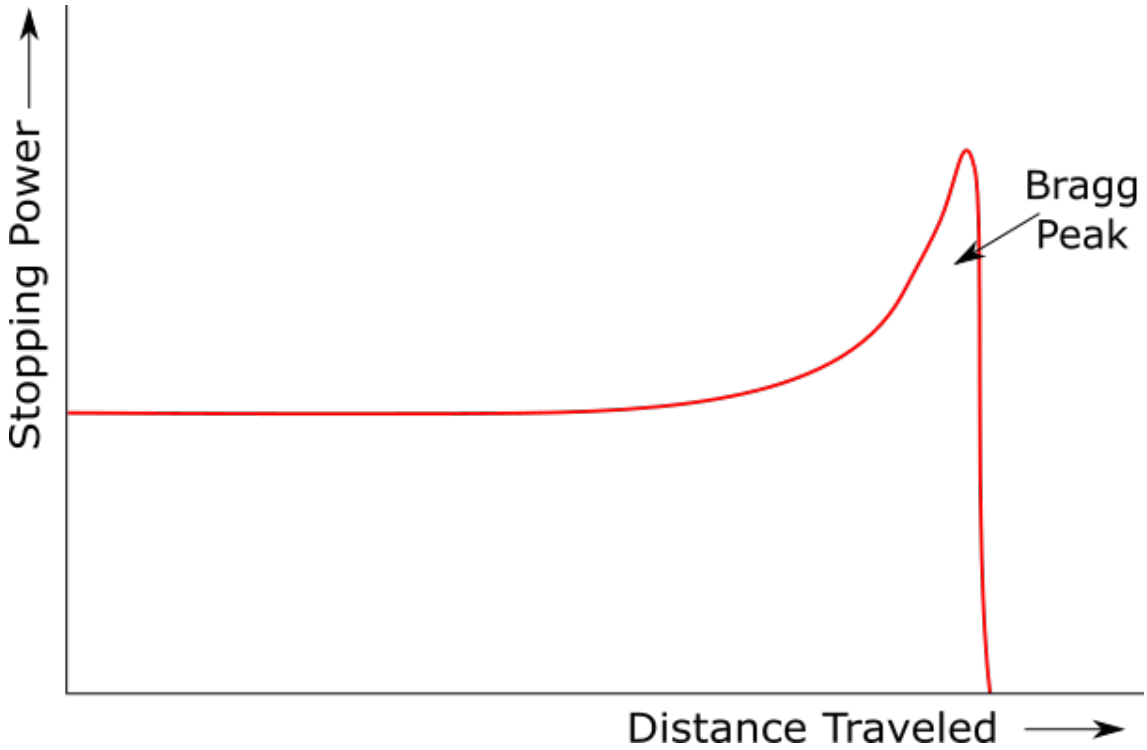

Figure 1.6: Pictorial representation of the Bragg peak. Sharp increase in stopping power with distance traveled.

sensor where a thicker cladding is used to discriminate against dose deposition from alpha particles (Figure 1.7).

Range

A consequence of an alpha particle's high ionisation 'power' is a much shorter path in a given medium than a beta particle of the same energy. In air, alpha particles have ranges of cm [29], however, in more dense materials like liquids and solids, the range is much shorter. The higher densities enable more collisions per path length for the alpha particles [31]. The range of alpha particles in more dense materials can be determined by the formula described by [33],

$$R_{cm} = 0.00032(A^{1/2}/\rho)R_{air} \tag{1.6}$$

where R_{cm} is the average range (cm) of the alpha particle, A is the atomic weight of the liquid or solid, ρ is the density (g/cm^3), and R_{air} is the calculated average linear range of the alpha particle in air from the formula, $R_{air} = 0.3E^{3/2}$ [34].

The alpha particles in the intended sensing environment travel tens of microns in liquids due to their energies. Therefore the scintillators may be packed closely together with very thin cladding's ($< 10\ \mu m$) and with diameters thick enough to maximise dose deposition (Figure 1.7).

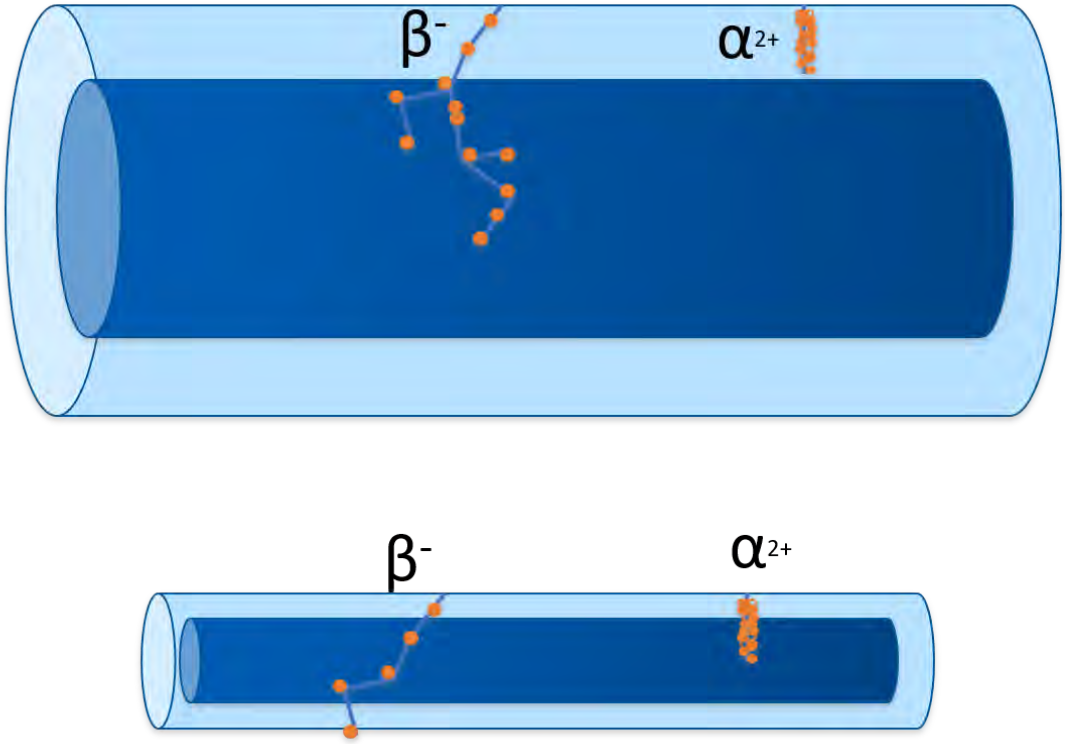

Figure 1.7: Pictorial representation of the fibre geometries for each sensor. The top represents the geometry for the beta particle sensor where the thicker cladding is used to discriminate dose from alpha particles and the thicker fibre maximises dose deposition from beta particles. The lower represents the geometry for the alpha particle sensor where the thinner cladding allows dose deposition from alpha particles and the thin fibre diameter minimises dose deposition from beta particles.

1.2.3 Photon Interactions With Matter

The absorption of electromagnetic radiation (gamma rays), by matter is fundamentally different than that of charged particles due to photons being neutral. These particles are absorbed or scattered in a single event or interaction with a nucleus. The maximum energy of the gamma rays emitted throughout the U-238 chain is ≥ 2 MeV. Therefore, they can interact by both low and high energy processes including; Rayleigh scattering, Photoelectric absorption, Compton scattering and finally Pair production.

Energy Loss Mechanism

The main interactions of photons with matter occur by (Figure 1.8),

- **Rayleigh scattering:** Low energy photon interactions with electrons. This is an elastic collision so the photon does not excite or ionise the atom, it is simply deflected from its path.

- **Photoelectric absorption:** The energy of an incident photon cannot be totally absorbed by a free electron [29]. This can only occur when the electron is initially bound in the atom. When this occurs, the photon is immediately followed by the emission of a photoelectron with energy equal to the photon energy minus the binding energy of that electron. The filling of this new vacancy in this shell, by an outer shell electron, causes the release of characteristic X-rays.

- **Compton scattering:** Compton scattering is the interaction of a photon and a free or stationary electron. When the energy of the photon is far greater than the binding energy of the electron, the electron can be considered as free [29]. The incident photon will collide with the electron, transfer energy and a new lower energy photon is created.

- **Pair Production:** For high energy photons, exceeding 1.02 MeV [29], a forth type of interaction becomes possible. This interaction occurs in the presence of the Coulombic field of a charged particles nucleus [31]. The photon is fully absorbed and its energy is converted into rest mass energy and kinetic energy of an electron-positron pair. Once the positron comes to rest it will annihilate with a nearby electron, emitting annihilation radiation (two 0.511 MeV gamma ray photons).

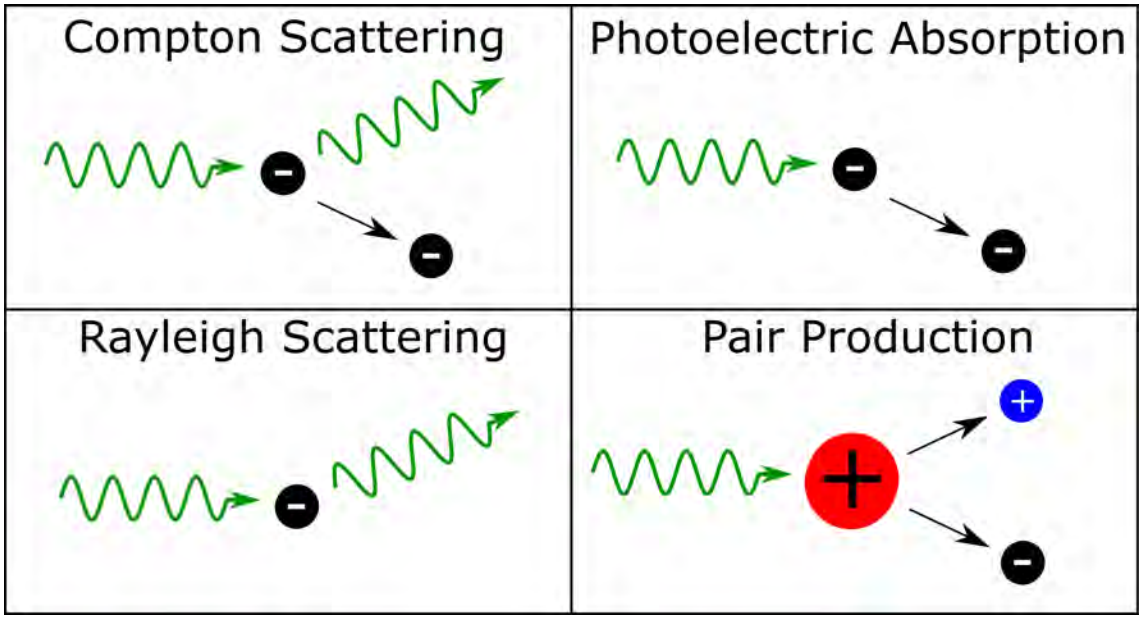

Figure 1.8: Pictorial representations of the possible interactions for gamma rays.

Attenuation in Matter

Photons have no charge, therefore the range of a photon is governed by the interaction probability (cross-section). This depends on the absorber and the energy of

the photon (predicts the interaction cross-section). The intensity that remains after travelling through an absorber of thickness, x, is predicted via Equation 1.7,

$$I = I_0 \exp(-\mu x) \tag{1.7}$$

where μ is the attenuation coefficient for a given photon energy and absorber material [1]. The transmitted photon intensity, I, is then proportional to the initial intensity, I_0. From Equation 1.7, the thicker and denser the absorber the greater probability of interaction and hence, energy deposition. Therefore, the thickness of the scintillators for alpha and beta detection is kept minimal to reduce dose deposition from gamma ray sources.

The geometries discussed above can be easily made by drawing optical fibres from scintillating polymers (plastics). These geometries allow for efficient discrimination between each type of ionising radiation and effective dose deposition. However, the sensitivity of these devices for real-time sensing depends on the quality of the scintillator used and the method of signal processing. A description of scintillator properties follows.

1.3 Scintillation Materials

A description of organic and inorganic scintillators is provided in this section to give context for the materials used in this thesis. The mechanisms discussed cover both plastic (organic) and crystals (inorganic).

In general, a useful scintillator should possess the following characteristics:

- **High photon production efficiency:** The deposited energy from incoming radiation should be converted into detectable photons with a high efficiency to give the highest signal to noise ratio.
- **Linear energy response:** A linear response to the incoming radiation is desired so that the light yield is directly proportional to the amount of incoming radiation.
- **High optical quality:** A high optical quality is required to reduce loss of the photons produced. Transparency at the scintillation photon wavelength(s) is also required to limit absorption. These qualities will allow for high light yields and high photon production efficiency.
- **Short decay time:** A shorter decay time allows for high count rates.
- **Emission wavelength:** The scintillation wavelength(s) should be emitted to best match to the spectral response of photodetector, in this case a PMT.

The scintillators used in this thesis were characterised in [3], they were found to possess these characteristics and therefore to be suitable for real-time sensing.

1.3.1 Organic Scintillators

In organic materials the scintillation emissions are produced by molecular energy level transitions. In the case of plastic scintillators, fluorescent organic molecules, called fluors, are dissolved into a polymer matrix. Each one of these fluor then acts as a scintillation centre. These molecules generally have symmetrical properties that form a π electron structure [32]. This structure allows for three kinds of photon emissions, prompt fluorescence, phosphorescence and delayed fluorescence. The relevant mechanism here is prompt fluorescence as this represents the majority of the light yield from a scintillating material.

The process of prompt fluorescence is shown in Figure 1.9, where an excited molecule undergoes a transition from an excited state back to the ground state with the emission of a photon.

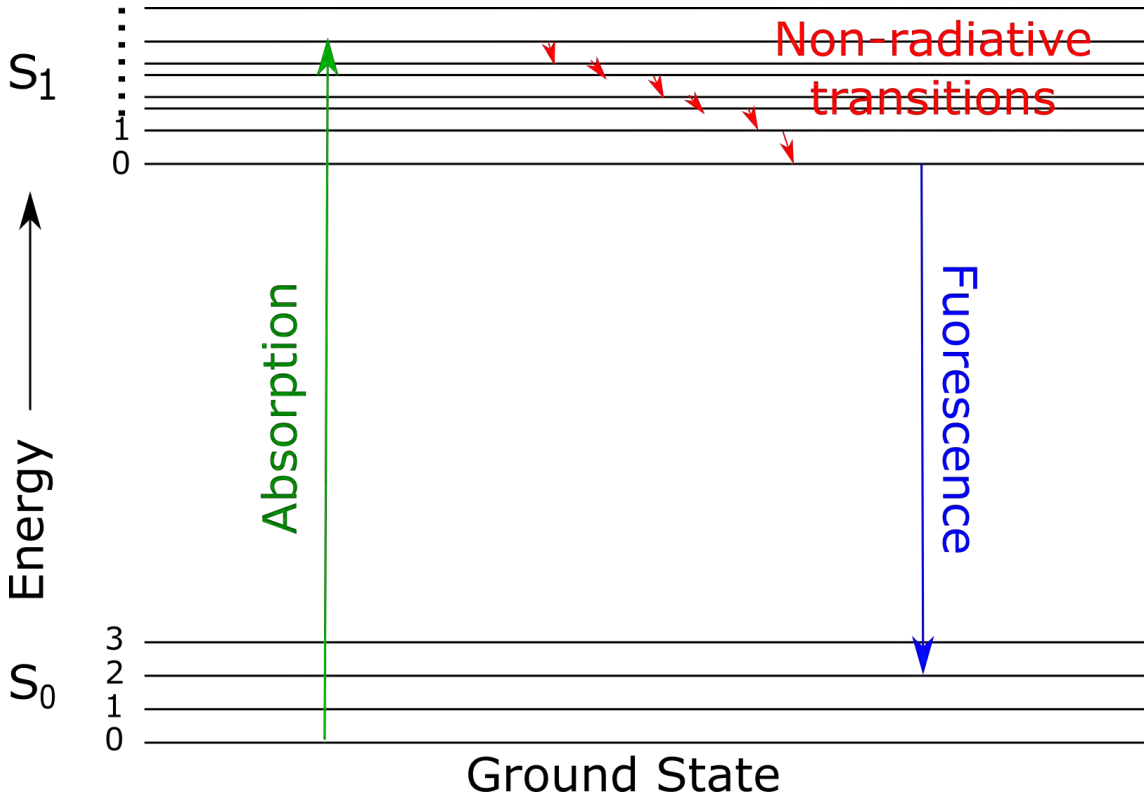

Figure 1.9: Energy level diagram of an organic molecule with π electron structure.

The molecule begins in the ground state, or singlet state (S_0), that is divided into several vibrational states (S_{00}, S_{01}, S_{02} etc). With the absorption of energy from incoming radiation, the molecule is excited to one of the excited states (S_1 or S_2 etc) or a vibrational state therein. Any transitions to a state above S_{10} will result in the almost instantaneous de-excitation back to the S_{10} state by non-radiative transitions (internal conversion). All of these transitions will occur in nanoseconds [29]. When

the molecule de-excites back to the ground state, or one of the vibrational states of the ground state, scintillation photons are emitted.

1.3.2 Inorganic Scintillators

In inorganic materials the scintillation emissions are related to the band structure of the crystalline lattice of the material. Incoming radiation or some other source can transfer energy to the electrons within the material. Sufficient energy will promote an electron to the conduction band, leaving behind an electron hole. When this electron returns to the valence band a scintillation photon is emitted. This emission is typically quite inefficient and its wavelength lies in the ultraviolet region that is prone to high optical losses due to self absorption.

With the addition of dopants, the material can be modified such that these emissions lie in the visible region. This is achieved by making special luminescence sites in the band gap (between the valence and conduction bands) to which the electrons de-excite before continuing to the valence band [29]. As the energy to the valence band is lower than that of the band gap the photons emitted have a longer wavelength, in the visible region.

1.4 Detection of Scintillation Photons

The number of photons that are captured by the photodetector are quite low even with the high light yields of the fibres used in these sensors. A highly sensitive photodetector and appropriate detection electronics is required for an effective radiation sensor. The detectors and electronics to maximise the efficiency of these detectors was investigated in [3].

1.4.1 Signal Processing and Detection Electronics

In the work presented here a ER9829B PMT was used since this device is designed for scintillation event counting.

The amplitude of the detector (PMT) output, the voltage pulse, allows the isolation of specific energy radiation events from the detector background noise. Thus, this is the most important characteristic of the output pulse. Analogue and digital processing can be used in order to extract information from this amplitude information in real-time.

The output from the PMT is converted to a voltage pulse via a charge-sensitive preamplifier (CR-Z-PMT) whose output is sent to a shaping amplifier within the multi-channel analyser (MCA-527), this manipulates the shape of the pulse to allow interpretation by the MCA. These interpreted signals form a pulse height spectrum

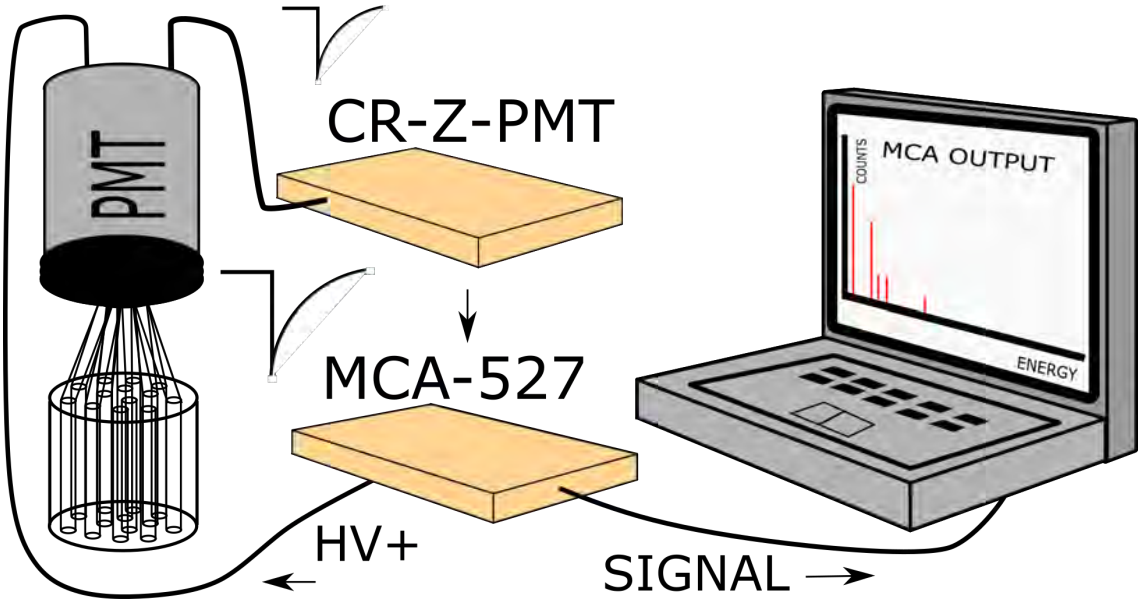

Figure 1.10: Equipment set up as described in section 1.4.1.

that provides energy information. This process is illustrated in Figure 1.10.

With these components, along with a fibre optic based sensing unit, real-time analyses of gross alpha and beta particles was shown to be possible in mineral processing liquids. The development of each sensor is described in the following chapters.

1.5 Polonium-Specific Sensor

The successful development of a near real-time polonium-specific sensor would be of high significance to the discipline of radiation monitoring and radiation safety, as Po-210 is notoriously difficult to measure in mixed RN samples due to it's low abundance, emission of almost solely alpha particle radiation, and high volatility. A real-time polonium-specific sensor would be highily advantageous in understanding polonium distributions in IOCG-U ore processing for process optimisation and monitoring.

This sensor is required to operate for long durations in concentrated acidic conditions and elevated temperatures of mineral processing liquids (specific conditions are outlined in Chapter 5). One goal of this research is to explore the efficiency of Po-210 deposition onto various metals in these processing conditions. The second is to investigate an appropriate scintillator to form the detector component. A sensitive scintillator coated in a film of metal is proposed to monitor Po-210 specifically in solution.

1.5.1 Polonium-210 Determination

The most common method of determining Po-210 concentrations in liquids is through alpha particle spectroscopy. This technique takes advantage of the fact that Po-210 spontaneously adheres to many metals which simplifies target preparation.

Spontaneous Deposition

Spontaneous deposition is the mechanism of a more noble metal atom in solution plating itself to the surface (a disk or some other substrate) of a less noble metal. From a thermodynamic perspective, spontaneous deposition occurs in a reaction where the standard Gibbs energy is less than zero ($\Delta G < 0$), that is the amount of energy available is greater than the energy loss due to entropy. Hence the reaction is spontaneous [35]. This process is governed by an atom's electronegativity, its tendency to attract a bonding pair of electrons, i.e. its tendency to form bonds with other atoms. The higher the value of an atoms electronegativity the more an atom attracts electrons.

The experiments in this thesis take advantage of this by plating Po-210 onto various metals. For example silver (Ag) has a electronegativity less than that of polonium, $1.93 < 2.0$, therefore polonium will spontaneously deposit itself into a silver substrate and any other metal with a lower electronegativity (or electrode potential). This mechanism is tested with various metals in the specific mineral processing conditions outlined above, including in the presence of contaminants, to identify if it can be used for near real-time determination of Po-210 in these harsh conditions.

Alpha particle spectroscopy

The most common transition metal used for counting targets in alpha spectroscopy is silver (Ag). There are various examples of this [36–40] using similar processes to determining polonium. However, the efficiency can vary depending on the conditions of the solution, hence investigation to determine which metal has the best efficiency for polonium uptake in the operating conditions is required.

As this sensor needs to operate as close to real-time as possible, the time between measurements must be minimised. This can be achieved by investigating a metal that Po-210 will adhere to quickly. In [36], various metals were investigated to determine which has the best uptake of Po-210 via spontaneous deposition in a short time frames of 15 minutes. It was found that nickel (Ni) had the best yield of 85%. Copper (Cu) was also found to be quite efficient at $\approx$ 70%. Each of these metals were considered for this sensor. In comparison it was found in [37] that Ag disks reached 90% but were left in solution for 3 hours to achieve that highest efficiency.

Temperature: The plating efficiency is heavily dependent on the temperature of the solution. In [39], a temperature of 70 °C was used, with a deposition time of

2 hours with rapid stirring. It was found that the deposition yield of Ag and Ni were unchanged but Cu increased to 85%. In [40], room temperature plating was performed. This process took at least 1 day to reach the same efficiencies, confirming the deposition yield is heavily dependent on the temperature of the solution. This was confirmed in [41]. Therefore, the temperature dependence is a key factor in the polonium uptake efficiency.

Acid: The most common acid used in alpha spectroscopy is hydrochloric (HCl) as it is found to be the most efficient for spontaneous deposition of polonium [42–44]. However, here we are concerned with uptake in sulphuric acid (H_2SO_4) which is commonly used in mineral extraction. Deposition of Po-210 in H_2SO_4 (and HNO_3) is hindered by low solubility of Po-210 in this medium [42, 45]. The Hallistadius method [46, 47] is the most widely used method for plating in H_2SO_4. This method involves using pretreatments and other chemicals within the liquid to combat this insolubility. This method is only viable in a controlled environment, not suitable for real-time sensing. However, this does give promise for efficient polonium uptake in H_2SO_4. The main limitation in using spontaneous deposition is the interactions of Po-210 with other compounds or ions in the solution. These compounds can be other metals present in the solution: most notable is the ferric ion (Fe^+) that can be present in mineral or environmental samples, and mineral processing liquids. There are various examples of pretreatments that can be used in order to counteract this effect [41,48–52]. In [41] it was found that hydroxylamine hydrochloride was useful in reducing interference. This was further supported in [49–51] who found the addition of sodium citrate was also effective. In [48] it was found that ascorbic acid reduces ferric ions efficiently, and it was found in [51] that ascorbic acid is more efficient at reducing Fe(III). As these pretreatments are made to the solution, not the sensor, this would need to be undertaken in a controlled environment so it is not suitable for real-time sensing in a mineral processing plant.

The feasibility of efficient deposition in mineral processing conditions is explored in Chapter 5.

1.5.2 Detector Geometry

The envisioned sensor relies on coating a scintillator in a thin coating of a transition metal to form a detector that actively attracts polonium to the sensor. Methods of achieving a thin coating are well known: electroless plating, and mechanical sputtering. Electroless plating is a process of metallic ions in solution being reduced onto another surface either spontaneously or by chemical activation. Mechanical sputtering is a process that deposits thin films onto a target. A source ejects atoms within a vacuum chamber that are not in thermodynamic equilibrium such that the atoms will stick to all surfaces within the chamber, including the intended target. This allows for thin films with low variation in thickness [53].

A viable candidate for this scintillator is a ZnS(Ag) screen. The geometry is easily coated via mechanical sputtering and efficient for coupling to a PMT.

1.6 Radiation Sources

The radiation sources used in this research consist of alpha, beta and gamma emitting RNs. Most of the sources used are unsealed sources with the exception of one source (Am-241). A brief description of each source used is given in the next section, along with any radiation safety procedures.

1.6.1 Sealed Source

Am-241 (5.486 MeV Alpha and 60 keV Gamma)

An Am-241 sealed source was used in this research for calibration of the "Daybreaker" counter (alpha counter) for testing the response of ZnS(Ag) screens. The source consists of a Au coated Ag foil with uniformly distributed americium dioxide that is contained within a stainless steel holder. The Au coating of the foil attenuates the high energy alpha particles as they are emitted from the foil. The low energy gamma rays (60 keV) are not significantly attenuated.

Both the alpha and gamma emissions from the Am-241 foils used in this project are very low activity levels and are low risk to the handler. Alpha particles at these energies are stopped by the dead layer of human skin so the only risk is internal. Gloves were worn when handling this source to prevent accidental ingestion.

1.6.2 Unsealed Sources

Potassium chloride (1.31 MeV Beta and 1.46 MeV Gamma)

Potassium chloride (KCl) contains the radioisotope of potassium K-40, which was used to create low concentration solutions for testing the beta particle sensors. K-40 emits beta particles and a small fraction of low energy gamma rays.

Beta particles are blocked simply with the glass beakers used to contain the solutions and the gamma rays are not considered dangerous at such low activities. The KCl is only toxic if ingested in large quantities. However, safety precautions were still taken by wearing gloves throughout handling and preparation.

Po-210 (5.4 MeV Alpha)

Po-210 was used for testing the sensitivity of the alpha sensors, in the polonium contamination prevention experiments and in the electrochemical experiments.

Po-210 is almost a pure alpha emitter with a short half-life. Po-210 is considered

extremely dangerous, however, in it's solid form this isotope is relatively harmless but when is volatilised it can be lethal. The lethal dose is less than 1 μg. Therefore, extra care was taken during preparation of solutions and throughout experiments involving this RN. All solutions were produced under a fume hood and gloves were worn at all times. Special consideration was taken for lab equipment used in these experiments, to not spread any contamination: routine checks were made using surface barrier detectors available in the lab.

Ra-226 (4.87 MeV Alpha)

Radium-226 was used to measure the response of the alpha sensors. Ra-226 is the most stable isotope of radium with a 1600 year half life and it emits an alpha particle.

Ra-226 is considered dangerous as it decays into Radon, a noble gas and an alpha emitter; this may be dangerous when inhaled in high concentrations. All samples of Ra-226 were prepared under a fume hood and gloves were worn throughout experiments. The concentrations of this RN were also kept very low.

1.7 Summary

The aim of the research presented in this thesis is to develop and test the feasibility of creating a class of sensors for the quantification of key RN contaminants during mineral processing of RN contaminated ores, and radiation protection during processing.

This chapter outlined the research scope along with discussion of relevant literature and theory. Further development of the optical fibre prototypes are found in chapters 2 and 3. Chapter 3 explores the use of various surfactants to remove accreted contamination on the surface of polymer fibres. Chapter 4 investigates the limit and possible components of the sensor background signal. Finally, the feasibility of a polonium-specific sensor is outlined in Chapter 5.

Chapter 2

Beta Particle Sensor

2.1 Introduction

This chapter details the development of a more sensitive beta particle detector including its scalability and performance in mineral processing liquids. Sensitivity is improved by increasing the sensing volume and therefore increasing the number of possible interactions with ionising radiation. This enabled a more detailed analysis of the sensor's noise floor. A periodic variation in the noise floor from an external source is described in this Chapter and a more fundamental investigation is found in Chapter 4.

2.2 Construction and Performance Testing

This device is an extension of the work by C.Whittaker [3]. To examine the scalability of these devices the number of fibres was increased, while the fibre and detector geometries remained the same. The construction protocol was changed to facilitate this increase (section 2.2.1). A performance test was also undertaken to ensure the sensors linear response to increasing amounts of ionising radiation remains consistent (section 2.2.2).

2.2.1 Construction

The scintillators used in this sensor were 15 cm long, 1.1 mm thick, plastic scintillating fibres (BFC12 from St. Gobain). A plastic frame was used to hold 200 fibres spaced 5mm apart (Figure 2.1), this separation was found to maximise the detection efficiency in [26]. Each end of the detector is held by an optical cement (EJ-500), chosen since it has the same refractive index as the plastic fibres (n=1.57). The detector face is brought together with a 1 inch diameter SM1 threaded ring. This detector face is then polished until optically clear to prevent loss of signal when coupling to a photomultiplier tube (PMT) with an internally SM1 threaded cap. The procedure for construction is found in Appendix A.

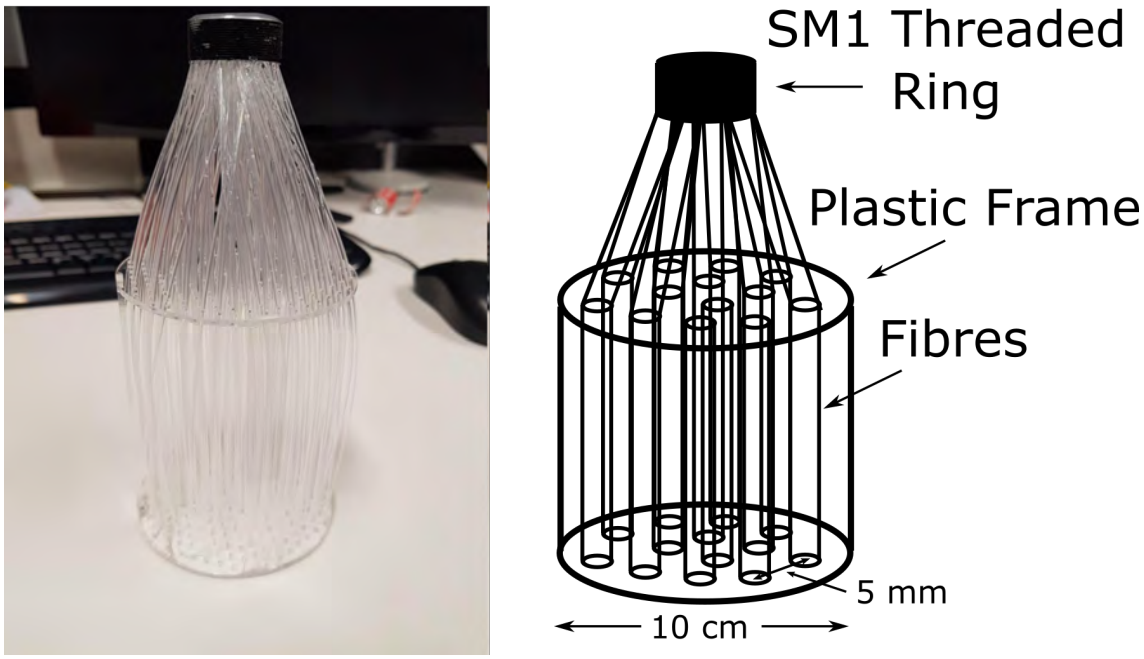

Figure 2.1: Picture of the completed sensor (left). Schematic drawing of the sensor (right).

2.2.2 Performance Testing

A response curve that tests this sensors response to solutions of different beta particle activity was generated by measuring known concentrations of radionuclides in solution. Ideally a pure beta particle emitter would be sourced for this purpose. However, a cheap, readily available, safe and practical source of beta particles is potassium chloride (KCl) which contains potassium-40 (K-40). This was used to create solutions of different activity concentrations determined by the Equation 2.1.

$$A_C = \frac{m_{KCl}}{V_T} \times A_s \tag{2.1}$$

where, m_{KCl} is the mass of KCl, V_T is the total volume of the solution prepared and A_s is the specific activity of KCl (16.08 Bq/g).

The gamma ray emission from K-40 constitute a very convenient means of measuring the activity of the solutions, to confirm their calculated activities. Multiple solutions of the same volume (600 ml, maximum for beaker used), but different concentrations were made using differing amounts of m_{KCl}, the details of each is found in Table 2.1. The activity concentrations were determined by gamma spectroscopy.

The experimental arrangement used for taking measurements is shown in Figure 2.2. The sensor is lowered into a 600 ml beaker containing the KCl solution and placed into a blackout box that minimises any light leakage from stray light sources.

Solution	Activity (Bq/ml)
1	0.097 ± 0.145
2	0.292 ± 0.127
3	0.492 ± 0.117
4	1.000 ± 0.0963
5	1.475 ± 0.0685
6	1.983 ± 0.0636
7	2.483 ± 0.0364
8	2.990 ± 0.0198
9	3.497 ± 0.0129
10	4.050 ± 0.0051

Table 2.1: KCl solution concentrations determined by gamma spectroscopy.

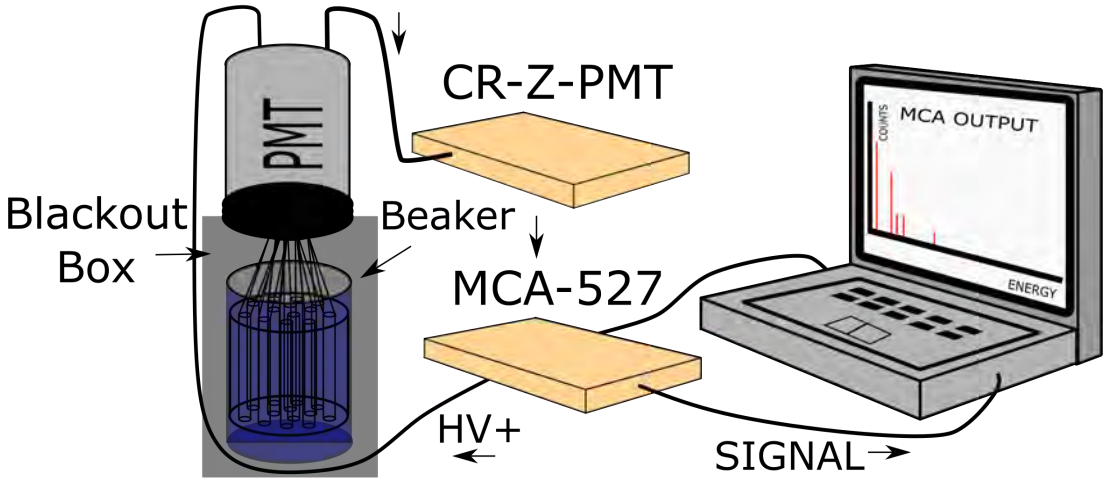

Figure 2.2: Experiment set up. Light produced from the sensor is guided to a PMT, this signal is then amplified in a preamplifier and fed to a MCA as outlined in section 1.4.1.

Multiple measurements of the pulse height spectra (PHS) using 100 second integration windows for each concentration is taken continuously over a period of 3 hours (108 windows). The background signal of 600 ml of deionised (DI) water is also taken for 12 hours to tightly define any background variations with time. The process of interpreting this data is detailed in the next section.

Data Analysis and Background Variation

The PHS of each solution is interpreted using a MATLAB code, shown in Appendix A. An example of a PHS for the 4.05 Bq/ml solution is given in Figure 2.3. It was found in [3], that the scintillation events generated by the gamma ray component of K-40 was accounted for by integrating the total events beyond a certain chan-

nel threshold. This threshold is set beyond the single electron peak (SEP) and the contribution of background radiation and cosmic rays (blue box). The beta particle events are dominant in the spectrum beyond this point (red box) due to their higher energies. The channel threshold is set to 300 for each measurement. The total counts in this region are integrated as the signal for a given measurement.

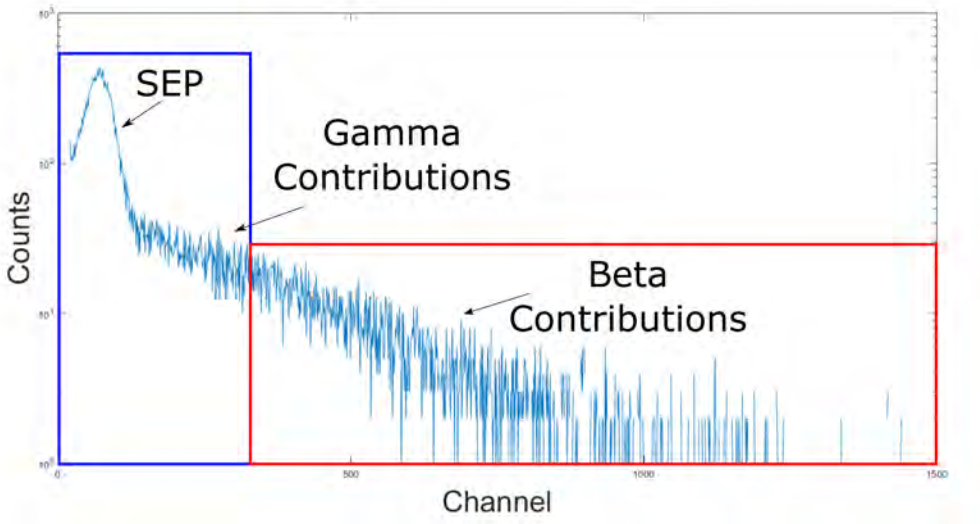

Figure 2.3: Pulse height spectrum for the 4.05 Bq/ml KCl measurement. The blue box contains the SEP and contributions from environmental sources. The red box contains the region dominated by beta emissions (channel 300+) and is integrated as the signal for this measurement.

The spread of this signal is due to two factors including; (1) the distribution of energies in the beta particles in solution and (2) the variable loss in beta energy due to different attenuation of the solution. The first factor is intrinsic to beta particle emissions where the energy is not fixed, as mentioned in Chapter 1. This process is outlined further in Section 2.3. The second is due to energy lost to the atoms and molecules within the solution along the beta particles path to the scintillator dependent on the beta particle path length between it's origin point and impacting the optical fibre and its subsequent path length within the optical fibre. Hence, each beta particle will experience a different attenuation from interactions with the solution forming a distribution of energies detected.

The variation, or uncertainty, is taken as the standard deviation of the total number of events within this region of the PHS. This uncertainty must also include variations in the background signal. It was found the background fluctuated dramatically over a period of a few hours (Figure 2.4). A Fourier transform of this signal (Figure 2.5) indicates the likely source is interference from nearby source. This effect was resolved by performing experiments in a laboratory located in a different building. The fluctuations were found to be significantly reduced, but they were still significant enough to required quoting the uncertainty in each measurement as the

reproducibility (Figure 2.6) since this value was larger than the uncertainty from poisson statistics.

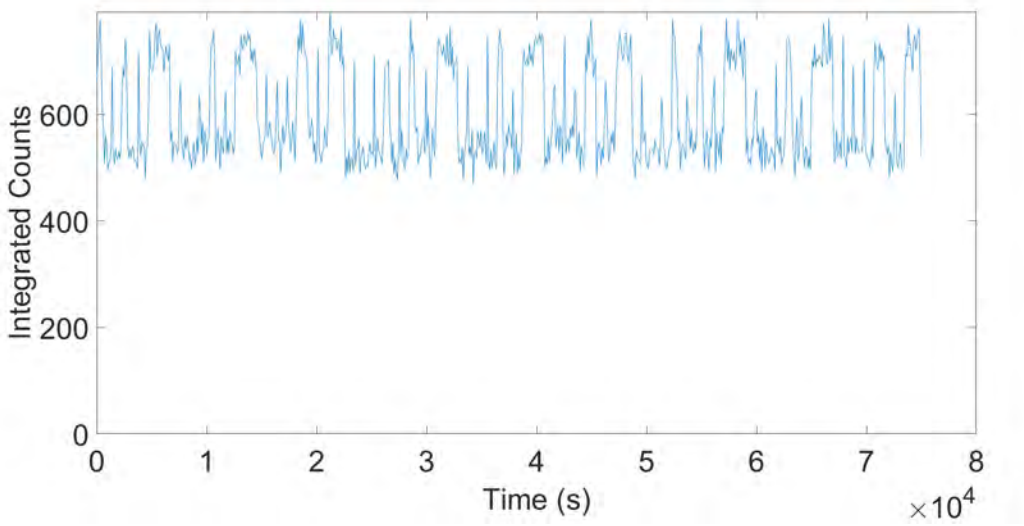

Figure 2.4: Background signal of the detector in DI water located in laboratory 1. Measurements were taken immediately after turning the HV on and at regular intervals (100 s). N_e is the number of scintillation events in 100 s.

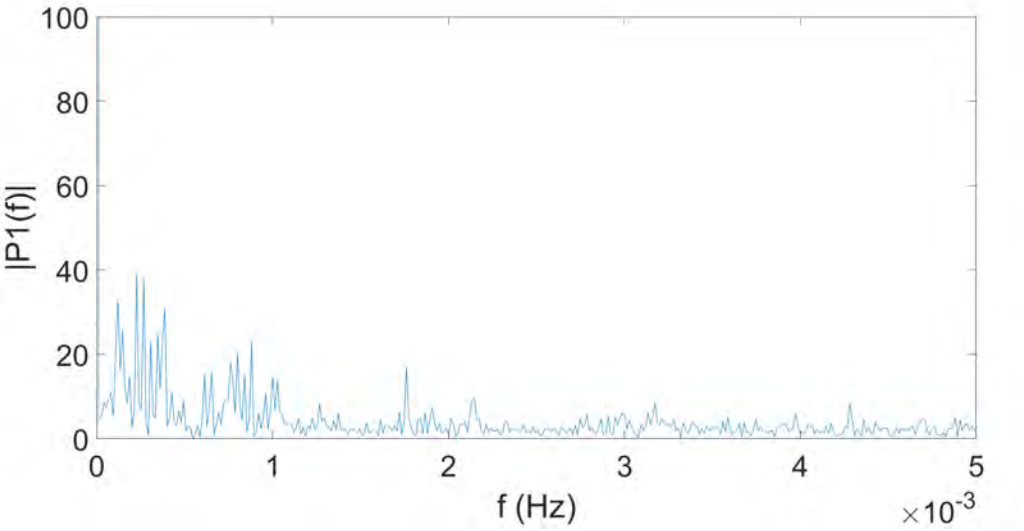

Figure 2.5: Background signal of the detector in DI water located in laboratory 1. Included is a Fourier transform of this signal, the low frequencies suggest the source is most likely from a nearby source, such as the temperature control of the lab.

The reproducibility σ_{rep} in each measurement is the standard deviation in addition to the standard deviation of the background signal (see Equation 2.2). This accounts

for any fluctuations in the background signal during each separate measurement.

$$\sigma_{rep} = \sigma_{bkg} + \sigma_{sig} \tag{2.2}$$

where σ_{bkg} is the standard deviation in the sequential background measurements and σ_{sig} is the standard deviation in the sequential KCl solution measurements. This analysis is undertaken for each solution subtracting the background signal. A line of best fit is found, forming a response curve.

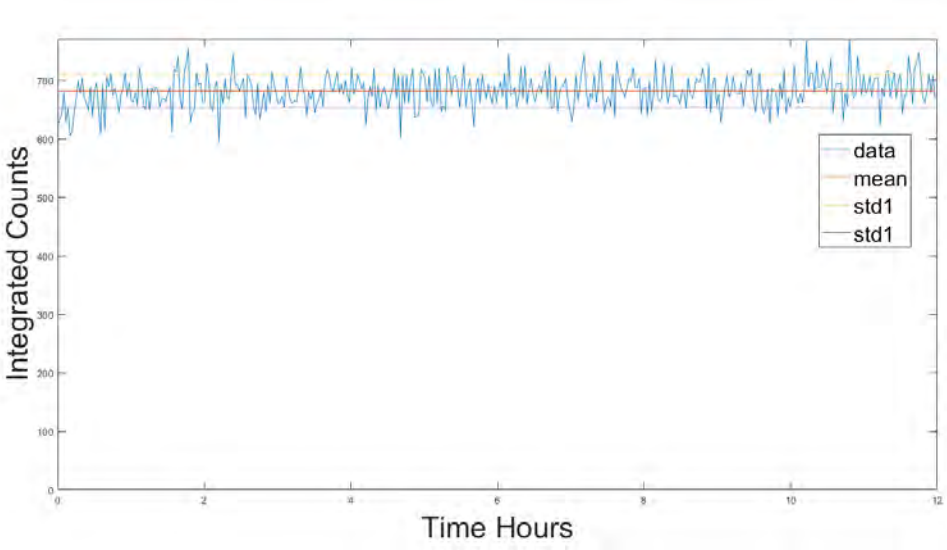

Figure 2.6: Background signal of the detector in DI water located in laboratory 2. Measurements were taken immediately after turning the HV on and at regular intervals (100 s). std = standard deviation

Results

The solutions in Table 2.1 were measured sequentially, starting with the lowest concentration so that any accumulation of KCl on the sensor wouldn't affect the subsequent measurement. The results of the PHS analysis are shown in Figure 2.7.

Each signal was distinguishable from the background signal and the uncertainty remained above background. There was also a linear increase in the number of events for an increasing RN concentration, as expected from [3, 26, 28].

A comparison between the previous generation of sensor [3] and the current is also made in Figure 2.7. It is seen that a 5-fold increase in the number of fibres resulted in a 4-fold increase in the number of counts in 100 s above background, instead of the 5-fold increase expected. Possible reasons for this effect are losses induced from (1) attenuation in the fibres or (2) coupling to the PMT.

The minimum detectable activity is now below 0.1 Bq/ml, a factor of ten below the original goal of 1 Bq/ml for mineral processing applications. This indicates that the signal strength increases with the number of fibres, as expected. A detailed noise analysis of these fibre systems is presented in Chapter 4. Understanding the noise in these sensors is needed to allow these to be used in applications requiring even lower detection limits, such as drinking water monitoring.

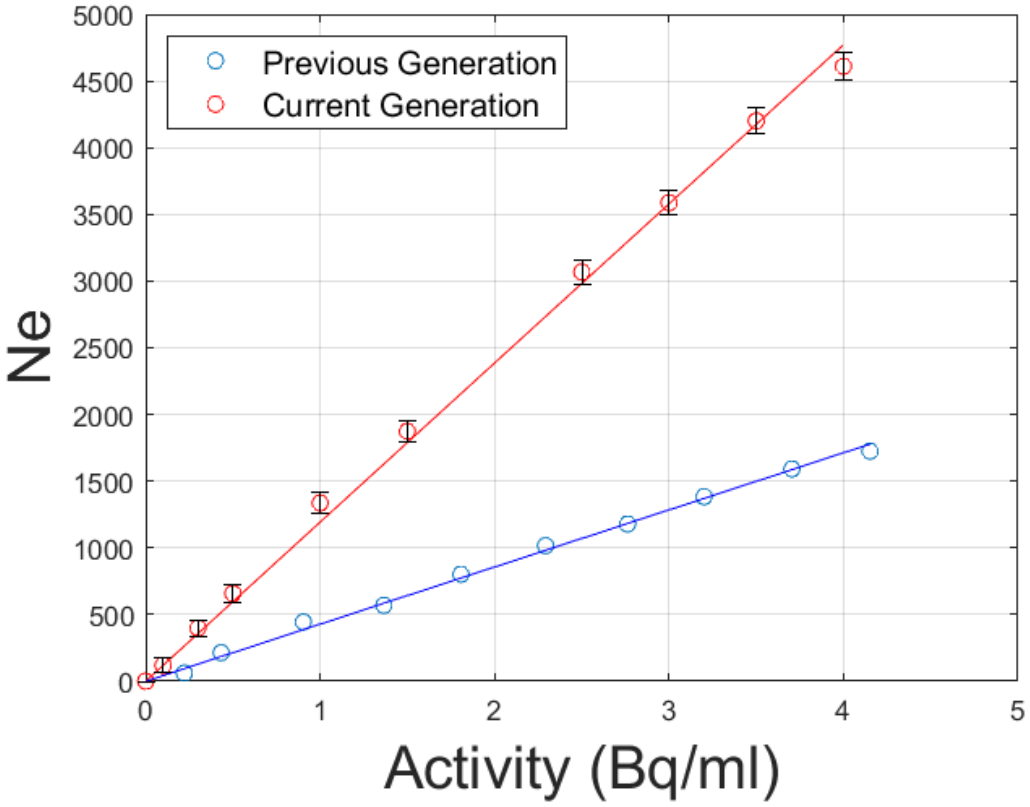

Figure 2.7: Comparison between the previous generation (blue) and current generation (red) of the beta sensor. N_e is the number of scintillation events in 100 s, background subtracted.

2.3 Mixed Radionuclide Measurements

To show the performance of this sensor in its intended field deployable state, the sensor was tested in mineral processing solutions. There are multiple stages throughout mineral processing, as described in Chapter 1. The RNs present and their concentrations will vary between each stage due to the removal of particular RNs. To gauge the performance of these sensors in mineral processing liquids a leach solution was provided for measurement by an industry partner in the ARC Australian Cu-U Hub from their Olympic Dam site. This contains mostly Pb-210 from later in the mineral processing chain; the RNs in this solution are indicated in Figure 2.8.

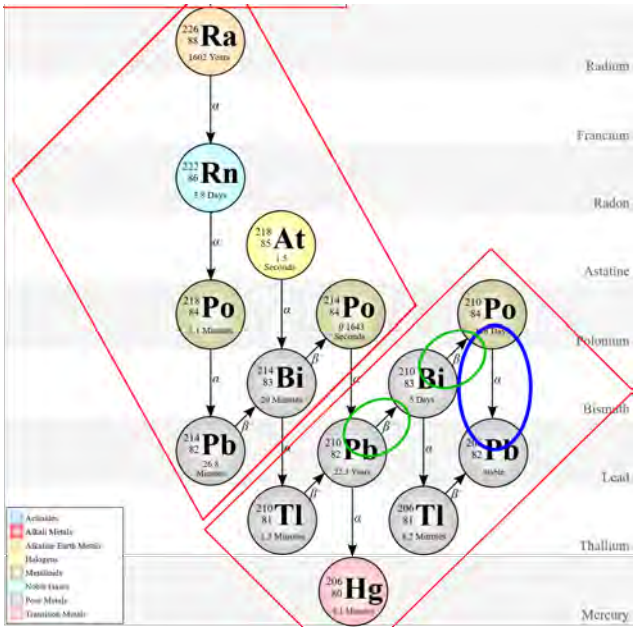

Figure 2.8: U-238 decay chain including half lifes of each daughter. The circled emissions are found in the leach solution measured in this section and those found in Chapter 3.

The leach solution was a 3 M HCl solution containing 1.8 Bq/ml (combination of Pb-210 and Bi-210) of beta emitting RNs. The measurement of this solution proceeded as in the previous section, including the data analysis. The result is shown in Figure 2.9.

The response of this sensor for a given beta particle concentration is expected to be the same for a given KCl concentration as per the results in [3, 26]. However, it is seen that the response of the sensor is far below the expected response in the leach solution. This appears to reflect the difference in the beta particle energies of the RNs present in this solution as described in the next section.

Energy Dependence

A beta particle emission is accompanied by the emission of an (anti)neutrino (depending on the charge of the emission). The energy emitted in a beta decay is then divided between the recoil nucleus, the beta particle and the (anti)neutrino. The average energy is a third of the total Q-value (mass difference between parent and daughter nucleus) [31, 54], an example of a beta emission spectrum is shown in Figure 2.10. The maximum range of a typical emission is then found from this energy.

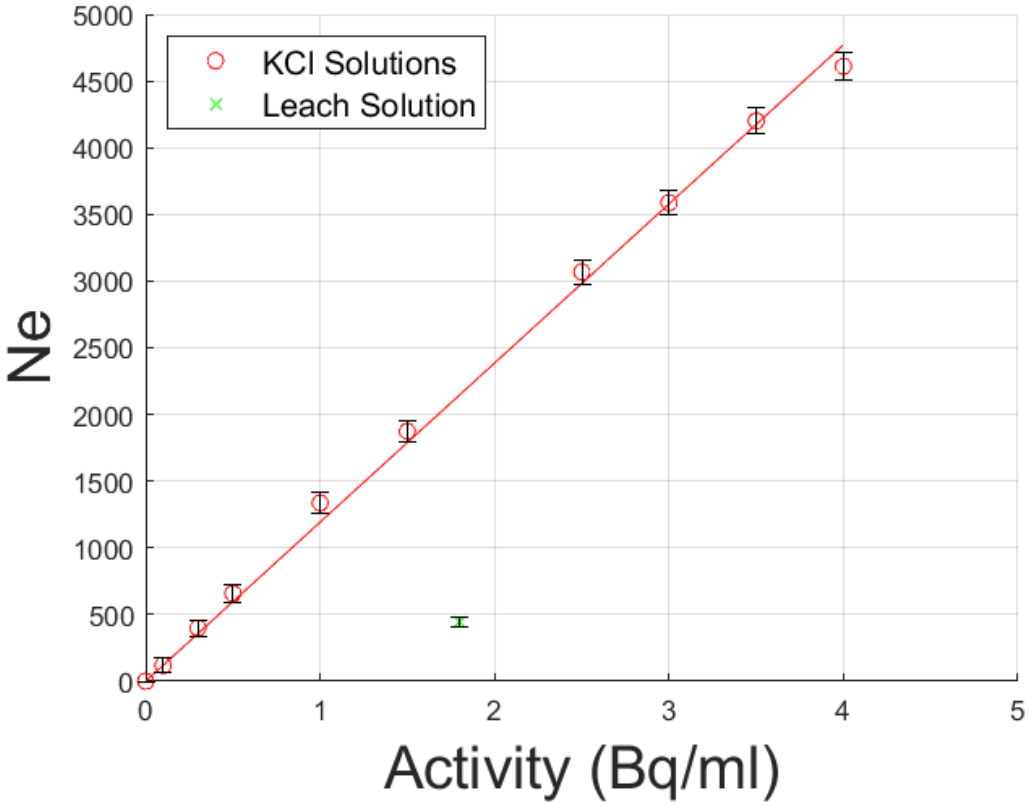

Figure 2.9: Comparison between the KCl calibration (red), a measurement in the leach solution (green). N_e is the number of scintillation events in 100 s, background subtracted.

The major factor that has affected these measurements is a difference in the range of the RNs within the solution. This range is dependent on the stopping power of the traversed material, calculated by the modified Bethe-Bloch formula (Chapter 1), which is dependent on the electron density of the material. This dependency comes from the number of interactions experienced by the incoming particle, progressively losing energy in each successive interaction. Beta particles of lower energies then have lower ranges in a given material. The probability of detecting a beta particle with this sensor is then dependent on the separation between each fibre. If the range is not sufficient to traverse this separation the probability of detection begins to decrease rapidly: too short and the particle will not be detected. The average energy of each beta particle and the maximum range at those energies in water for those present in this solution is shown in Table 2.2.

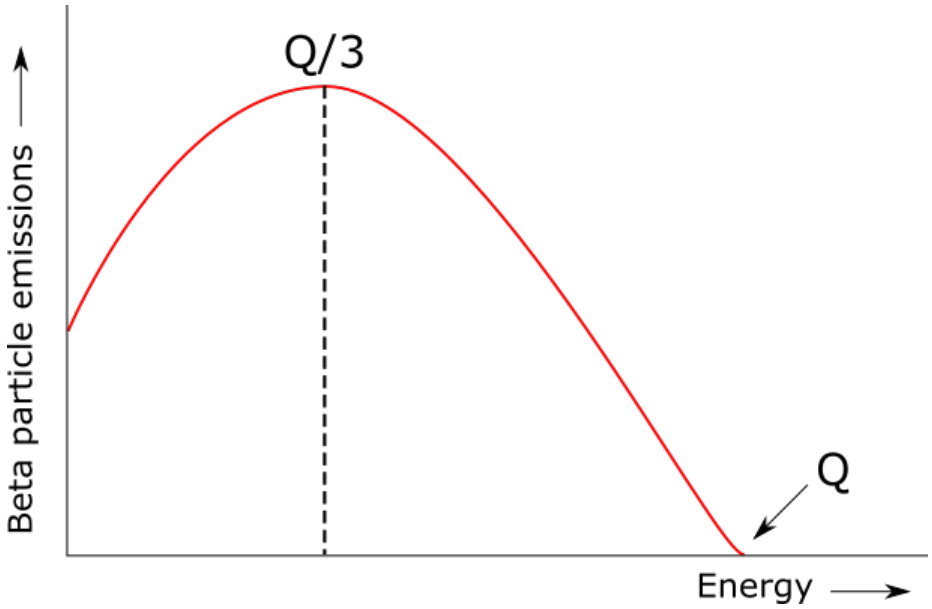

Figure 2.10: Example of a beta emission spectrum showing the concept of the Q-value.

Isotope	Average Energy (keV)	Branching Ratio (%)	Range in H_2O (cm)*
Pb-210	63 [55]	100	0.0006
Bi-210	387	100	1.3
K-40	437	89	1.5

Table 2.2: RN decay information for the beta emitters found in these solutions. *Range for the average energy is found from the NIST estar database.

The leach solution contains mostly Pb-210, however, each beta emission of Pb-210 is immediately followed by a beta emission from Bi-210 of higher energy. The total concentration of this solution was found to be 1.8 Bq/ml. Therefore, if the range of each RN is taken into account, the emission from Pb-210 will not deposit energy into the fibres since the beta range is not sufficient to traverse through the cladding, even if the emission was on the surface of the cladding (Figure 2.11). The signal is then only from Bi-210. The range of Bi-210 emissions is ≈15% lower than K-40, therefore, the difference in the volume is ≈30%. This noticeable difference between the signal in the leach solution compared to that of the KCl solutions can then be expected.

This correction was applied to the data in Figure 2.9 and is shown in Figure 2.12. It is seen that the data follows the trend of the energy dependence suggested. This indicates that tailored sensors will need to be created for each mineral processing stage. The separation between fibres and fibre claddings could be optimised to allow the emitters at each stage to deposit the maximum dose. An approach to this issue is discussed in the next section.

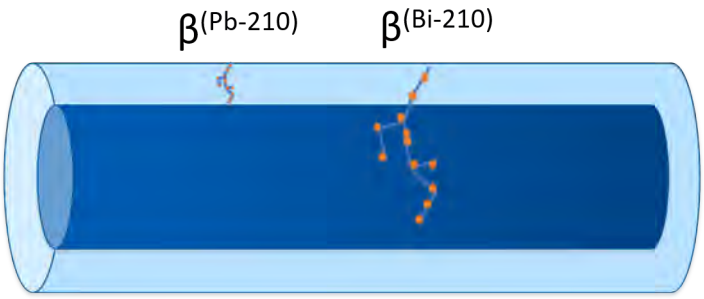

Figure 2.11: Visualisation of each beta particle emitting RNs relative range showing the likelihood of interaction with the core of the optical fibre.

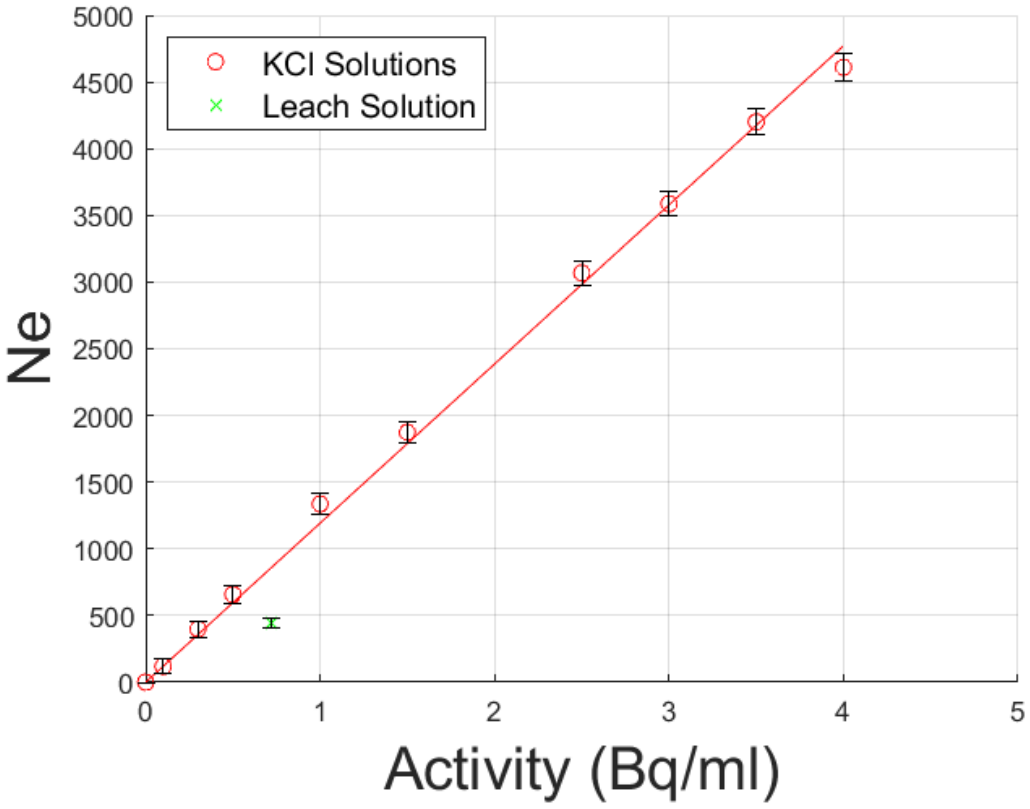

Figure 2.12: Corrected comparison between the KCl calibration (red), a measurement in the leach solution (green). N_e is the number of scintillation events in 100 s, background subtracted.

2.4 Future Directions

These sensors are not only required to be tailored to the type of emission (alpha or beta particles), but also indicate a requirement for specifically tailoring their geometry to the RNs present in each processing stage.

As the range of beta particles can vary significantly due to the nature of their interactions with matter (see Section 1.2.1 of Chapter 1), Monte Carlo simulations of each situation are required. Parameters that could be optimised are,

- Various fibre spacing's to maximise dose deposition
- Different fibre cladding thicknesses to prevent screening of low energy events
- Size of the detector to optimise the signal to noise ratio for low concentration solutions

These simulations could also be used in conjunction with standards of quantified (by alpha and gamma spectroscopy) leach liquors, each from different processing stages. A specific sensor geometry could then be designed and then calibrated for each processing stage.

With sensors calibrated for each stage of mineral processing, field deployable devices could be created. These devices could be placed in a flow cell between each processing stage or samples from each stage could be brought to the sensor in an isolated chamber. With suitable electronics and photodetectors these devices could then take real-time measurements of RNs throughout mineral processing stages.

2.5 Summary

In this chapter the construction and testing of a new generation of radiation-sensitive fibre-optic sensors has been achieved. The sensitivity limit for these new sensors was lowered from 0.3 Bq/ml to 0.1 Bq/ml. It was found that increasing the sensing volume 5-fold resulted in a near linear increase in the signal strength. The sensitivity of these devices can be improved further by employing the findings of the investigation in Chapter 4. An energy dependence of these sensors was identified and suggestions for future work around this topic are given, including Monte Carlo simulations and calibrations in mineral processing liquid standards.

Chapter 3

Alpha Particle Sensor

3.1 Introduction

This chapter investigates three aspects of a fibre-optic based alpha particle sensor,

- The scalability of this sensor (Section 3.2)
- The performance in mineral processing liquids (Section 3.3)
- The removal and prevention of polonium contamination (Section 3.4)

The scalability of this sensor was achieved by increasing the number of fibres used and, therefore increasing the total sensor volume. The performance of the sensor was assessed, including measurements in the same mineral processing solution as in Chapter 2. The investigation into polonium contamination was required due to results found in [3, 27], where polonium appears to adhere to the surfaces of the fibres. This effect has implications on the sensors operation, thus, methods or removal and prevention required investigation.

In contrast to the previous sensor, this sensor utilises a geometry that maximises dose deposition from alpha particles. This is achieved by minimising the attenuation of alpha particles utilising fibre cladding with a thickness that is less than the path length of alpha particles in these materials (largest path length considered here is 40 μm). The thickness of the fibres is also kept minimal to reduce the contribution from beta particles.

3.2 Construction and Performance Testing

As previously noted, this device is the extension of the work by C.Whittaker [3] and the same materials and geometry were used but with an increase in the number of fibres to test scalability, along with a new batch of higher quality (lower loss) fibres. The number of fibres was increased from 1500 [3] to 2500. The construction of the detector is outlined in Section 3.2.1 and the performance testing in Section 3.2.2.

3.2.1 Construction

The fibres used are 10 cm long, 250 μm thick plastic scintillating fibres (BFC12, from St. Gobain). The fibres are brought close together like the hairs of a paint brush, they do not need to be separated as in the previous sensor given the ranges of alpha particles in liquids is short. The sensor (Figure 3.1) consists of 2500 fibres which is optical cemented into a 1 inch, SM1 threaded adaptor. This detector face is then polished until optically clear to prevent loss of signal when sent to a photomultiplier tube (PMT). The procedure for construction is described in Appendix A.

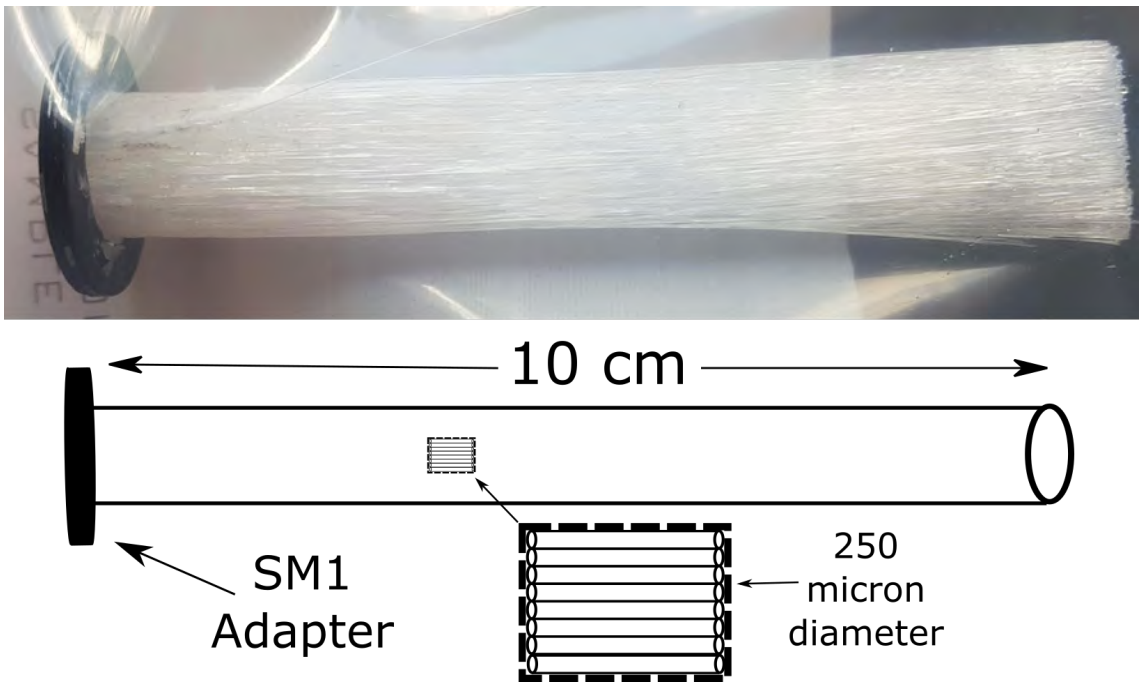

Figure 3.1: The completed sensor, 2500 BCF12 optical fibres from St. Gobain kept in place with EJ-500 optical cement. The detector face was constructed by polishing it flat until it was virtually free from flaws and optically clear, with each fibre terminating in a polished end face.

3.2.2 Performance Testing

The performance testing of these sensors is achieved using Po-210 solutions, as mentioned in Chapter 1. However, it was found in [3] that Po-210 adheres to the fibres causing a variable background signal between measurements, and causing the signal to rise with time. The removal of this contamination and prevention is critical for real-time operation and is explored later in this Chapter.

A duty cycle approach where the sensor background is measured in between measurements can be used to accurately test these sensors. However, as an alternative for this new sensor, a performance test in Ra-226 solutions was performed and compared to Po-210.

First, to show that Ra-226 does not adhere to these fibres, a sensor was placed in a 4 Bq/ml Ra-226 solution for 20 minutes. The result is shown in Figure 3.2.

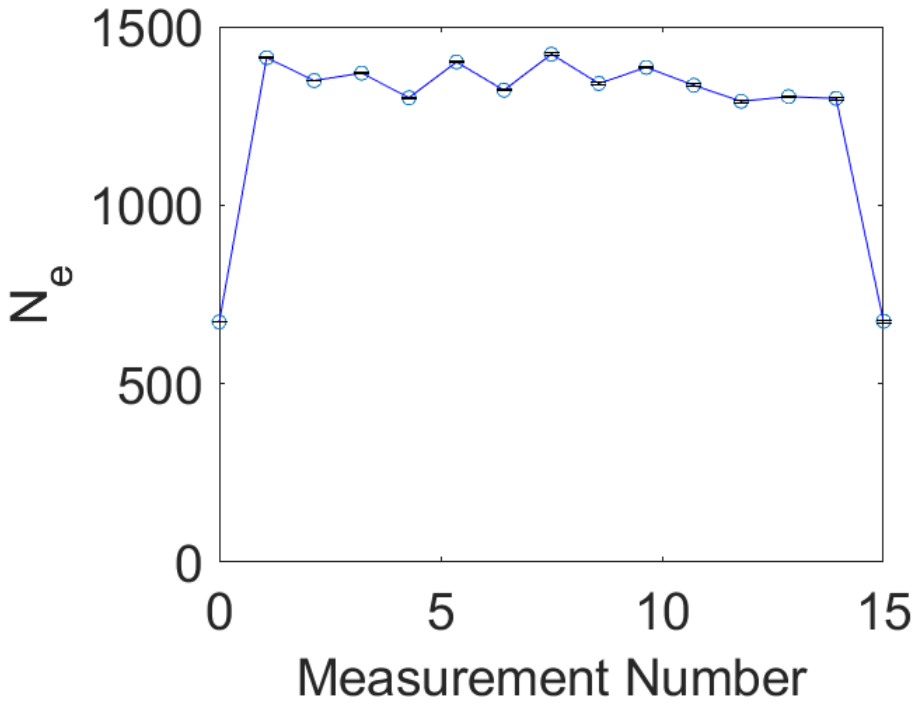

Figure 3.2: A continuous measurement of a 4 Bq/ml, 0.3M HCl solution. The first and final points are measurements of a blank 0.3 M HCl solution. N_e is the number of scintillation events in 100 s.

A response curve for Ra-226 was generated by measuring solutions of different activity concentrations (Figure 3.3). Each solution is a dilution of an original concentrate, the concentrations were determined by gamma spectroscopy. The solution concentrations can be found in Table 3.1. The total volume for each solution is 40 ml.

Ra-226 Solution	Concentration (Bq/ml)
1	0.100±0.00327
2	0.811±0.0267
3	1.5047±0.0493
4	3.0517±0.0996
5	4.615±0.1505
6	6.228±0.2027

Table 3.1: Ra-226 solution activity concentrations determined by gamma spectroscopy.

The apparatus and data analysis used for this sensor was the same as for the sensor investigated in Chapter 2. However, the channel threshold is set to 400 instead of 300. This threshold is set to eliminate any contribution from beta particles and environmental sources, that lie in the lower energy portion of the PHS compared to the contribution from alpha particles. The solutions are also left for 23 days to ensure secular equilibrium. An attempt to eliminate Radon (Rn) and its daughters is made by aerating the sample before measurement. This was done in an attempt to reduce the number of interactions with these RNs and measure purely Ra-226. This process also reflects the real world situation of Rn escaping from solution. However, this sample still contained a small concentration of Pb-210 due to it's age and, unfortunately, could not be removed as this would require a lengthy chemical separation. If this was achieved, returning to secular equilibrium is required for determining the solution's activity concentration and, therefore, the Pb-210 would still be present. This situation can only be resolved by using an alpha particle emitter that does not decay into a beta particle emitter, like Po-210 which will not allow for ease of measurement as we require. Thus, Ra-226 was still the preferred alpha particle emitter for this performance testing.

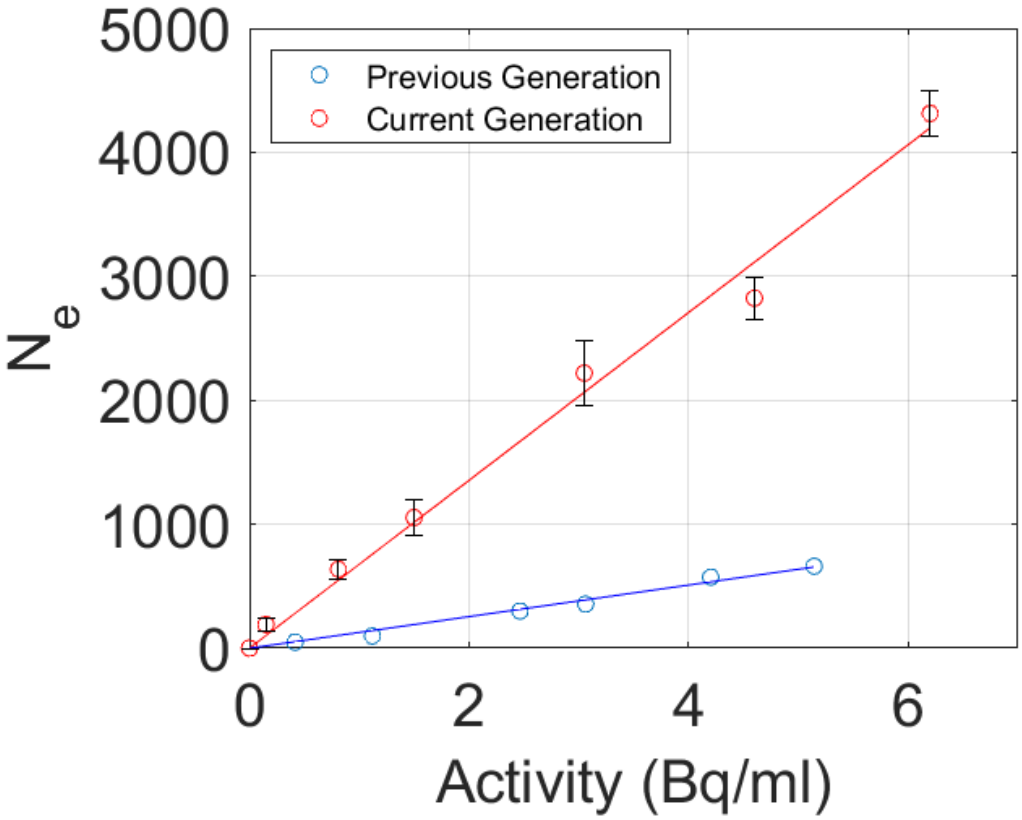

Figure 3.3: The performance of this sensor in liquids containing Ra-226 (red) compared to the response of the previous sensor to liquids containing Po-210 (blue). N_e is the number of scintillation events in 100 s, background subtracted. The uncertainty values here reflect the reproducibility of each signal and are determined in the same way as in Chapter 2.

The performance of this sensor in Ra-226 is shown in Figure 3.3. Also shown is the response of the previous generation of sensor to increasing activity concentrations of Po-210. The energy of alpha particles emitted from Ra-226 is lower than those emitted from Po-210 so the difference in sensitivity may actually be larger and not directly quantifiable. However, the response remains linear and the sensitivity limit has been pushed beyond 0.15 Bq/ml.

3.3 Mixed Radionuclide Measurements

This sensor was also tested in the same mineral processing leach solution as used in measurements reported in Chapter 2. However, the alpha emitter concentrations are now relevant. The contributions from beta emissions are accounted for using the appropriate threshold in the PHS as mentioned previously.

The leach solution measured here was a 3 M HCl solution containing 0.5 Bq/ml

(Po-210) of alpha emitting RNs. The alpha emitters within each solution are listed in Table 3.2. The response of the sensor to the solution is shown in Figure 3.4.

Isotope	Average Energy (MeV)	Branching Ratio (%)	Max Range in H_2O (μm)*
Po-210	5.304	100	40
Ra-226	4.784	94.45	35

Table 3.2: RN decay information for the alpha emitters found in these solutions. *Range for the average energy is found from the NIST astar database [1].

The energy dependence seen here is consistent with the measurements of these solutions reported in Chapter 2. The Ra-226 alpha particle has a shorter range than the Po-210 alpha particle so the measurement of the leach solution should lie above the Ra-226 response curve (Figure 3.5). The large difference observed here is also possibly caused by the presence of the beta emitting RNs in this solution (Pb-210) which was twice as concentrated as for the Ra-226 solution of a similar activity concentration. The diameter of this sensor would allow for the beta emissions to deposit the majority of their energy, accentuating the signal response. This issue can be resolved by performing differential measurements with a replica sensor that discriminates alpha particles (thicker cladding) or simply calibrating the response of this sensor in standard samples of this solution at different activity concentrations.

3.4 Polonium Contamination

In this Section the removal and prevention of polonium contamination from three types of fibres is explored. In Section 3.4.1 chemical treatments to remove the contamination after measurements is explored. A method of preventing the contamination whilst in solution is explored in Section 3.4.2.

3.4.1 Contamination Removal

An effective method for removing chemical contamination from surfaces is to use surfactants. A common chemical treatment for radionuclide laboratories is DECON 90. The information given from the manufacturer (DECON Laboratories) states "DECON 90 is a complex emulsion of highest quality anionic and non-ionic surface active agents, stabilising agents, alkalis, non-phosphate detergent builders and sequestering agents, in an aqueous base". Here DECON 90 was tested for its effectiveness to remove the polonium contamination on single fibres, to increase the longevity of the alpha sensors and to remove the build up of polonium between measurements throughout the duty cycle process.

In order to explore the active ingredient/chemical in DECON 90 that removes polonium specifically (in this case a positive ion) multiple surfactants and chelators were

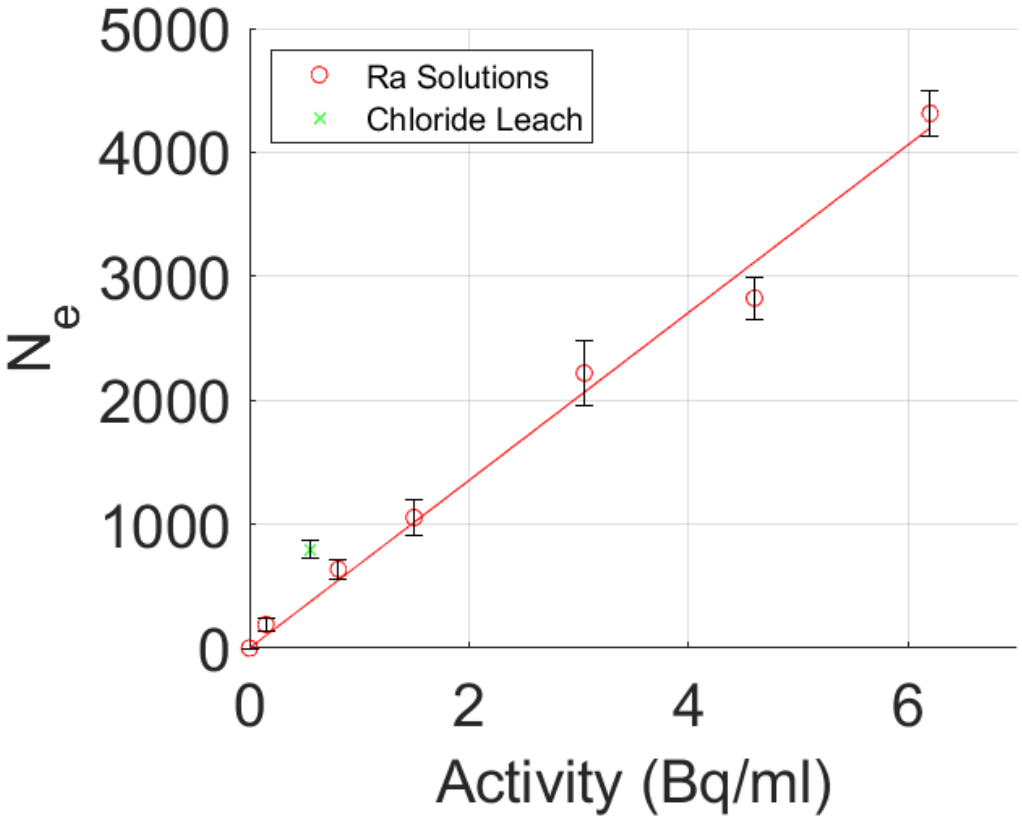

Figure 3.4: Comparison between the Ra-226 calibration (red), a measurement in the chloride leach solution (green). N_e is the number of scintillation events in 100 s, background subtracted. The uncertainty values here reflect the reproducibility of each signal and are determined in the same way as in Chapter 2.

tested in the same way. If these chemicals perform similarly or better than the DE-CON 90 treatment this could save cost to the end user, and also potentially help identify the oxidation or bound state of polonium within these mineral processing solutions.

Experiment

The equipment used in this experiment is shown in Figure 3.6. A clamp-on fibre jacket holding a short sample of fibre (44 mm in length) was held at an adjustable height above a magnetic stirrer. The horizontal post that held the fibre jacket could slide down the vertical post such that the fibre could be easily lowered into and removed from a vial containing a liquid sample. A "stopper" was fixed on the vertical post to ensure the same length of fibre is exposed to the solution each time it is lowered.

Multiple samples of the same total volume but with different concentrations of each chemical treatment listed in Table 3.3 were prepared along with concentrated Po-

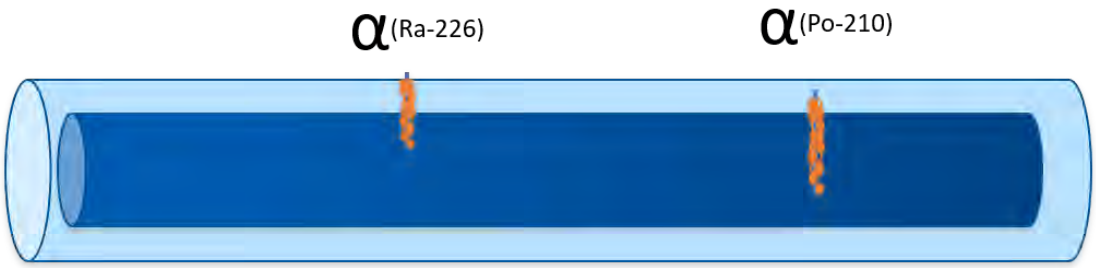

Figure 3.5: Visualisation of each alpha particle emitting RNs relative range showing the likelihood of interaction with the core of the optical fibre.

210/HCl solutions (≈10 Bq/ml). The efficiency of Po-210 removal of each of these chemicals was tested by comparing the amount of Po-210 on the fibre sample before and after treatment.

Name	Type
Cetrimonium bromide (CTAB)	cationic (+ve) surfactant
Sodium hydroxide (NaOH)	inorganic compound
Ethylenediaminetetraacetic acid (EDTA)	chelator (complexes with metal ions)
DECON 90	Complex Mixture

Table 3.3: Name and type of chemicals used to attempt Po-210 removal from fibre surfaces.

The treatment proceeded as follows,

- First the fibre is lowered into a Po-210 solution for 15 minutes, with agitation. This allows Po-210 to adhere to the surface of the fibre.
- After 15 minutes, the fibre is removed and rinsed in DI water.
- The fibre is then lowered into a chemical sample for 1 minute, with agitation.
- The fibre sample is then rinsed with DI water again and allowed to dry.

This process is repeated for each concentration of each chemical. For comparison, a fibre sample undergoes this process but without a chemical treatment. The relative surface activity of the fibres were then measured using an alpha counter (Daybreak 582).

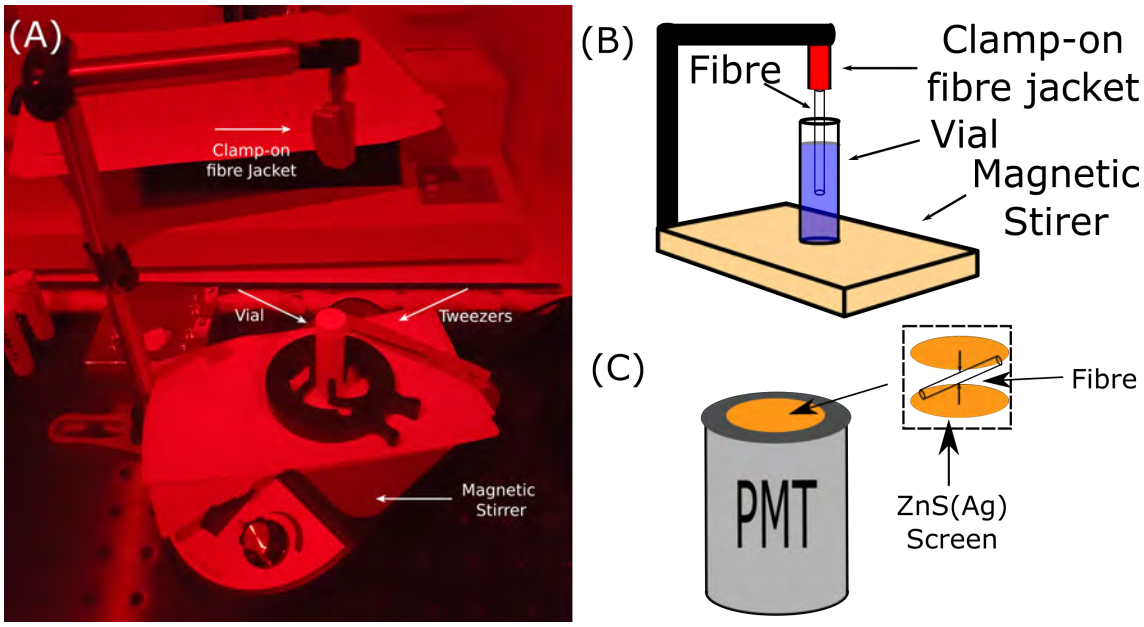

Figure 3.6: (A) The experimental set up for the contamination removal experiments. The clamp-on fibre jacket was used to hold each fibre at the same height for each exposure. Plastic tweezers are used to remove the fibre after the exposure without removing polonium. The magnetic stirrer was used to assist with diffusion of polonium onto the surface of the fibre. (B) Schematic drawing for the contamination removal experiments. (C) Schematic drawing for the alpha counter used for determining the surface activity of the fibres. Each fibre was wedged between two ZnS(Ag) screens and placed on a calibrated PMT that thresholds any contributions from non-alpha particle interactions with a ZnS(Ag) screen. The counting electronics determines the number of events that occur.

Results

The following Figures show the results of a pretreatment of these chemicals to different types of fibres. DECON 90 removed the greatest proportion of polonium from the surface of the each type of fibre, polymer, fluorinated acrylate coated and silica. Other types of fibres were tested to find possible candidates for future sensor designs. The amount of polonium on the surface of the fibre gives units of Bq/mm^2. This unit is used to directly compare the removal efficiency for different sized fibres. The uncertainties stated in Figures 3.7, 3.8 and 3.9 reflect the standard error from Poisson counting for each fibre surface area.

The results show that a DECON 90 treatment performed far better than any other chemical treatment for the removal of Po-210 from each type of fibre. The use of NaOH on polymer and silca fibres appears to show feasibility. CTAB and EDTA appear to have an effect but to a far less extent than DECON 90. These results

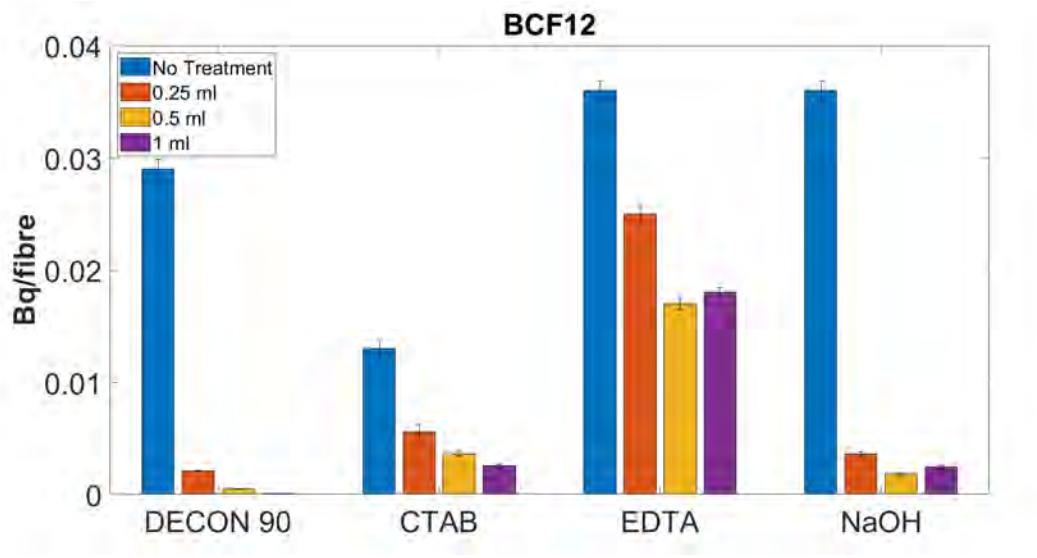

Figure 3.7: Removal of Po-210 from the surface for polymer (BCF12) fibres using different concentrations of (A) DECON 90, (B) CTAB, (C) EDTA and (D) NaOH. The value represents the amount of each chemical used in the 5 ml solution. A ratio of 4:1 of DECON 90 removed all of the polonium contamination.

make speculation on the active ingredient in DECON 90 that removes polonium specifically impossible. It is more likely that it is the balance of this mixture that makes DECON 90 so effective.

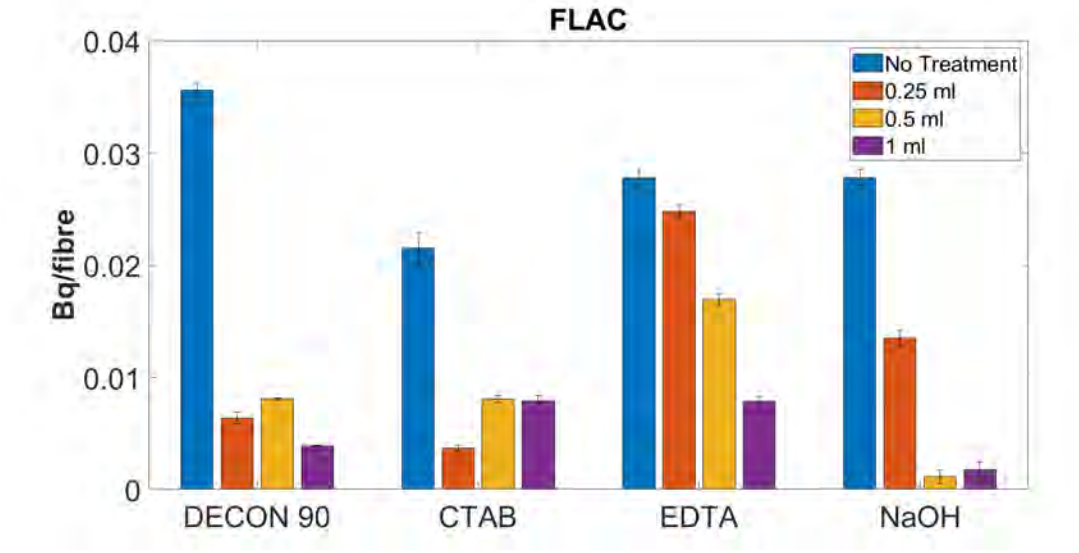

Figure 3.8: Removal of Po-210 from the surface of fluorinated acrylate (FLAC) coated fibres using different concentrations of (A) DECON 90, (B) CTAB, (C) EDTA and (D) NaOH. None of the amounts used showed full removal of the contamination.

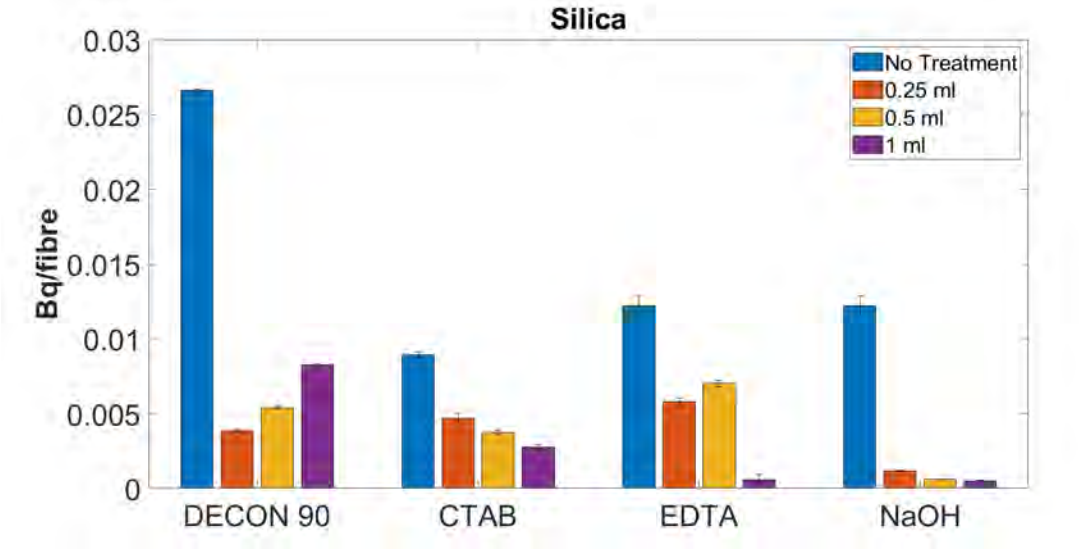

Figure 3.9: Removal of Po-210 from the surface for silica fibres using different concentrations of (A) DECON 90, (B) CTAB, (C) EDTA and (D) NaOH. The amount of contamination appeared to increase with some fibres. This effect could be the result of the large surface area of these fibres that decreases the detector efficiency, generating larger uncertainties.

3.4.2 Contamination Prevention

The removal of Po-210 contamination by DECON 90 will improve the operational life of these sensors. However, active contamination prevention of the fibre surface would allow a real-time sensing solution and will avoid the added complication of

a duty cycle operation. A possible mechanism is to saturate the sensor with Po-209 before entering solutions containing Po-210. As these isotopes act the same chemically in solution (hence the use of Po-2109 as a "spike" for quantification in alpha spectroscopy), it's possible this isotope of polonium will prevent Po-210 adhesion. Therefore, an experiment similar to Section 3.4.1 was performed with a pretreatment of Po-209.

Experiment

The experimental set up for this experiment is the same as in Section 3.4.1. Solutions of 1 Bq/ml of each Po-209 and Po-210 were made, these concentrations were limited by the availability of Po-209. The active prevention of contamination is tested with BCF12 fibres in the following situations,

Fibre 1

- Exposed to Po-209.
- Then allowed to dry.

Fibre 2:

- Exposed to Po-209.
- Then allowed to dry.
- Then exposed to Po-210.
- Then allowed to dry.

Fibre 3:

- Exposed to Po-209.
- Then immediately exposed to Po-210.
- Then allowed to dry.

Fibre 4:

- Used to test for any diffusion back into solution, it was exposed to Po-210.
- Then immediately into a HCl solution.
- Then allowed to dry.

Each exposure was 45 minutes long and the surface activities were measured using the Daybreak alpha counter.

Results

The result of each exposure is shown in Figure 3.10. The second bar indicates that allowing the Po-209 to dry before the Po-210 exposure provides no active contamination prevention. However, the third column indicates that the immediate exposure to Po-210 without drying the Po-209 allows for active contamination prevention. The final column, indicates that Po-210 will diffuse back into solution.

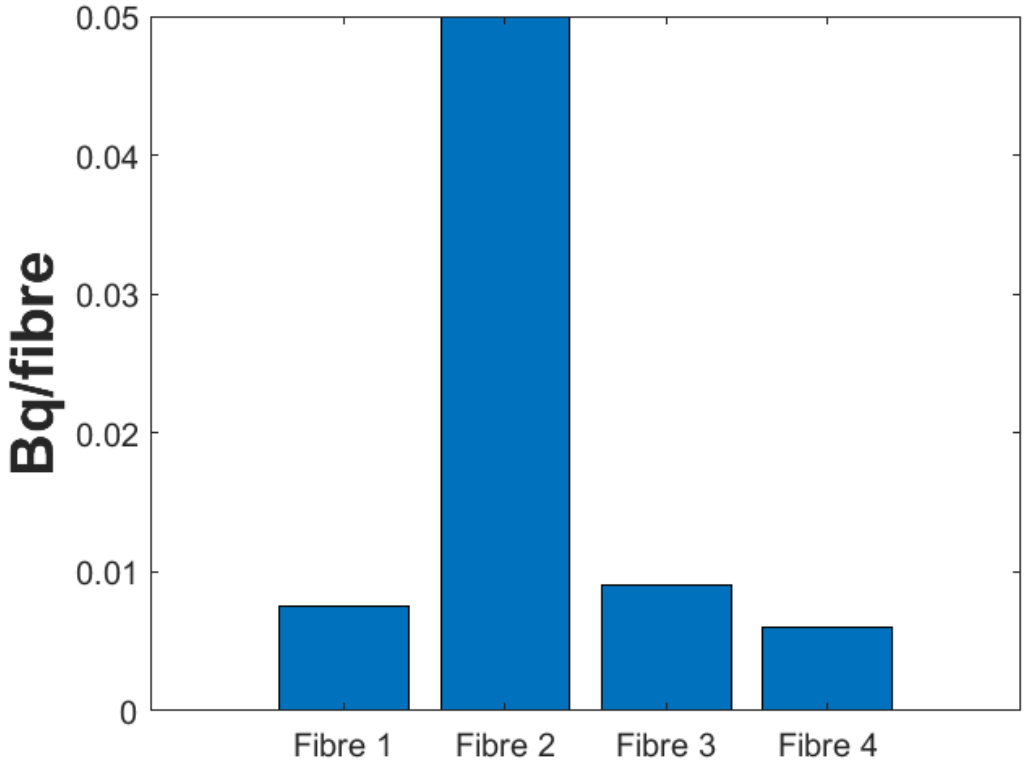

Figure 3.10: Results of the active contamination prevention testing. All values are found by measurements with an alpha counter.

The prevention of Po-210 adhesion due to the presence of Po-209 has implications for how polonium adheres to these surfaces. It was found in [56] that the amount of Po-210 that can be deposited onto a silver disk is 2.95 millicuries/cm^2 or 110 MBq/cm^2 in a monoatomic layer. So, if the polymer (BCF12) fibre behaves similarly, with a surface area of 0.35 cm^2 it can "hold" almost 40 MBq of Po-210. However, it should be noted, the alpha particle sensor has been seen to "saturate" at much lower concentrations of Po-210, indicating that Po-210 only bonds to specific defects or sites on the polymer surface, rather than in a monoatomic layer. These results indicate that not only does both species of polonium behave similarly in solution. Therefore, this suggests that pre-exposure to Po-209 fills the sites that would allow Polonium adhesion thereby preventing build up of Po-210. The prevention of contamination

with a Po-209 pretreatment is then feasible but requires further examination.

A more extensive research effort should be undertaken at higher polonium concentrations, with fully constructed sensors and measurements of each solutions polonium concentration before and after each exposure, using alpha spectroscopy to reduce uncertainty. This would indicate on-site usability and provide greater accuracy and quantification of this pretreatment method.

3.5 Summary

In this chapter the construction and testing of a new generation of these sensors has been achieved. It was found that increasing the number of fibres resulted in an increase in the sensors response. The sensitivity limit for these sensors was lowered by the improvements reported here from 0.4 Bq/ml to 0.15 Bq/ml. The sensitivity of these devices can be improved further by employing the findings of the investigation in Chapter 4

The removal of Po-210 contamination was achieved using a DECON 90 treatment and active contamination prevention was shown to be feasible using a Po-209 pretreatment.

Chapter 4

Polymer Fibre Background Investigation

4.1 Introduction

During the performance testing of the beta sensor, a background signal was noticed beyond the set channel threshold in the PHS (300+). Although this sensor has already surpassed the sensitivity requirements of mineral processing, this background signal will restrict the sensitivity of this detector for environmental RN monitoring applications, such as municipal water sources.

This chapter outlines an investigation into the source of this background signal. Possible sources were:

- **KCl contamination:** The background signal lies in the same region as the signals from K-40 found in Chapter 2. So the contamination of the sensor by trace amounts of KCl was possible. We investigated this source by performing measurements before and after cleaning the sensor with DECON 90. A oscilloscope was used here to confirm this signal is produced by scintillation events.
- **Environmental Background Radiation:** Interactions with environmental gamma rays were found to be a major contributor to the background signal. We investigated this source by suppressing the gamma rays with extensive lead shielding. This shielding completely encompassed the detector during measurements. This shielding was then employed for each of the following tests.
- **Photomultiplier Noise:** Any contribution from additional noise from the PMT was investigated by taking measurements without the sensor present, both with and without the photocathode exposed.
- **Natural Polymers:** Individual measurements of the optical cement and the polymer fibres were taken to confirm the background signal is physically produced/located within the fibres. This observation lead to an investigation of the precursor used to create these fibres, to rule out the possibility that they contain natural sources.

- **Muons:** The final possible source for this background signal was muons. Calculations of the expected event rate from muons and measurements with a purpose built muon detector are compared to the background signal from the beta sensor.

4.2 KCl Contamination

A simple test to gain insight into this background signal was to clean the detector after measurements in KCl. This ensured no residual KCl was causing scintillation in the fibres when removed from solution.

The detector was cleaned for an hour in a solution of DECON 90. A measurement was taken before and after the cleaning procedure with a oscilloscope. This approach was taken to ensure the events were scintillation events rather than a RF noise source. The signal from the PMT was sent directly to the oscilloscope, which was visualised on a nearby laptop (Figure 4.1). Figure 4.2 shows the comparison between each measurement.

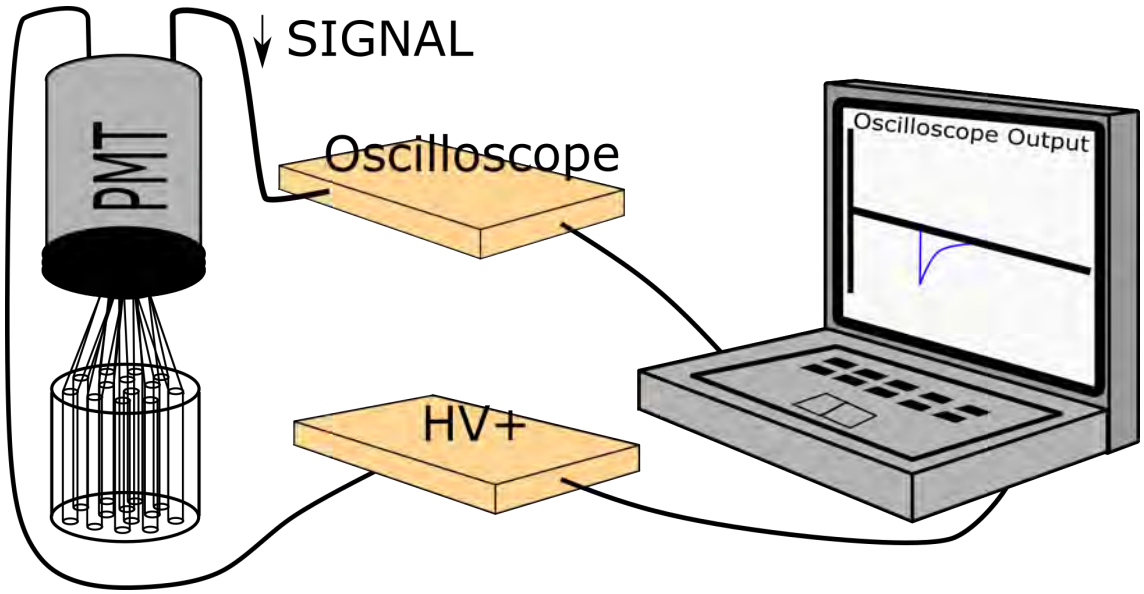

Figure 4.1: Schematic diagram of the experimental arrangement for these measurements. The signal from the PMT was sent directly to the oscilloscope for viewing on a nearby laptop. The high voltage (HV+) was supplied by a 1200 V source.

The number of events in each measurement are the same (within error). Therefore, no change is observed after cleaning the sensor and there is negligible KCl residue. The pulse shapes and rise times also remained the same confirming this background is caused by scintillation-producing events.

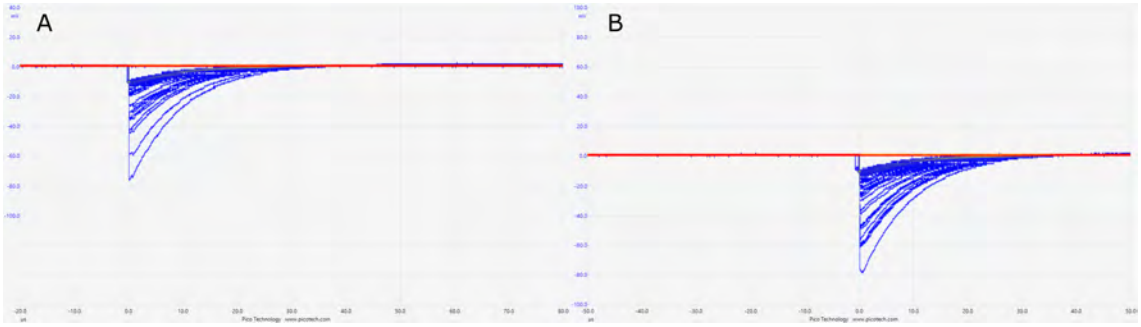

Figure 4.2: Pulse shapes (A) before (40 counts) and (B) after a DECON 90 rinse (38 counts).

4.3 Background Radiation

Another possibility for this signal was interactions with environmental background radiation whose signal lies beyond the set channel threshold in the PHS. Low radioactivity lead is commonly used to attenuate the effects of environmental gamma rays [57, 58]. So a 20 cm thick, lead shielding was sourced to completely encompass the detector. This shielding was formed with an iron drum that was filled with low radioactivity lead shot, forming lead shielding that is effectively 20cm thick.

First, the attenuation of the environmental background radiation by this shielding was measured using a Sodium Iodide (NaI) detector. To show the effect of this shielding, a comparison between measurements inside and outside the shielding was made (Figure 4.3).

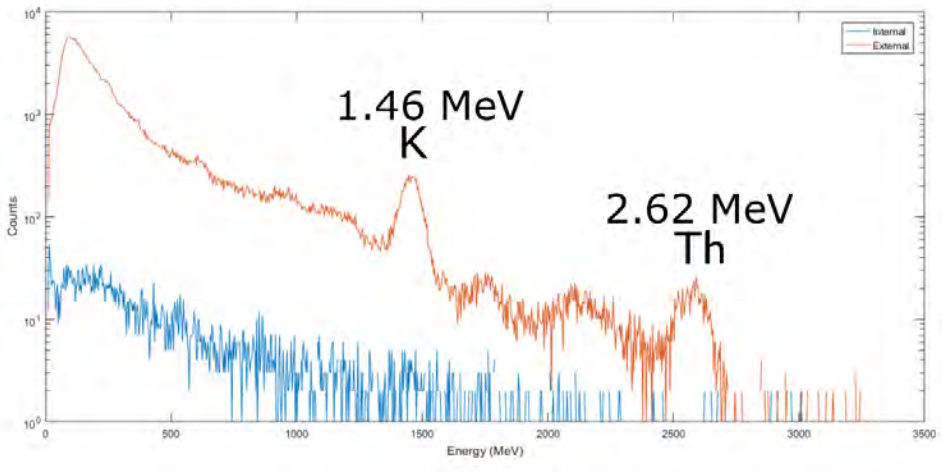

Figure 4.3: A 20 minute measurement of the environmental background signal inside and outside the lead shielding, determined with a NaI detector. The potassium-40 (K) and thallium-208 (Tl) peaks are denoted.

We see the gamma ray signal from natural sources is almost completely suppressed inside this shielding including the Tl-208 peak at 2.62 MeV [59].

Measurements with the beta sensor were taken both inside and outside the lead shielding. The spectra was also shown in Figure 4.4 and the total number of events in 100 s for channels 300+ is shown in the embedded figure. This channel threshold is set as the noise variation (fluctuating SEP) between measurements is independent of the noise beyond this point. It was expected that the background noise would be completely suppressed. However, counts were still seen beyond the channel threshold (300+).

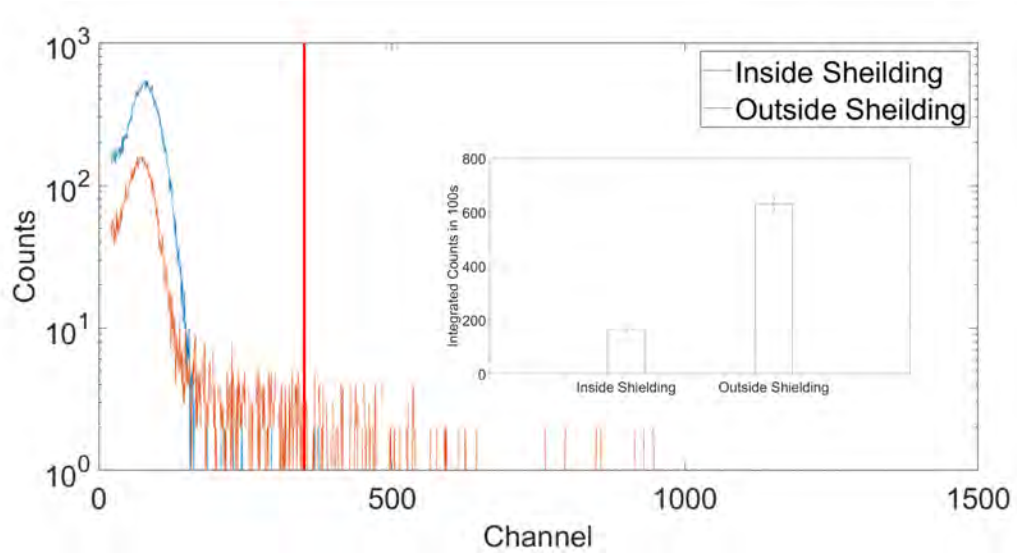

Figure 4.4: Spectra for two measurements comparing the response of the beta particle sensor inside and outside of the lead shielding. The channel threshold is set to 300, denoted by the red line. This threshold is set to mitigate the fluctuating SEP. N_e = number of events. Embedded: Total integrated counts inside and outside of the lead shielding beyond the channel threshold.

This result shows the majority of the background signal is removed by the addition of lead shielding, but a component is not a consequence of interactions with environmental background radiation. However, with the addition of shielding the signal-to-noise ratio is improved suggesting the need for lead shielding for applications requiring greater sensitivity.

4.4 Photomultiplier Noise

The background noise from the PMT was assumed to lie in the first two peaks in each of the spectra (PHS) shown. The first peak is caused by electrical noise and the second is caused by the photocathode dark noise [3] and contributions from low energy environmental radiation. To ensure this background signal is not sourced from

the PMT, measurements with the PMT cap on and off were taken (Figure 4.5). This situation reflects the photocathode exposure whilst taking a measurement.

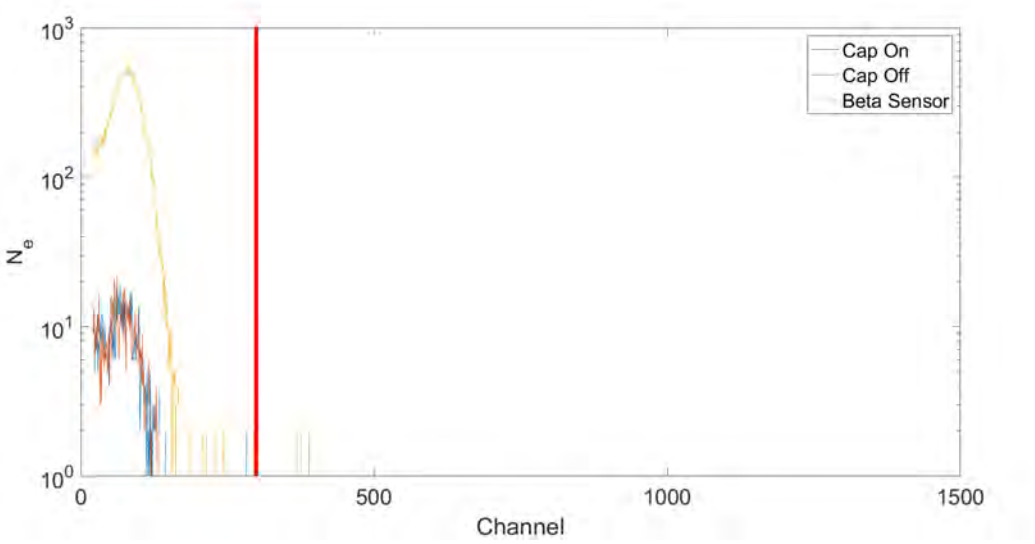

Figure 4.5: Spectra of measurements taken inside the lead shielding from the photocathode unexposed, exposed and the beta sensor. This result shows the background signal is not sourced from the PMT. The channel threshold is set to 300 denoted by the red line. N_e = number of events.

The spectra in Figure 4.5 show the background signal is not due to additional noise from the PMT beyond the channel threshold. The amount of events present is less than 20% of the total number of events seen with the beta particle sensor. This indicated the background signal was being produced within the sensor itself.

4.5 Natural Polymers

Another possibility requiring investigation was that of an internal source of these scintillation events within this sensor. Individual measurements of the separate components that construct the sensor were tested. The same amount of fibres from the same spool used to construct the sensor were bundled together without resin. The optical cement (resin) was also tested by filling a spare SM1 threaded ring with the resin, approximately the same amount used when constructing the sensor. Measurements of each were taken inside the lead shielding and compared to the measurement of the sensor (Figure 4.6).

The total counts reflect that the fibres themselves are the cause of this background signal since the total counts for the resin without fibres present is similar to the previous experiment with no observable scintillation events present. This signal is possibly some form of scintillation produced within the fibres from an unknown

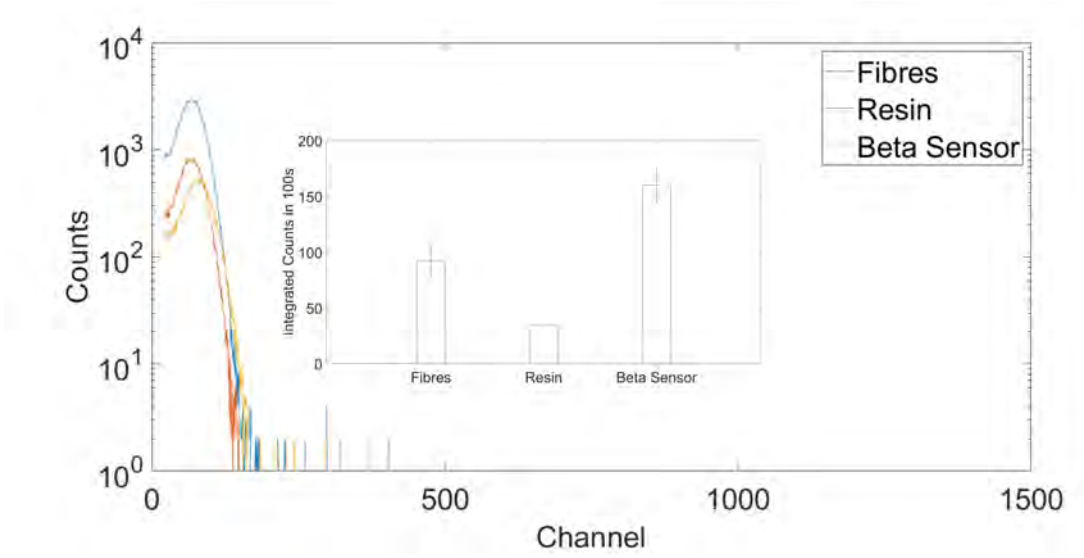

Figure 4.6: Total background counts for 100 s measurements using the fibres, resin and beta sensor. Spectra are shown for the fibres, resin and then beta particle sensor. Embedded: Total integrated counts in each measurement. This result indicates that the spurious signal is from the fibres and not the resin. The difference in counts for the fibre measurement and the sensor can be attributed to the unpolished ends of the fibres. The channel threshold is set to 300, as with all other measurements with this sensor indicated by the red line. N_e = number of events.

source, however, the total count is far less than the sensor. This effect is due to the loss in efficiency from the unpolished fibre ends scattering light.

This result is further supported by the spectra of each measurement found in Figure 4.6. The background of the resin appears to mimic the previous test and the spectra of the fibres lies within the region of the sensor, increasing the likelihood that the fibres are the source of this background signal. The scintillation events that make up this background signal have been shown to originate within the sensor itself.

A possible source is the presence of Carbon-14 (C-14) within the polymer fibres if they were manufactured with natural (non-fossil carbon, contains C-14) rather than synthetic (contain fossil carbon, does not contain C-14) polymers. Natural polymers are sourced from the environment, therefore, they contain C-14. This isotope of carbon is a beta particle emitter and forms the basis of radiocarbon dating [60]. Synthetic polymers are synthesised from petroleum oil [61] and contain 'dead' carbon (stable isotopes of carbon) since it is much older than the C-14 half-life.

A calculation of the expected event rate from the amount of C-14 that could be present was undertaken to determine the validity of C-14 as a source of this signal. First the expected amount of C-14 within the beta sensor was calculated. The commercial provider of the fibres quotes a carbon atom density of 4.85×10^{22}

atoms/cm^3.Using this value and the natural abundance of C-14 is 10^{-12} (ppt) [62] we can find the atom density of C-14 to be 4.85×10^{10} atoms/cm^3. A density can be found by using the number of C-14 atoms per gram (3.3×10^{10}). This results in a value of 1.47 g/cm^3. With the total volume of the sensor being 28.5 cm^3 a total expected mass of 41.86 g can be found for C-14. Given the specific activity of C-14 is 13.56 (decays/min)/(gram Carbon) [62], the expected event rate from the presence of C-14 is 10 Bq/s. This value is higher than the background signal seen, however, with low collection efficiencies and other losses present in this system this possibility warranted further investigation.

To determine if the fibres actually contained C-14 at anything like these activity levels, a sample was sent to an off-site carbon dating lab (Beta Analytic Inc, North Sydney, NSW, Australia). No Carbon-14 was found, therefore, the background signal cannot be explained by C-14 contamination of the polymer used: this indicated an external source for this background signal.

4.6 Muon Interactions

Another possibility for this background signal is identified from consideration of the data presented in Figure 4.3. The background signal appears at low count rates in the higher energy channels, which indicates a likely source is muons. Therefore the possibility of muon interactions is investigated in this Section.

Muons are produced after the interaction of a high energy primary particle (proton) with a nucleus within the upper atmosphere. This interaction produces a shower of short lived particles (pions). These particles will have their own interactions with the atmosphere producing muons that continue in a cascade towards the Earth's surface (sea level).

Muons are fundamental particles (leptons) with the same charge as an electron, but a much greater mass ($>$ 200 times). Muons decay, on average, after 2 μs [63,64] but posses high energies and travel at high speeds (relativistic) allowing them to easily reach and surpass sea level during this lifetime. Muons mainly interact by electromagnetic processes with matter, losing little energy via ionisation so are still quite energetic by the time they reach sea level ($\approx$GeV) and can typically travel through meters of rock or concrete [65].

The data in Figure 4.3 shows muons are not suppressed by the lead shielding. This is expected as the stopping power in lead is 1.122 MeVcm^2/g [65]. Therefore, muons will have plenty of energy to deposit into the beta article sensor.

The muon flux at sea level is 1/cm^2/minute [63] for an acceptance angle of 2π steradian. Using this value, the expected event rate from muons can be calculated

for a 100 s measurement, using the cross section of the sensor. The cross section of the beta sensor is 100 cm^2, therefore in 100 s we expect 167 muon events. This value falls within error of the background signal seen. Muons are then the likely source of this final component of the background signal.

Measurements with a purpose built muon detector further supports this calculation.

A purpose built muon detector was sourced, that was able to fit within the lead shielding. The operation of this sensor is similar to the ones developed in this document. A light-tight container houses a PMT that is optically coupled to a NaI scintillator. The signal from the PMT is interpreted by purpose built circuitry which thresholds any electrical noise and signals from background radiation (unlike the polymer fibre detector). Both PMT and scintillator are 120 mm in diameter and the scintillator is 100 mm thick.

To house the detector within the lead shielding, seen in Figure 4.7, it was necessary to lay the detector horizontally rather than its usual upright position: this allowed for the cross section of the detector to become more comparable to the cross section of the beta particle sensor.

The number of counts seen by this detector was 63 ± 9 in 100 s which is comparable to the number of counts seen from the beta sensor. The small difference can be explained by the difference in signal processing of each detector: the muon detectors pulse height threshold is set far higher than in the beta sensor, so any low energy events would be lost. This process is shown pictorially in Figure 4.8. Hence, any signals from a muon's trajectory that doesn't pass entirely through the scintillator (deposits a small amount of energy) will not be triggered by this threshold gate. Unlike the beta sensor, therefore is has a higher count rate due to lower thresholding. The muon flux is known to be a constant rate so this final component of the background signal could be more accurately determined with detectors of a larger cross section.

This experiment confirms that the likely cause of this background signal is the interaction of muons with this detector. This finding suggests this is a hard restriction on the scalability of these detectors, since increasing the size of the detectors will exacerbate this problem due to the increase in cross section, and cannot in practise be removed with effective shielding.

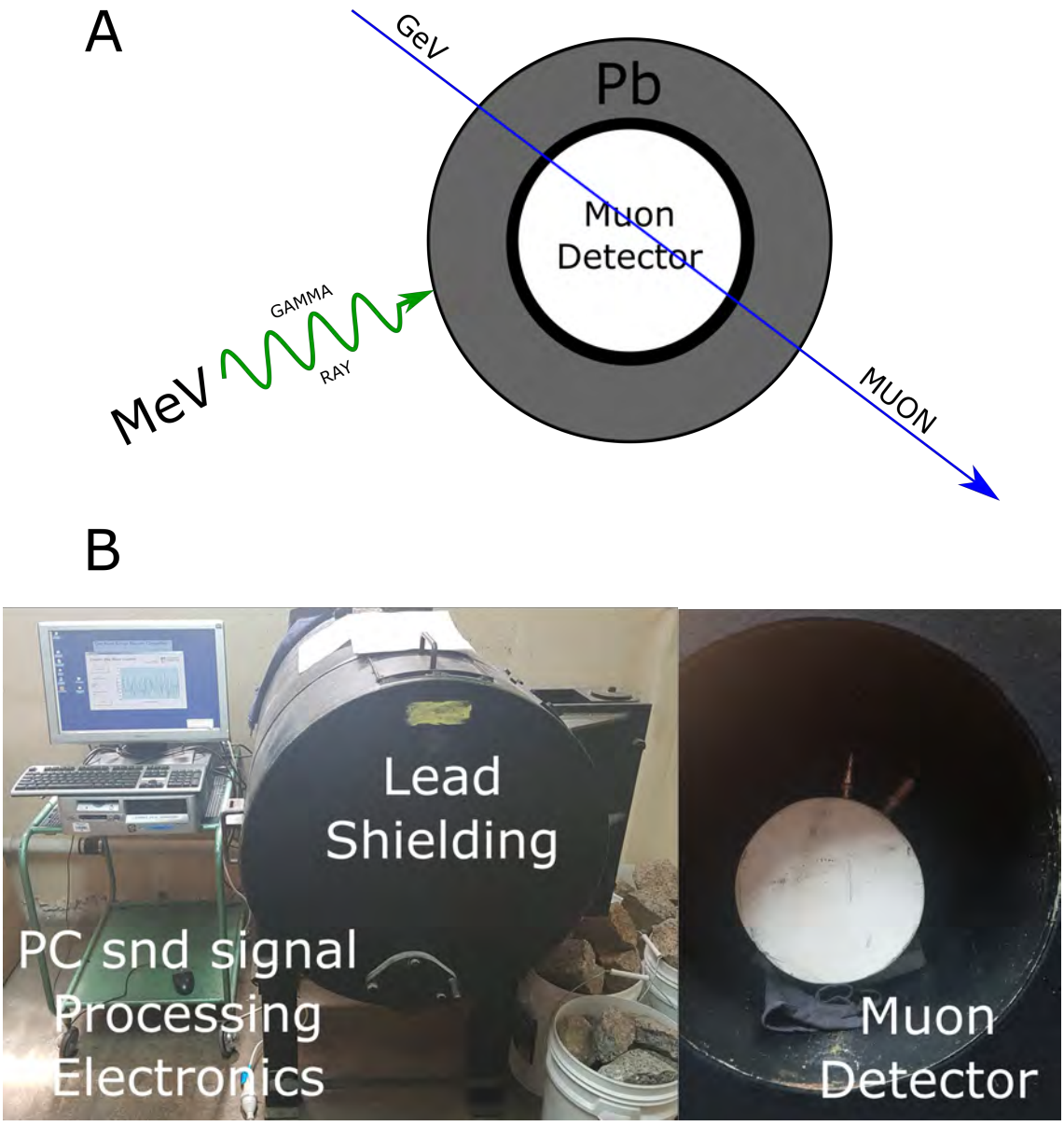

Figure 4.7: A: Schematic diagram of the functionality of the lead (Pb) shielding. Gamma rays are blocked but muons are not. B: Muon detector inside (right) and outside (left) the 20 cm thick shielding.

4.7 Implications for On-site Design

Due to the implications of the above trials, two additions to the sensor design must be made to maximise the sensitivity. The first being the addition of lead shielding. These sensors easily achieve the sensitivity required for in-line sensing during mineral processing so shielding isn't necessary. However, for applications demanding a higher sensitivity, like municipal water supply water monitoring, it is necessary to engulf the sensor in a similar lead shielding as used in Section 4.3. Openings into

this shielding could then form a flow cell where water is allowed to fill the cell, a measurement be taken, then the water is ejected, allowing near real-time measurements. However, the contribution from muons limits this operational sensitivity.

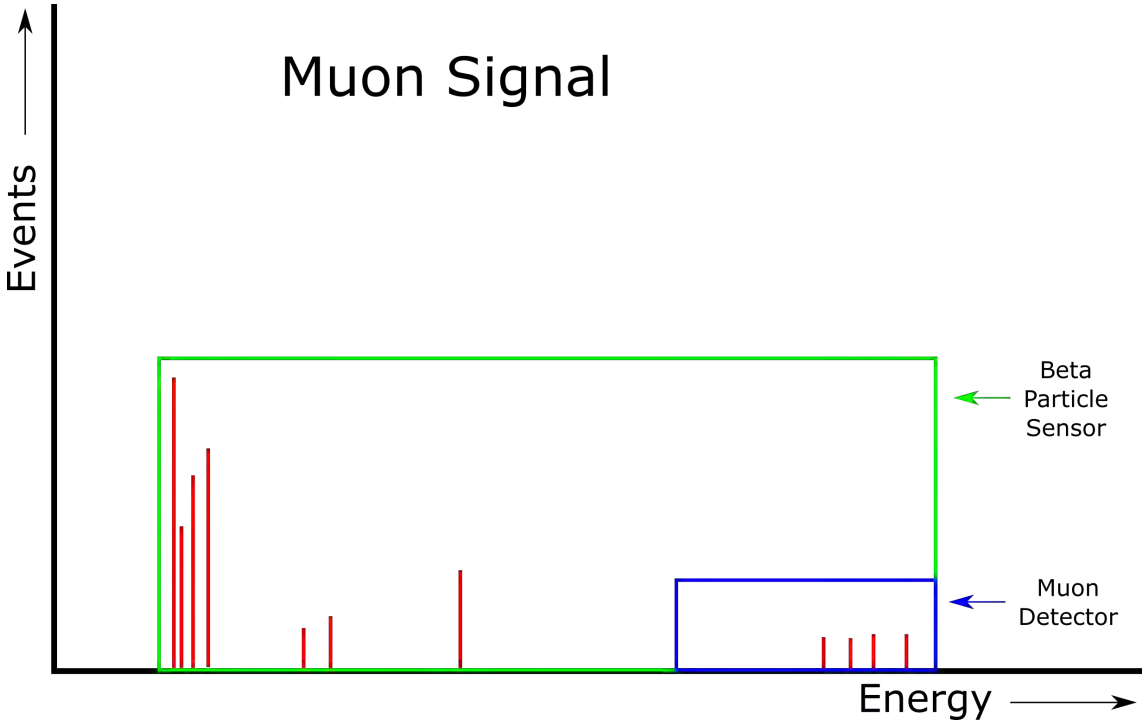

Figure 4.8: Pictorial demonstration of the difference in thresholding of each detector.

The second addition is accounting for the interactions with the muons. Once again this adjustment is not required for in-line sensing during mineral processing. However, for other applications this is crucial as this background is the fundamental limit for this device' s sensitivity. Since the muon signal cannot be effectively shielded this signal must be removed differentially by coincidence counting. This technique is readily employed for detecting muons [66], and takes advantage of the large distance traversed by muons. Using two detectors, it is assumed that any coincident events in both detectors indicates a muon interaction, enabling the muon background to be removed in real-time.

A feasible design for such a detection system would then be a cylindrical lead shield, similar to the one used in this Chapter, to remove contributions from environmental gamma radiation. To account for muon signals, a beta particle sensor can be surrounded by a hollow cylindrical scintillator. This geometry would ensure coincident detection of all incoming muons. The measurement procedure would then proceed as indicated earlier.

4.8 Summary

The expected beta particle sensor constructed for this project showed unexpectedly high background. The obvious avenues of investigation into the source of this background have been taken. This lead to the identification of two components that contribute to the background signal: gamma rays from environmental sources and muons from cosmic sources. It was found that with adequate shielding the contribution from gamma rays was suppressed. However, muons are not attenuated by this shielding forming the fundamental limit for the scalability for these devices. The implications for future designs are outlined, however, these are not necessary for the intended application in mineral processing.

Chapter 5

Polonium-Specific Sensor

5.1 Introduction

Monitoring of RNs such as Po-210 throughout different mineral processing stages is critical for improving product purity and in addition, assists in securing the safety of workers. As mentioned in Chapter 3, it is common for Po-210 for adhere to glasses and various plastics. This gave inspiration for a sensor utilising electrochemical processes to specifically sense Po-210 in mineral processing liquids by assisting adhesion to the detector face. The feasibility of such a sensor is explored in this Chapter.

5.2 Sensor Operation

The desired operation for this sensor is a duty cycle measurement, like the sensor in Chapter 3, but specifically for Po-210. This mode of operation enables the user to determine the Po-210 concentration in near real-time. The duty cycle will allow a differential measurement between (1) a measurement with Po-210 present and (2) a measurement without Po-210 present (background measurement). This operation could be greatly enhanced by effective polonium adhesion to a sensitive detector. In this case, a metal coated scintillating material placed at the photocathode of a PMT. The feasibility of this operation is explored in this Chapter.

The first step is to efficiently attract Po-210 specifically to the sensor, avoiding other RNs that would also stimulate a signal within the scintillator. A mechanism that achieves this is spontaneous deposition (auto-plating) which is the act of an ion in solution being reduced onto a metal surface. This should allow specific pickup of Po-210, however, the efficiency reduction due to the interference from contaminants present in solution (Iron (Fe), Copper (Cu) etc) may render this technique infeasible.

The intended sensor operation is depicted in Figure 5.1. The Po-210 is allowed to spontaneously deposit onto the coated scintillator. The alpha particles emitted will produce scintillation events (photons) to be detected by a PMT.

By keeping this metal layer thin (1-2 μm maximum), the alpha particles emitted

from Po-210 will deposit the majority of their energy into the scintillating material. However, not all of the alpha particles are emitted in the direction of the scintillator as these emissions are isotropic. The sensor would then require calibration in mineral processing liquid standards with different concentrations of Po-210 present.

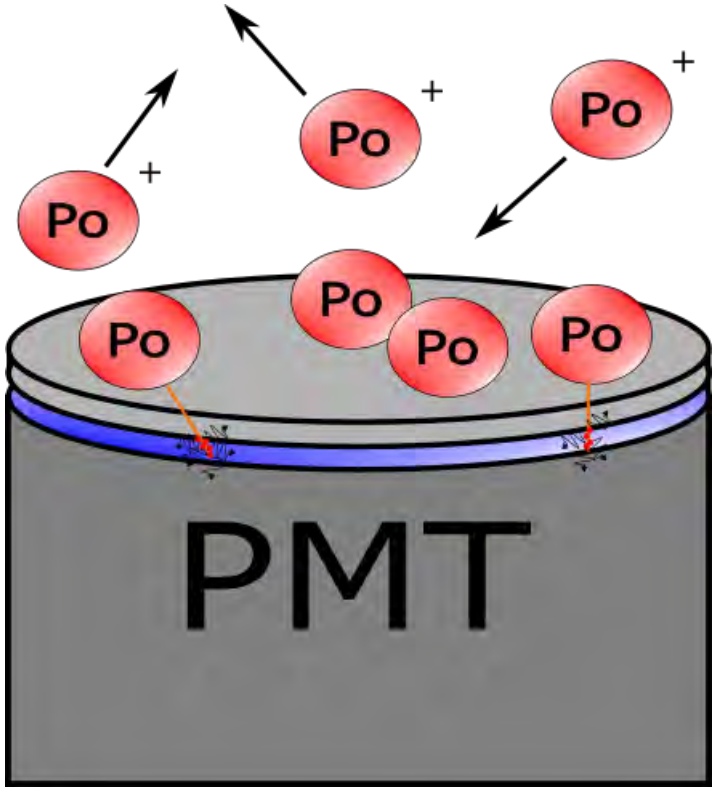

Figure 5.1: Operation of the polonium-specific sensor. A measurement at regular intervals should find the concentration of Po-210 in near real-time.

The first step in testing the feasibility of such a device is to determine an appropriate metal to be coated.

5.3 Transition Metals Selection

The chosen metal must withstand the conditions typical of mineral processing solutions and also efficiently plate Po-210 spontaneously. The conditions of mineral processing solutions are; 60°C, 150g/L (1.6 M) H_2SO_4 ($<$ pH $=$ 1) for 30 hours (according to the sponsor).

Obtainable metals were chosen based on their electrode potentials (directly related to their electronegativity) as this governs if polonium will deposit spontaneously to that metal. The electrode potential must be below polonium, $\approx$0.8 V for deposition. Metals that could be obtained that fit this criteria were; Copper (Cu), Silver

(Ag), Gold (Au), Nickel (Ni), Tungsten (W), Tantalum (Ta), Molybdenum (Mo), Tin (Sn), Brass and other alloys that contained Fe and Ni.

These metals resistance to mineral processing conditions are tested by the method outlined in Section 5.3.1, the results are presented and discussed in Section 5.3.2.

5.3.1 Method

For each selected metal a 1 cm^2 sample was cut. They were polished and cleaned with methanol to remove any contaminants. Au was not used as this metal is well known for being resistant to H_2SO_4 in these conditions. Samples of these metals were placed into test tubes filled with 1.6 H_2SO_4. These test tubes were submerged in a larger beaker containing water. One of these test tubes remained vacant for a thermometer to estimate the temperature in the other test tubes. The beaker can then be placed on a hotplate at 60°C for 30 hours. The results of the experiment were interpreted using an electron microscope.

5.3.2 Results

The results of this experiment are shown in Table 5.1. Each sample was analysed with an electron microscope (FE1 Quantum 450), located at Adelaide Microscopy, to look for signs of corrosion or other surface effects. After the 30 hour period some of these metals had definite signs of corrosion and the Ferrochrome (FeCr) sample completely dissolved. The metals that showed signs of corrosion were mostly the alloy metals, brass etc. The metals that withstood these conditions were: Cu, Ag, Au, Ni, W, Ta, and Mo.

Metal	Electrode Potential (V)	Condition
Cu	0.3402	Untarnished
Ag	0.7996	Untarnished
Ni	0.23	Untarnished
W	0.1	Untarnished
Ta	0.71	Untarnished
Mo	0	Untarnished
Sn	0.14	Corroded
Au	1.42	Not tested
Po	0.8	Not tested
Brass	-	Corroded
FeCr	-	Dissolved

Table 5.1: Results of the metals testing. Shown is the electrode potential and the condition of each metal after the test. An electrode potential of '-' is given for any alloy as this value can vary depending on its elemental make-up.

The results of this experiment showed that many of the metals in Table 5.1 can withstand the conditions provided by the sponsor. Electrodes (wires) of Cu, Ag, Au, Ni, W, Ta, and Mo were purchased for the next stage of this experiment. The metals of interest here are Cu, Ta, Ni and Ag as they all have an affinity for polonium deposition.

5.4 Spontaneous Deposition Experiments

The metals that can withstand mineral processing conditions were identified. The next step was to explore their affinity for Po-210 deposition. Spontaneous deposition (Chapter 1) is the act of reducing a metal ion from solution to metal surface. The efficiency of deposition for each metal was tested in a clean solution with only Po-210 present. This allowed the testing of Po-210 affinity specifically.

5.4.1 Preliminary experiment

This experiment had a dual purpose; familiarisation with spontaneous deposition and also identifying any obvious candidate metals. Factors that diminish the efficiency of the plating were identified. Changes made to reduce these effects are discussed and used in the next experiment.

Method

The apparatus used in this experiment is illustrated in Figure 5.2. A glass dish was used to house a test tube rack forming a hot water (60°C) bath. The rack held multiple test tubes filled with a preprepared 4.9 Bq/ml Po/H_2SO_4 (1.6 M) solution.

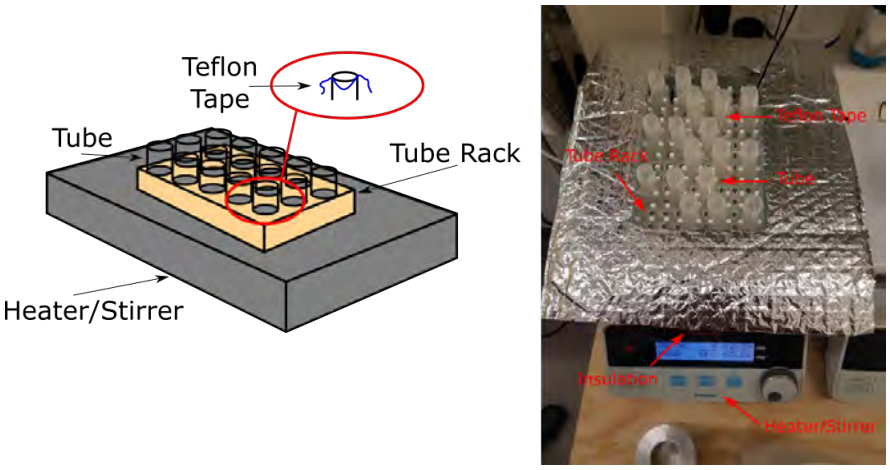

Figure 5.2: Apparatus for the spontaneous deposition experiment. A heater is used to keep a glass dish filled with water at 60°C. This dish is used to hold a test tube rack filled with each sample.

The solutions used in this experiment were dilutions from a Po/H_2SO_4 solution whose concentration was determined via alpha spectroscopy at ANSTO. A bulk dilution of 100 mL at a concentration of 4.9 Bq/ml was created from this solution. Each test tube for each test was then filled with 5 mL of this solution for plating.

Each test tube had two slits cut into each side of opening, to assist in draping Teflon tape across the opening of the tube. The bent wires can then be hung over this tape for ease of placement and removal from the tube. The tape was draped such that the entire piece of 44 mm wire was submerged in the solution to maintain the same total area was submerged for each metal wire. The tubes were labelled and placed into the test tube holder.

Once the solutions were warmed to 60°C the metals were placed in their individual test tubes and left for one hour. The placement and removal of the wires were conducted so that each wire was submerged for the same amount of time.

After the wires were removed they were rinsed with DI water and allowed to dry. Using ZnS(Ag) screens the amount of Po-210 on each wire was determined using alpha counters. This value was then compared to the amount of Po-210 removed from solution using alpha spectroscopy.

Results

The amount of Po-210 removed from a solution by each metal wire is shown in Figure 5.3. The expected result was for Ag, Ni and Cu to perform best according to [39]. However, this was found for solutions of HCl, at a different concentration of acid (pH) and using plates rather than wires.

The results showed W performed best, but was only more efficient than Ag and Ni by 5%. This result was promising as W would then be a cheaper alternative to Ag.

Another result of interest is the amount removed by Au. The high removal of Po-210 by Au was unexpected due to its position in the reactivity series. Po-210 ions should not be able to spontaneously absorb to the Au wire since Au is a more noble metal (higher electronegativity). However, this result could be due to impurities within the wire as often Ag and Cu are present along with Au.

The data for Cu is not shown here since the presence of an insulating coating that was not completely removed hindered the deposition of Po-210. This was avoided in the next experiment and showed better results. This result was not repeated as the next experiment was performed before the results of alpha spectroscopy were known.

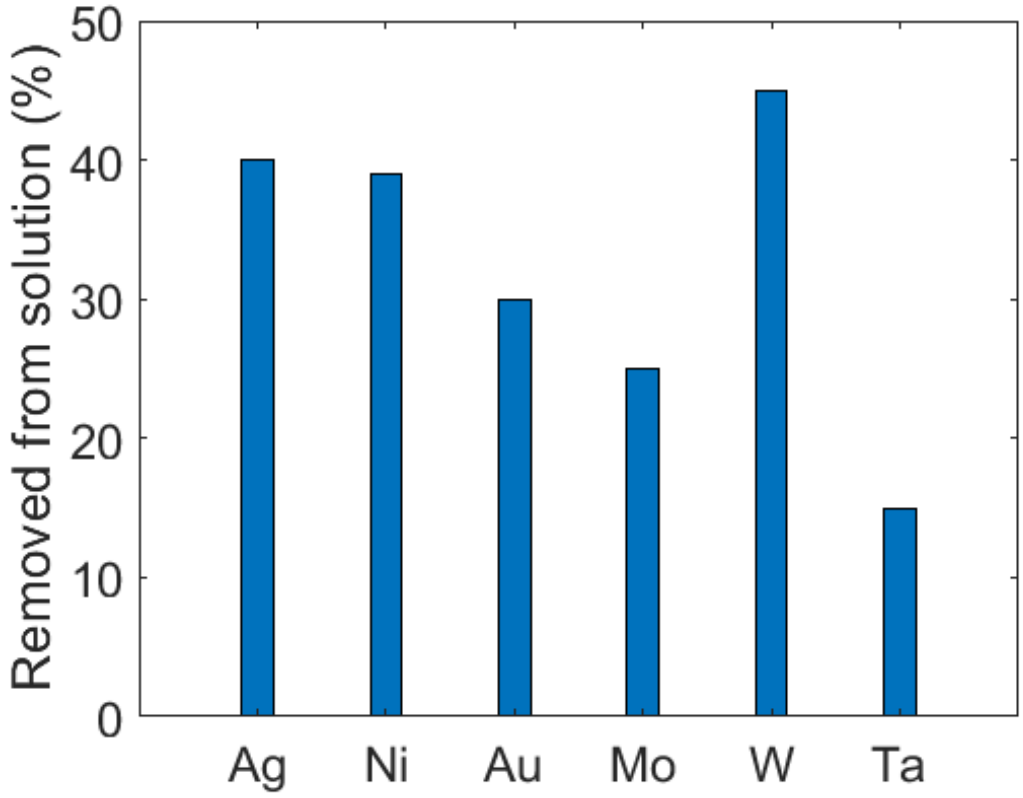

Figure 5.3: Results of the preliminary spontaneous deposition test. The amount of Po-210 removed (in percent) from a single solution.

Figure 5.4 shows the amount of Po-210 present on each wire determined by the alpha counter. The amount removed from solution should match the amount deposited onto the wires. This result indicates the values determined by the alpha counters were affected by the geometry of the metals tested. The literature indicates that to determine the true amount deposited onto a metal the geometry must be flat and smooth [47]. This requires plates of each metal of a known surface area and for those plates to be polished flat. The flat geometry will allow for less attenuation of the alpha particles and will ensure the majority of the particles will interact with the scintillating screen, giving a higher collection efficiency. Also, any coatings or films including layers of the oxidised metal (an important factor in the case of Ag) is removed with the inclusion of a polishing step. These factors are accounted for in the next experiment by using thin 1 cm^2 sheets of each metal (excluding Au) polished before entering the Po-210/H_2SO_4 solutions.

5.4.2 Spontaneous Deposition of Po-210 in H_2SO_4

The preliminary experiment showed that the plating of Po-210 in H_2SO_4 was quite inefficient due to its low solubility, agreeing with the literature [42, 45]. However, factors were identified that would improve the deposition of Po-210 including pol-

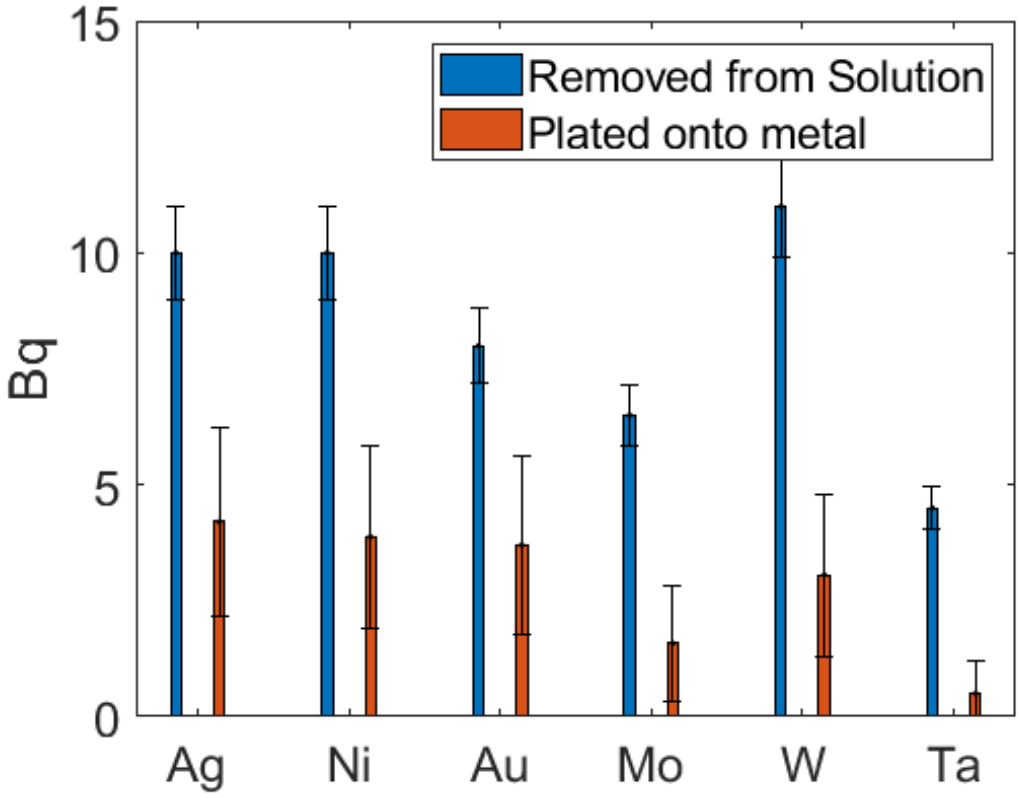

Figure 5.4: Comparison between the total amount of Po-210 removed from each solution determined by alpha spectroscopy and the amount present on each wire determined by the alpha counter. Here we can see an obvious discrepancy caused by the geometry of the tested metals. The uncertainties stated here reflect the standard error from Poisson counting for each sample.

ishing and a flat geometry. In addition to these factors, agitation of these solutions is employed via stirring: this has been shown to drastically increase the deposition efficiency as this disrupts concentration gradients at the surface of the disk [47].

In this section the deposition efficiency is explored utilising the results of the preliminary experiment.

Method

The sheets of metal had a small hole punched into the corner for ease of removal from solution. Au is excluded here as sheets of a high purity were not sourced. However the attraction of using Au for this purpose is low as Au is expensive and polonium doesn't spontaneously deposit onto Au efficiently.

Once the metals were cut to size one face was polished and cleaned to remove surface contaminants. The back face is then covered with tape like in [47] to ensure

deposition on only the exposed side of the metal. Teflon tape was then threaded through the corner hole.

The volume of each solution used was increased to 30 ml, so larger samples of solution could be taken for analysis by alpha spectroscopy. This change allowed faster measurements and greater accuracy as the measured sample was less dilute. This removed the need for using the alpha counters. The solutions contained the same amount of Po-210 as in the previous experiment so the two experiments could be comparable and the effect of polishing and geometry could be seen. The metals were placed in each solution at 60°C and agitated via a magnetic stirrer. After 15 minutes, the metals were removed, rinsed with DI water and allowed to dry. The amount of Po-210 deposited was determined by the amount removed from each solution.

Results

The results of this experiment is shown in Table 5.2. The amount of Po-210 removed from each solution was evaluated by alpha spectroscopy. The uptake of Po-210 was best for the squares of Ag followed by Cu and Ni. Molybdenum, W and Tantalum appear to have poor uptake of Po-210. W appears to perform well, however, the total amount removed is half that of Ni. The measurements for Ta, W and Mo were affected by the low concentration of the solutions used which decreases the accuracy of alpha spectroscopy.

Metal	Counts/s before	Counts/s after	% Removed
Ag	1.18	0.22	81%
Cu	0.96	0.79	18%
Ni	1.25	0.80	36%
Ta*	0.63	0.68	7%
W*	0.40	0.28	30%
Mo*	0.15	0.19	+26%

Table 5.2: Results of the auto-plating trials for the six metals. A significant decrease in counts/s indicates a large uptake of Po-210 from the solution. * Ta, W and Mo have be affected significantly by the low concentrations of Po-210 in the starting solution that affect the accuracy of alpha spectroscopy.

It is concluded that even in these non-optimal conditions Ag is still the best metal for Po-210 uptake. This result is backed up by the literature and the electronegativity of Ag. After this was confirmed, this experiment was repeated in a mineral processing leach liquor.

5.4.3 Spontaneous Deposition of Po-210 in H_2SO_4 onto Silver Disks in Mineral Processing Liquids

As the final feasibility test, Ag disks were used in three different situations. A H_2SO_4 leach solution, a pure Po/H_2SO_4 solution as a comparison and finally in an Po-210/HCl solution. The leach liquor contained the contaminants typical of mineral processing (Fe, Cu etc) along with U-238 and other RNs from the early stages in the U-238 decay chain. The HCl solution was used to identify if a different acid in similar concentrations performs better than H_2SO_4. However, the concentration was not optimal for Po-210 deposition [39, 42, 45]

Method

The key differences between this experiment and the previous section was the use of disks and the sampling interval. The disks had a larger surface area which allowed for greater amounts of Po-210 to deposit. The sampling interval was increased to also allow for more Po-210 deposition. These adjustments were made to accommodate deposition in the heavily contaminated leach liquor. They also allowed the amount of Po-210 to be visualised via an alpha spectrometer. The preparation and treatment of disks was kept the same as the previous experiments.

The solutions were prepared differently in each case; The leach solution was spiked with Po-210 (4.5 Bq/ml) and kept at 60°C, the HCl solution was a 1 M HCl solution with an ascorbic acid pre-treatment at 90°C (similar to the conditions used in alpha spectroscopy) and the uncontaminated H_2SO_4 was prepared as with the previous experiment.

Results

The results of this trial is found in Table 5.3 and Figure 5.5. Each experiment was repeated twice (Trial 1 and Trial 2) to ensure the results were consistent. Unsurprisingly the HCl solution performs well but surprisingly, the H_2SO_4 solution performs similarly. The literature (see Chapter 1) indicates that the plating efficiency in H_2SO_4 compared to HCl is limited by polonium's solubility. However, the solubility in 1 M HCl is also low [67] and is the likely cause of the performance in each of these liquids. Changing the concentration to 0.5 M would increase the efficiency of plating. Similar data for H_2SO_4 could not be sourced. It is seen also that hardly any Po-210 is plated from the leach solution.

To visualise the effect of each trial, the spectra for each deposition is shown in Figure 5.6. It is seen that a clear peak is present for the non-contaminated solutions, but, the peak in liquor solution is smeared by the contaminants on the disks surface, attenuating the alpha particles emitted by Po-210.

This result suggests that spontaneous deposition of Po-210, without pre-treatments

Trail (b/a)	H_2SO_4 solution	Liquor solution	HCl solution
1b	100%	100%	100%
1a	63%	102%	54%
2b	100%	100%	100%
2a	57%	94%	63%

Table 5.3: Results of the auto-plating trials. (b/a) = before (b) the trial started or after (a) 30 minute trial

or appropriate filtering, in these leach solutions is not feasible and cannot be used for accurate determination of Po-210 concentrations. However, after the leach solution trials a surface effect on the silver disks was noticed. A comparison between a silver disk used in the leach solution trial and one used in the H_2SO_4 solution trial is made in Figure 5.7. The surface contaminant was investigated using an electron microscope (FE1 Quantum 450). This analysis (Figure 5.8) revealed an AgCl layer had developed on the disk during the trial. This layer has prevented the deposition of Po-210 onto the disk surface, hence, the low efficiency of Po-210 uptake from these solutions.

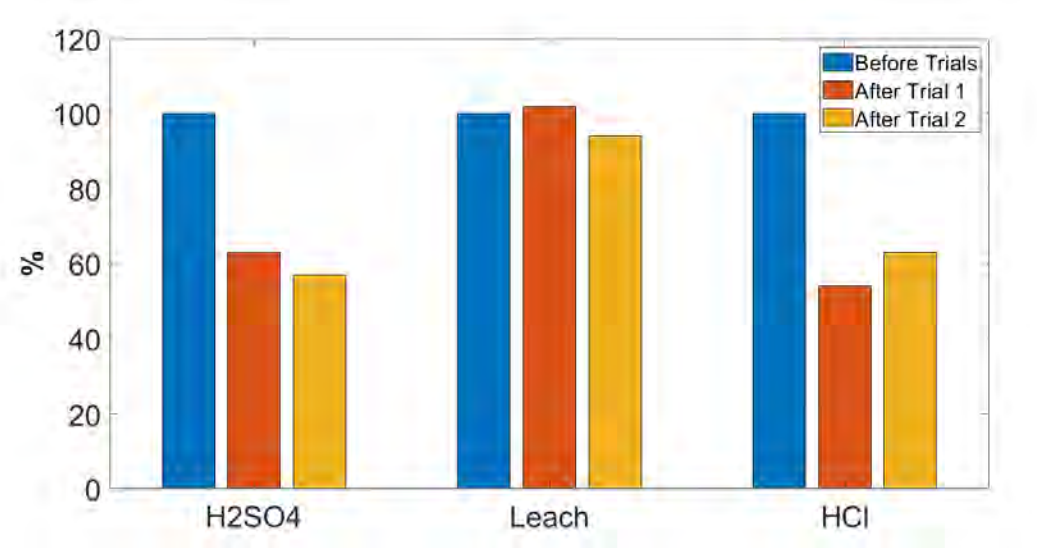

Figure 5.5: Results of the auto-plating trials. This result shows that each acid performs the similarly for a 30 minute trial but Po-210 uptake is heavily hindered in these leach solutions. Each experiment was repeated twice for these solutions (Trial 1 and Trial 2).

The literature has shown that an excess of chloride (Cl) present in solution will develop a AgCl layer onto silver disks as Cl and Ag have a high affinity for each other [68]. It has also been shown that Fe and Cu are active catalysts of AgCl formation [42, 69, 70]. It was revealed after the experiments that this leach solution contains HCl. Therefore, with the high abundance of Fe and Cu present a AgCl layer developed, preventing the deposition of Po-210 from this solution.

Fortunately, it has been observed that lower concentrations of such solutions drastically improves plating efficiency [71]. Therefore, with appropriate dilution this mechanism could be used to attract Po-210 to a silver coated scintillator. This process would allow for off-line determination of Po-210 in near real-time via a feed from the processing chain to a specialised dilution procedure.

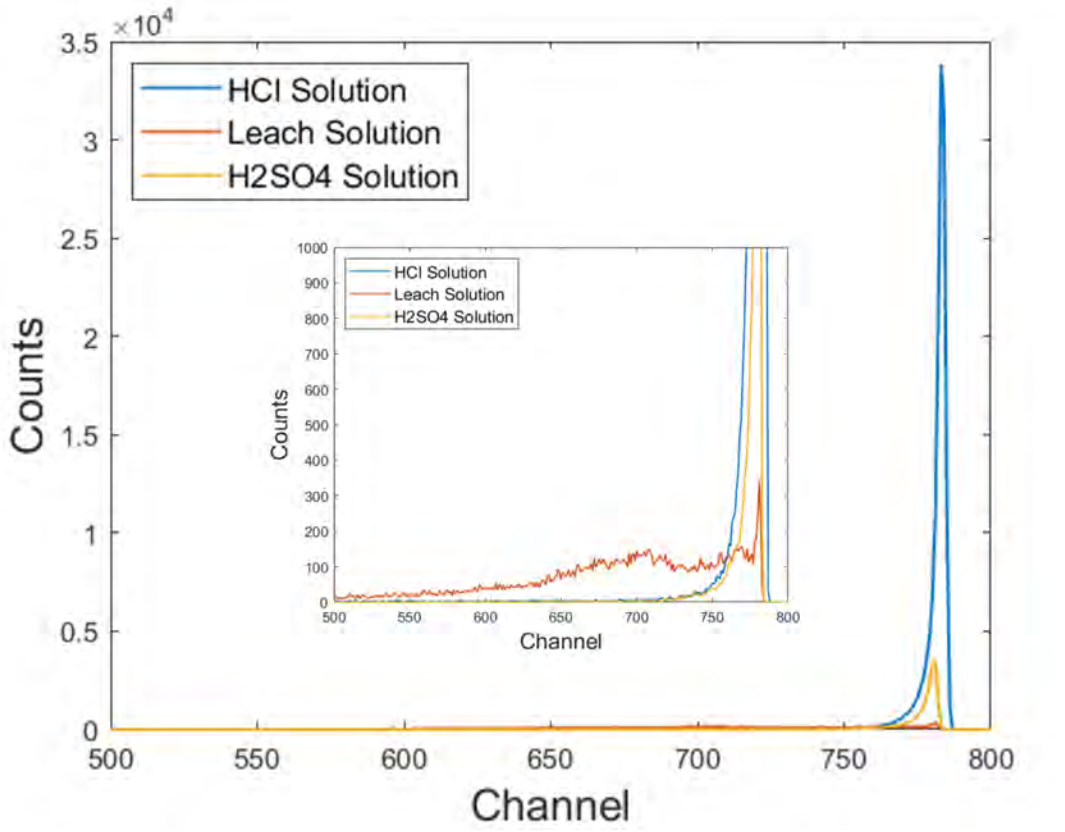

Figure 5.6: Spectra for each solution trialed. The inserted graph (zoomed) clearly shows that alpha spectroscopy measurements are hindered by the contaminants in the liquor solution. Without a defined peak the analysis cannot be achieved.

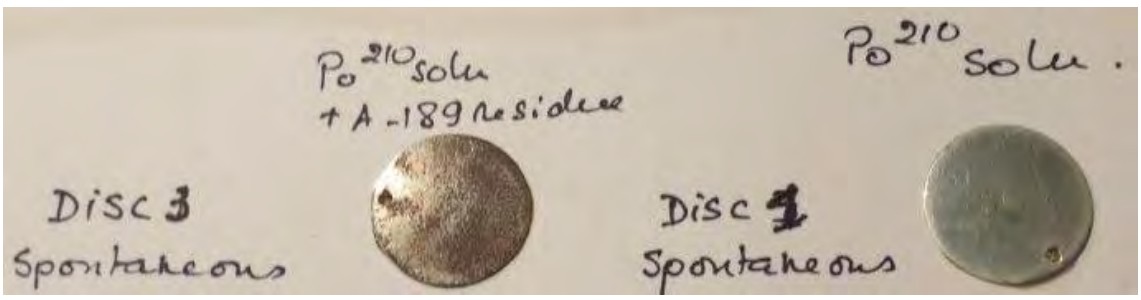

Figure 5.7: Silver disks used in the leach solution (left) measurement compared to the H_2SO_4 solution (right).

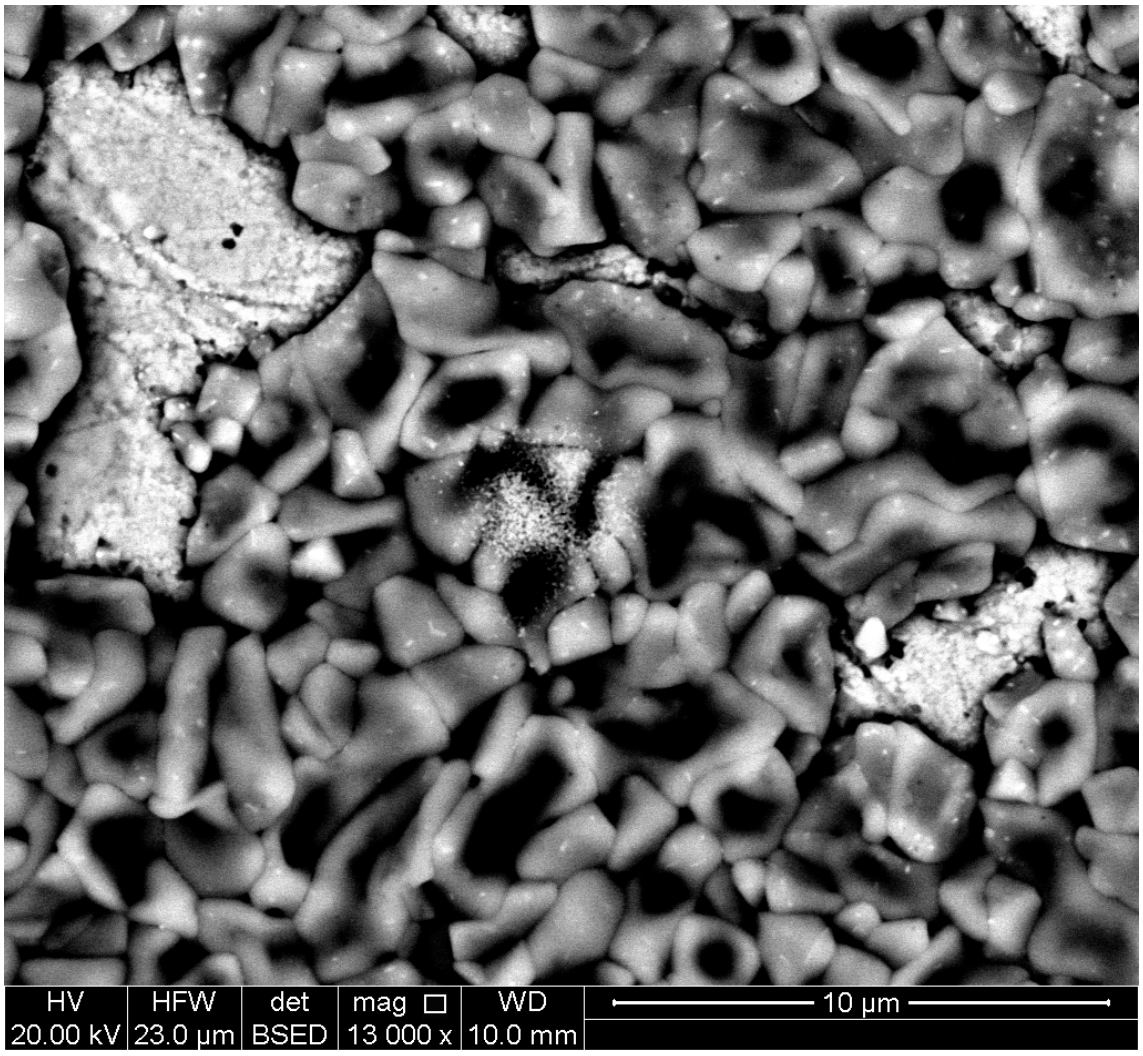

Figure 5.8: Image taken of the silver disks surface using the electron microscope (FE1 Quantum 450). The contamination on the surface revealed that a AgCl layer was present.

5.5 Scintillator Choice

The next component to investigate was the candidate for the scintillator material to be used for this sensor. A cheap and available scintillator is a ZnS(Ag) screen. It was assumed that coating one of these screens in Ag will not only protect it from the harsh environments but will also allow Po-210 ions to be spontaneously deposited. With the use of a PMT, this will allow for the detection of alpha particles emitted from Po-210 as they come in contact with the coated screen. To test the feasibility of such a sensor a ZnS(Ag) screen was coated with Ag via mechanical sputtering (performed by experts at Adelaide Microscopy) and the response of this screen to alpha particles was measured with a PMT and radioactive standard.

5.5.1 Ag Coated ZnS(Ag) Screen

The thickness of the Ag layer must be as thin as possible ($< \mu m$) to maximise the path length of alpha particles in the scintillator after penetrating the metal coating and therefore maximum dose deposition by alpha particles into the ZnS(Ag) screen. A process that enables this is mechanical sputtering, where atoms are deposited in a thin film. ZnS(Ag) screens were coated with various thicknesses of Ag atoms to test for any reductions in scintillation efficiency due to the attenuation of alpha particles by the Ag coating or damage to the scintillating screen.

A comparison of the efficiency before and after the application of the Ag layers is found in Figure 5.9. Here, an Am-241 (1 μC) source with a pinhole mask was used along with the alpha counter to determine the scintillation efficiency with the same standard.

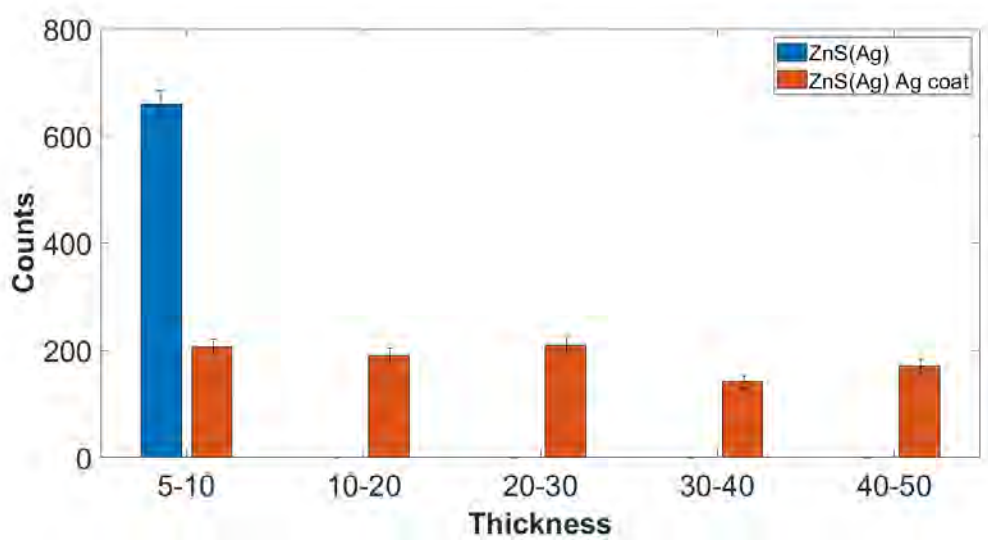

Figure 5.9: The response of ZnS(Ag) screens to a masked alpha particle standard before and after the application of a Ag layer of various thickness.

The efficiency of the screen dropped by over 50% with the application of each Ag screen. However, the response is very similar for each coating thickness. This is due to the fact that 5.486 MeV alpha particles travel 1.18 μm in Ag [1]. As each layer is less than 1 μm thick, it is fair to assume that the drop in scintillation efficiency is not due to the attenuation of the alpha particles, but damage caused to the screen from the sputtering process.

Investigations into the surface of each screen showed a layer of silver-oxide (Ag_2O) developed on the face of each coated screen due to the sputtering process. This effect faded as the layers were applied to the screens, indicating that this effect could be due to the 'warm up' time of the sputterer, so the application of layers was held for

some time during the next attempt (Section 5.5.2). This was recommended by the operator of the sputterer at Adelaide Microscopy [72]. This oxide layer may have damaged the scintillating crystals on the surface of the screen so a Au layer will also be applied before the Ag layer to test if this will reduce the oxidation of Ag when applied to the screen (a similar process is used when coating jewellery).

5.5.2 Ag and Au Coated ZnS(Ag) Screen

The process in Section 5.5.1 was repeated with two additional steps. The application of a 10 nm Au layer was laid on each screen and the sputterer was ran for sometime before the application of the Ag layer. The response of each screen to the Am-241 source is shown in Figure 5.10.

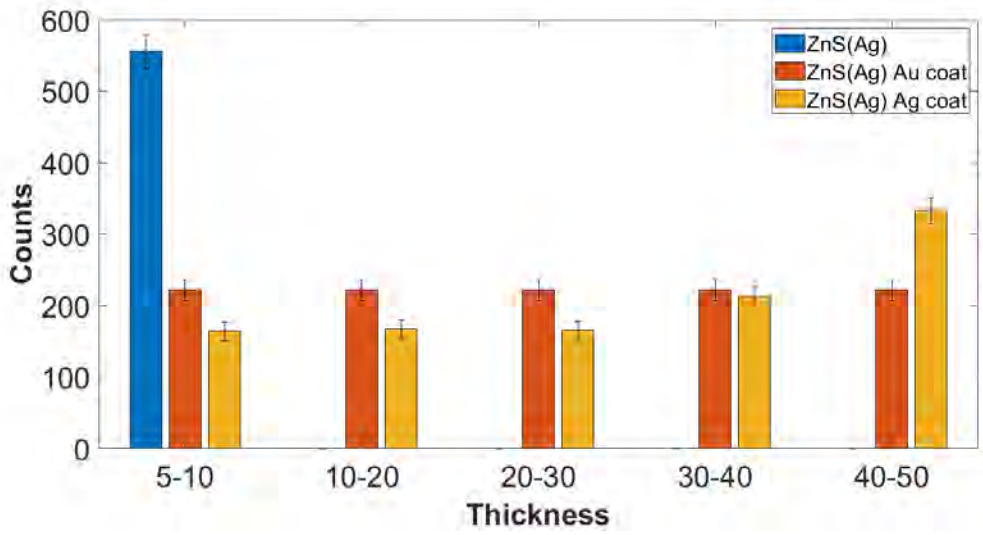

Figure 5.10: The response of a ZnS(Ag) screen to a masked alpha particle standard (i) before sputtering, (ii) after the application of a 10 nm Au layer and (iii) after the application of a Ag layer of various thickness.

The response is very similar for each coating thickness as with the previous test, so the sputtering process still damages the scintillator. The application of a Au layer does not appear to mitigate the effect or the control of the Ag oxidation.

The next step is to investigate the damage caused to this scintillator by observing the effect of sputtering on the response of the scintillating screen with a MCA.

5.5.3 Scintillator Response to Sputtering Process

To visualise the drop in efficiency for these coated screens, the response to an Am-241 source of each was observed using an MCA. A PHS was then recorded for each screen. The result of each measurement is shown in Figure 5.11.

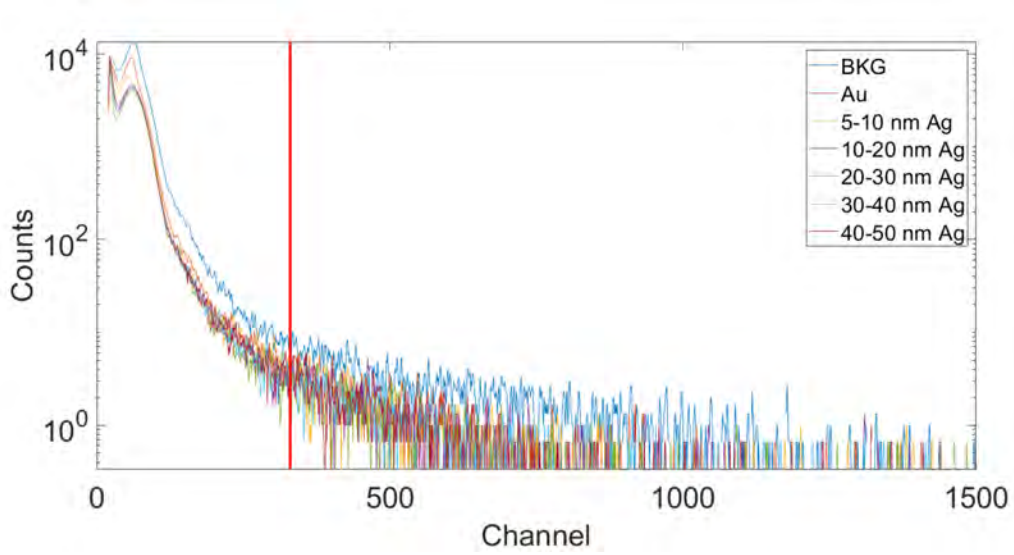

Figure 5.11: Spectra for each of the coated ZnS screens response to an Am-241 source. For all of the coated screens the same drop in efficiency is observed.

The drop in efficiency is seen in all of the coated screens and is consistent with other findings. This confirms that the sputtering process does damage the scintillator, decreasing the amount of light produced. An alternative method to apply the thin layers of Ag must then be sourced or an alternative scintillator that can withstand this process can be tested, such as polymers such as those used in the alpha and beta particle sensors.

5.6 Future Work

The results of the spontaneous deposition trials indicate that even Ag is not effective at Po-210 uptake from leach solutions. It will have restrictions for in-line detection of Po-210. This requires a clearly defined peak in the energy spectrum for polonium-specific sensing. Fortunately, it was found that with appropriate dilution, the results of spontaneous deposition can be improved. However, determining the appropriate dilution factor and any other requirements would require an extensive research effort that surpasses the extent of this project. The future directions of this research would be to identify inexpensive, effective methods of dilution and simple filtering or pre-treatments for this purpose.

The coating of ZnS(Ag) disks by sputtering appeared to have the possibility of creating a simple, cheap and interchangeable sensor unit. However, as the act of sputtering damages the screen another method of applying thin films of Ag should be found, such as using a Tollen's reagent (used for coating glass to form large mirrors). Alternatively, a different scintillator could also be used such as a plastic scintillator or an inorganic crystal (such as NaI).

With these other avenues to explore the next steps for this research effort are to find alternative scintillators and pre-treatments for solution.

5.7 Summary

In this Chapter, the feasibility of a polonium-specific in-line detector was explored. The use of spontaneous deposition onto various metals was trialed extensively, resulting in the feasible use of Ag to specifically uptake Po-210 in mixed RN and contaminated solutions. However, more work is required for in-line sensing. A cheap and easily disposable scintillator was explored as the sensor component, but the method of coating damaged the scintillator response to radiation, indicating further research is required including alternative coatings and scintillators.

Chapter 6

Conclusion

The research documented in this thesis outlines the development of different RN detection techniques for in-situ monitoring of RNs in mineral processing liquids. The detection of alpha and beta particles in mineral processing liquids was achieved by constructing and utilising new, more sensitive, fibre-optic based prototypes. These sensors allow reliable monitoring of low concentration RNs continuously and in-situ.

Techniques for improving future on-site devices were explored including: (1) Decontamination and (2) background suppression. Surface contamination was removed and prevented by techniques that allow for these sensors to operate continuously. The fundamental sensitivity limit for these devices was identified and indicated the importance of certain modifications to further improve the device sensitivity for more demanding applications than mineral processing.

A novel technique for the specific-sensing of Po-210 enabled by electrochemical techniques and a thinly coated scintillator was explored. It found that selective deposition of Po-210 in mineral processing liquids is prevented by contaminates within the liquids. The chosen scintillator was found to be infeasible for this application. The results of these experiments indicate further exploration is required in the form of pretreatments, filtering and alternative scintillators.

Real-time in-situ monitoring of the variations and low abundances of RNs throughout the processing of IOCG-U ores provides a valuable tool for understanding these variations, allowing for improvements in processing that yield high quality concentrates of valuable metals for export that comply with modern trade regulations.

The achievements of this research are:

- **Beta particle detection:** A new, more sensitive beta particle detector was constructed and tested. The sensing volume was increased 5-fold compared to the previous sensor resulting in a near linear increase in the signal strength. This increase in signal strength resulted in a lowering of the sensitivity limit to 0.1 Bq/ml. The performance of this detector was found to be dependent on the RNs present in solution, however, the sensors still operate as intended in mineral processing solutions.

- **Alpha particle detection:** Another more sensitive detector for sensing alpha particles was constructed and tested. It was found that by increasing the sensing volume resulted in a near linear increase in the signal strength lowering the sensitivity limit to 0.15 Bq/ml. The performance of this sensor was dependent on the RNs present in solution, as with the previous sensor.

- **Contamination removal and prevention:** The removal of Po-210 contamination and active contamination prevention was tested indicating that DECON 90 can be used to improve longevity of the sensors and a Po-209 pre-treatment could possibly allow for active contamination prevention in solution.

- **Sensitivity limitations:** If the sensitivity limit could be reduced further, these sensors could be used in more stringent applications, such as municipal water source monitoring. An effort was then made to reduce the noise floor that limits the sensitivity of these devices. The obvious avenues of investigation into the noise floor of these sensors were explored. It was found that the "noise floor" is due to the sensitivity of the detector to environmental background radiation, as shown by greatly suppressing the radiation background with effective shielding. However, the signal from muons cannot be shielded in practice, serving as the fundamental limit for these devices scalability.

- **Polonium-Specific sensing:** It was found that the use of Ag to specifically uptake Po-210 in mixed RN and contaminated solutions is in-feasible. The attenuation of alpha particles by plated contaminants makes determination of Po-210 concentrations impossible.However, dilution of these solutions could allow for a off-line detection protocol. A cheap and easily disposable scintillator was explored as the sensing component, but the method of coating damaged the scintillator response to radiation, indicating further research is required.

The directions of future research for the alpha and beta particle sensors centre on field deployability and improving sensitivity for other applications. To become field deployable these sensors require calibration in standards of mineral processing liquids. This could be achieved by sampling each stage of mineral processing and appropriately diluting those samples to vary the concentrations of RNs. By determining the concentrations of each RN with lab based techniques these samples can be used to form a calibrated response curve for these sensors to different concentrations. With this calibration these sensors could be deployed in mineral processing.

Although these sensors easily surpass the sensitivity required for mineral processing, other applications arise with the addition of appropriate shielding and coincidence counting. The use of lead shielding, like in Chapter 4, suppresses environmental gamma rays. The performance of these sensors could be repeated in an appropriately developed lead shielding, that allows liquid samples, to determine the sensitivity limitation. An optimisation of these additions along with Monte Carlo simulations would allow design and development of more sensitive detectors.

The results of the electrochemical trials indicated that further research into appropriate filtering and pretreatments is required. The contaminants present in solution also plated onto the Ag disks which then attenuate the alpha particles emitted from Po-210. This attenuation "smears" the signal from Po-210 making the concentration impossible to determine through alpha spectroscopy. If the contaminants could be filtered and removed from the mineral processing samples this effect could be reduced significantly, allowing the determination of Po-210 concentrations. The efficiency of Po-210 deposition is still quite low in these solutions so exploring pretreatments to increase this efficiency should be explored before this method could become feasible with the addition of filtering.

It was found that sputtering damages the ZnS(Ag) screens used in these trials. There is then a need for a different method of applying thin films of Ag allowing use of these cheap scintillators. Alternatively, a different scintillator could also be used such as a plastic scintillator or an inorganic crystal such as NaI. These aspects of this sensor must be explored to make this sensor feasible.

In conclusion, the development of different RN detection techniques for in-situ monitoring of RNs in mineral processing liquids is documented in this thesis. Continuous, in-situ monitoring of low concentration alpha and beta particle emitting RNs in mineral processing solutions was achieved. Each sensor was a new, more sensitive version of the previous generation and possess sensitivity limits an order of magnitude lower than was required by the sponsor. These sensors remove the need for lengthy, off-site analysis techniques and can be deployed for on-site analyses. This novel technique for specifically monitoring Po-210 was investigated and was found to show possible feasibility, however, this requires much further research.

Bibliography

[1] Coursey J. Zucker M. Berger, M. and J. Chang. ESTAR, PSTAR, and ASTAR: Computer Programs for Calculating Stopping-Power and Range Tables for Electrons, Protons, and Helium Ions (version 1.2.3), [Online]. Available: `https://physics.nist.gov/PhysRefData/Star/Text/ASTAR.html` [2019, December 23]. National Institute of Standards and Technology, Gaithersburg, MD., 2019.

[2] A Murray, R Marten, A Johnston, and P Martin. Analysis for naturally occuring radionuclides at environmental concentrations by gamma spectrometry. *Journal of Radioanalytical and Nuclear Chemistry*, 115:263–288, 1987.

[3] C. Whittaker. *Radiation sensitive optical fibres for radiation detection and dosimetry.* PhD thesis, University of Adelaide, 2018.

[4] International Atomic Energy Agency. *Assessing the need for radiation protection measures in work involving minerals and raw materials.* IAEA, 2006.

[5] J Martin. *Physics for Radiation Protection.* Wiley VCH Verlag & Co. KGaA, 2013.

[6] L. Myers and A. Brush. Counting of alpha- and beta-radiation in aqueous solutions by the detergent-anthracene scintillation method. *Analytical Chemistry*, 34(3):342–345, 1962.

[7] T. Oikari, H. Kojola, J. Nurmi, and L. Kaihola. Simultaneous counting of low alpha- and beta-particle activities with liquid-scintillation spectrometry and pulse-shape analysis. *International Journal of Radiation Applications and Instrumentation. Part A. Applied Radiation and Isotopes*, 38(10):875 – 878, 1987.

[8] J. McKlveen and W. McDowell. Some studies of reflector construction and electronics configurations for optimizing pulse-height and pulse-shape resolution in alpha liquid-scintillation spectrometry. *Nuclear Technology*, 28(1):159–164, 1976.

[9] J. McKlveen. Liquid-scintillation energy and pulse-shape detection applied to low-level alpha radioassay. *Radiation Research*, 66(2):199–214, 1976.

[10] J. McKlveen and W. McDowell. Liquid scintillation alpha spectrometry techniques. *Nuclear Instruments and Methods In Physics Research*, 223(2-3):372–376, 1984.

[11] M. Patterson and R. Greene. Measurement of low energy beta-emitters in aqueous solution by liquid scintillation counting of emulsions. *Analytical Chemistry*, 37(7):854–857, 1965.

[12] B. Coursey, W. Mann, A. Malonda, E. Garcia-Toraño, J. Los Arcos, J. Gibson, and D. Reher. Standardization of carbon-14 by $4\pi\beta$ liquid scintillation efficiency tracing with hydrogen-3. *International Journal of Radiation Applications and Instrumentation. Part A. Applied Radiation and Isotopes*, 37(5):403 – 408, 1986.

[13] John Betteley Birks. Scintillations from organic crystals: specific fluorescence and relative response to different radiations. *Proceedings of the Physical Society. Section A*, 64(10):874, 1951.

[14] G. Alkhazov, A. Komar, and A. Vorob'ev. Ionization fluctuations and resolution of ionization chambers and semiconductor detectors. *Nuclear Instruments and Methods*, 48(1):1 – 12, 1967.

[15] E. Steinbauer, P. Bauer, M. Geretschläger, G. Bortels, J. Biersack, and P. Burger. Energy resolution of silicon detectors: approaching the physical limit. *Nuclear Instruments and Methods in Physics Research Section B: Beam Interactions with Materials and Atoms*, 85(1):642 – 649, 1994.

[16] Steinberg. *Nature*, 182, 1958.

[17] Steinberg. *Nature*, 183, 1959.

[18] K. Jang, B. Lee, and J. Moon. Development and characterization of the integrated fiber-optic radiation sensor for the simultaneous detection of neutrons and gamma rays. *Applied Radiation and Isotopes*, 69(4):711–715, 2011.

[19] S. Jackson, S. Monk, and K. Lennox. Testing of a scintillator and fibre optic based radiation sensor. *Radiation Measurements*, 59:50 – 58, 2013.

[20] S. Yamamoto, K. Yamasoto, and T. Iida. Development of a real-time radon monitoring system for simultaneous measurements in multiple sites. *Nuclear Science, IEEE*, 46:1929 – 1933, 2000.

[21] A Ramli, DA Bradley, S Hashim, and H Wagiran. The thermoluminescence response of doped sio2 optical fibres subjected to alpha-particle irradiation. *Applied Radiation and Isotopes*, 67(3):428–432, 2009.

[22] Juha-Pekka J. Laine, Peter Miraglia, and Jr. H. Charles Tapalian. High efficiency fiber-optic scintillator radiation detector. `https://patents.google.com/patent/US7791046B2/en`.

[23] Hiroshi Sugihara. Optical fiber, optical fiber cable, and radiation detecting system using such. `https://patents.google.com/patent/US6671451B1/en`.

[24] H. Blumenfeld, M. Bourdinaud, P. Rebourgeard, and J. Thevenin. Production and test of coherent bundles of plastic scintillating microfibers. *Nuclear Instruments and Methods in Physics Research, Section A*, 278(2):619–621, 1989.

[25] I. Kim, I. Lee, A. Appleby, E. Christman, M. Liepmann, and G. Sigel Jr. Airborne alpha emitters monitored by a glass fibre scintillator bundle. *Radiation Protection Dosimetry*, 61(1-3):77–80, 1995.

[26] C. Whittaker, C. Kalnins, H. Ebendorff-Heidepriem, N. Spooner, and D. Ottaway. A fibre optic based approach and device for sensing beta radiation in liquids. *Sensors and Actuators A: Physical*, 296:101 – 109, 2019.

[27] C. Whittaker, C. Kalnins, H. Ebendorff-Heidepreim, D. Ottaway, and N. Spooner. A fibre optic based approach and device for sensing alpha particles in liquids. *Sensors and Actuators A: Physical*, 299:111573, 2019.

[28] C. Whittaker, A. Santos, C. Kalnins, H. Ebendorff-Heidepriem, D. Ottaway, and N. Spooner. Evaluating the energy dependence of various polystyrene based plastic scintillators. *Radiation Measurements*, 122:57 – 62, 2019.

[29] J. Birks. *The theory and practice of scintillation counting*. Pergamon Press Oxford, England, 1964.

[30] W. Burcham. *Nuclear Physics: An Introduction*. Longmans, 1973.

[31] M. L'Annunziata. *Chapter 1 - Radiation Physics and Radionuclide Decay*. Academic Press, Amsterdam, third edition, 2012.

[32] G. Knoll. *Radiation detection and measurement*. John Wiley & Sons, 2010.

[33] M. L'Annunziata. *Radionuclide tracers*. Academic Press, London (UK), 1987.

[34] E. Fenyves and O. Haiman. *The physical principles of nuclear radiation measurement*. Academic Press, New York, 1969.

[35] S. Djokić and P. Cavallotti. *Electrodeposition: Theory and Practice*. Springer New York, 2010.

[36] U. Rieth, H. Hummrich, and J. Kratz. Electrodeposition of Po-210 on various electrode materials.

[37] P. Vesterbacka and T. Ikäheimonen. Optimization of 210Pb determination via spontaneous deposition of 210Po on a silver disk. *Analytica Chimica Acta*, 545(2):252 – 261, 2005.

[38] H. Narita, K., W. Burnett, S., and W. McCabe. Determination of 210Pb, 210Bi and 210Po in natural waters and other materials by electrochemical separation. *Talanta*, 36(9):925 – 929, 1989.

[39] T. Karali, S. Ölmez, and G. Yener. Study of spontaneous deposition of 210Po on various metals and application for activity assessment in cigarette smoke. *Applied Radiation and Isotopes*, 47(4):409 – 411, 1996.

[40] G. Benoit and H. Hemond. Improved methods for the measurement of 210Po, 210Pb, and226Ra. *Limnology and Oceanography*, 33(6):1618–1622, 1988.

[41] W. Flynn. The determination of low levels of polonium-210 in environmental materials. *Analytica Chimica Acta*, 43:221 – 227, 1968.

[42] P. Figgins. The radiochemistry of polonium. Technical report, Mound Lab., Miamisburg, Ohio, 1961.

[43] L. Johansson. *Determination of Pb-210 and Po-210 in aqueous environmental samples*. PhD thesis, Gottfried Wilhelm Leibniz University Hannover, 2008.

[44] M. Haissinsky. Electrochemistry of polonium. *Transactions of The Electrochemical Society*, 70(1):343–371, 1936.

[45] Curie, I. Extraction et purification du dépôt actif à évolution lente du radium. *J. Chim. Phys.*, 22:471–487, 1925.

[46] L. Hallstadius. A method for the electrodeposition of actinides. *Nuclear Instruments and Methods in Physics Research*, 223(2):266 – 267, 1984.

[47] M. Crespo. A review of electrodeposition methods for the preparation of alpha-radiation sources. *Applied Radiation and Isotopes*, 70(1):210 – 215, 2012.

[48] K. Kostadinov, V. Petrova, and D. Todorovsky. A method for the determination of polonium in air. *Journal of Radioanalytical Chemistry*, 42(2):411–415, 1978.

[49] G. Jia, G. Torri, and M. Petruzzi. Distribution coefficients of polonium between 5aqueous hydrochloric and nitric acids. *Applied Radiation and Isotopes*, 61(2):279–282, 2004. Low Level Radionuclide Measurement Techniques - ICRM.

[50] A. Aarkrog. A rapid method for the separation of 210Po from 210Pb by tioa extraction. *Journal of Radioanalytical and Nuclear Chemistry*, 249(3):587–593, 2001.

[51] T. Church, N. Hussain, T. Ferdelman, and S. Fowler. An efficient quantitative technique for the simultaneous analyses of radon daughters 210Pb, 210Bi and 210Po. *Talanta*, 41(2):243 – 249, 1994.

[52] J. Smith and T. Hamilton. Improved technique for recovery and measurement of polonium-210 from environmental materials. *Analytica Chimica Acta*, 160:69 – 77, 1984.

[53] J. Boehm, A. François, H. Ebendorff-Heidepriem, and T. Monro. Chemical deposition of silver for the fabrication of surface plasmon microstructured optal fibre sensors. *Plasmonics*, 6(1):133–136, 2011.

[54] Iarc Official Publication. *Ionizing Radiation, Part 2 : Some Internally Deposited Radionuclides*. World Health Organization, 2001.

[55] P. Medley. Pb-210 determination using liquid scintillation counting (LSC). Internal report 627, Department of the Environment and Energy, 2016.

[56] M. Whitaker, W. Bjorksted, and A. Mitchell. Preliminary report on a quick method of depositing polonium on silver. *Phys. Rev.*, 46:629–630, 1934.

[57] P. Airey, T. Hinton, and J. Twining. Chapter 1 - the scientific basis. In John R. Twining, editor, *Tropical Radioecology*, volume 18 of *Radioactivity in the Environment*, pages 1 – 57. Elsevier, 2012.

[58] M. Tajiri, M. Sunaoka, A. Fukumura, and M. Endo. A new radiation shielding block material for radiation therapy. *Medical Physics*, 31(11):3022–3023, 2004.

[59] R. Grasty and B. Minty. A guide to the technical specifications for airborne gamma-ray surveys. australian geol. surv. *Organization Record*, 60, 1995.

[60] Sheridan Bowman. *Radiocarbon dating*. Univ of California Press, 1990.

[61] Anshuman Shrivastava. *Introduction to Plastics Engineering*. Plastics Design Library. William Andrew Publishing, 2018.

[62] G. Choppin, J. Liljenzin, J. Rydberg, and C. Ekberg. Chapter 13 - cosmic radiation and radioelements in nature. In *Radiochemistry and Nuclear Chemistry (Fourth Edition)*, pages 373 – 404. Academic Press, Oxford, fourth edition edition, 2013.

[63] Tanabashi M. et al. Review of particle physics. *Phys. Rev. D*, 98:030001, 2018.

[64] D. B. Chitwood, T. I. Banks, M. J. Barnes, S. Battu, R. M. Carey, S. Cheekatmalla, S. M. Clayton, J. Crnkovic, K. M. Crowe, P. T. Debevec, S. Dhamija, W. Earle, A. Gafarov, K. Giovanetti, T. P. Gorringe, F. E. Gray, M. Hance, D. W. Hertzog, M. F. Hare, P. Kammel, B. Kiburg, J. Kunkle, B. Lauss, I. Logashenko, K. R. Lynch, R. McNabb, J. P. Miller, F. Mulhauser, C. J. G. Onderwater, C. S. Özben, Q. Peng, C. C. Polly, S. Rath, B. L. Roberts, V. Tishchenko, G. D. Wait, J. Wasserman, D. M. Webber, P. Winter, and P. A. Żołnierczuk. Improved measurement of the positive-muon lifetime and determination of the fermi constant. *Phys. Rev. Lett.*, 99:032001, Jul 2007.

[65] J. Ziegler. The effect of concrete shielding on cosmic ray induced soft fails in electronic systems. *IEEE Transactions on Electron Devices*, 28(5):560–565, May 1981.

[66] B. Rossi. Interpretation of cosmic-ray phenomena. *Reviews of Modern Physics*, 20(3), 1948.

[67] R. Ram, J. Vaughan, B. Etschmann, and J. Brugger. The aqueous chemistry of polonium (Po) in environmental and anthropogenic processes. *Journal of hazardous materials*, 2019.

[68] K. Bagnall. The chemistry of polonium. *Quarterly Reviews, Chemical Society*, 11(1):30–48, 1957.

[69] N. Sethy, A. Sutar, P. Rath, V. Jha, P. Ravi, and R. Tripathi. A review of radio chemical analysis and estimation of 210po in soil matrices. *Journal of Radiation Research and Applied Sciences*, 8(4):590 – 596, 2015.

[70] W. Mahmood, Z. Uyun, N. Mohamed, N. Azlin N. Ariffin, and A. Ishak. Improved optimum condition for recovery and measurement of ^{210}Po in environmental samples. 2012.

[71] Danielle Questiaux. Personal communication, 2019.

[72] Adelaide Microscopy. Personal communication, 2019.

Appendix A: Sensor Construction Procedure and Specifications

Beta Sensor Construction Procedure

The following contains steps necessary to construct the device investigated in this thesis to the specifications found below.

1. Cut to length 200 (actually 207), 1.1 mm diameter plastic fibres (BCF12). Preferably with a sharp knife or surgical blade but as the end face of these fibres are polished later in this procedure scissors can be used. Another alternative is a pipe cutter of appropriate size.

2. With the plastic jig (with appropriate hole spacing), place a rigid sheet underneath and begin positioning and inserting the fibres into each hole. This is best done with tweezers in hand and placing the fibres into the jig in a spiral pattern from the inside to the outside. Once the jig is full the end face (bottom of the sensor that does't require polish) can be cemented into place.

3. The cement used for these sensors is Eljen's EJ-500, follow the SDS for the preparation procedure. Once prepared lay out a doubled over sheet (in case the first layer breaks!) of "Glad-Wrap". This allows for the cement to stay in place whilst drying onto a non-stick surface. Pour the cement over the surface of the sheet spacing it out to the size of the end face of the sensor. This also allows one to know if they've made enough cement.

4. With the "Glad-Wrap" layed, hover your filled jig and rigid sheet over the cement and slowly pull the sheet away from the sensor. The fibres will drop down onto the cement. With care allow the plastic jig to 'fall' into the cement as well. Leave overnight. Once dried simply peel off the "Glad-Wrap".

5. For the detector face, the fibre ends will be brought together and cemented into a SM1 externally threaded ring. Cut a plastic film canister in half and line the inside with "Glad-Wrap". Check the length by inserting the detector face. Mix together a smaller amount of cement than previously used and pour into the canister. Wrap the thread of the ring with tape so that no resin embeds

itself into the threading. Then with the sensor upside down, held with a clamp and retort stand, insert the detector face into the canister. Ensure that the ring and fibre ends sit firmly at the bottom of the canister. With the sensor aligned, leave overnight to dry. Once dried, remove the detector face from the canister, removing the "Glad-Wrap".

6. The detector face can then be polished and the edge of the detector face can be filed down. The polishing of the detector face can be achieved using a disk polisher/grinder. Using grits of higher grade (increasing number value) the surface will be come more transparent and more fibre ends will appear at the detector face as a result.

Alpha Sensor Construction Procedure

The following contains steps necessary to construct the device investigated in this thesis to the specifications found below.

1. Cut to length 2500, 250 μm diameter plastic fibres (BCF12). With a sharp knife or surgical blade. In this procedure scissors can't be used, nor a pipe cutter, as these fibres are significantly more delicate than the 1.1 mm fibres. It is advised that after every 10 fibres that are cut they are grouped together and placed onto a black piece of paper. This saves time and frustrations when cementing the fibres together.

2. Using a thin sheet of Teflon/silicon and some cable ties, bring the fibres together into a tight cylinder. Leave the end to be cemented hanging free from the sheet a few cm to ensure it doesn't stick to the fibres.

3. Using the same procedure for the previous sensor, mix up the optical cement (about the same as for the previous sensors detector face) and lay out some "Glad-Wrap". For this sensor use a surface with a 'dimple' or a circular indent that is larger than the ring opening but smaller that the entire ring. With the thread covered with tape, place it on the "Glad-Wraped" surface, align the hole and the ring such that when the fibres are placed then ends will sit lower than the ring.

4. Place a small amount of resin within the indent, it is important to use a small amount here as the resin finds it easy to capillary up along fibres. The result is a group of fibres all cemented together. Then place the group of fibres into the ring, stabilising with claps and a retort stand appropriately. Leave overnight. This process may need to be repeated depending on the amount of resin used.

5. As with the previous sensor, the detector face can then be polished using a disk polisher/grinder.

Sensor Specifications

The following contains the specifications of the sensors constructed and tested in this thesis.

Sensor Type	Num. of Fibres	Length	Diameter
Beta	207	15 cm	1.1 mm
Alpha	2500	10 cm	250 μm

Table 1: Specifications of the sensors constructed and tested in this thesis

Pulse height analysis MATLAB code

```
clear all
close all
clf
format long g

% Specify what folder the data is in
inputDir='D:\ZnS(Ag)\MCAdata';

% Specify what the filename prefix is
%fileNamePrefix = '1000s_';
time_int = 100; %measuring time
BKG_time_int = 7200; %2hours
% Get number of .spe files in folder
n=dir([inputDir,'\*.spe']);
N= length(n); %handy for later

% Read all the spe files into the variable 'data'.
% Here the A4_ is part of the file name that you specified
% The %d bit puts the for loop number i into that spot in
% the sprintf name
for i=1:7

        % To pad this filename with leading zeros, use %02d
        filename = fullfile(inputDir, sprintf('%d.spe', i));

        data(:,i)=dlmread(filename,',',[43 0 4138 0]);
end
for i=10:18

%           To pad this filename with leading zeros, use %02d
```

```
        filename = fullfile(inputDir, sprintf('0000%d.spe', i));

        data(:,i)=dlmread(filename,',',[43 0 4138 0]);
end
for i=100:108

%         To pad this filename with leading zeros, use %02d
        filename = fullfile(inputDir, sprintf('000%d.spe', i));

        data(:,i)=dlmread(filename,',',[43 0 4138 0]);
end

% Time vector for checking any variations with time
t_axis = (linspace(0,i,i)*100)/3600;


% Integrate regions of the spectrum
high=sum(data(300:length(data),:));

% Mean value and standard deviation
high_mean = mean(high);
% Generate vectors for comparison to t_axis
mean_val_y = zeros(size(t_axis)); %empty array the size of t axis
for i = 1:length(t_axis)
    mean_val_y(i) = high_mean; % vector of high_mean
end

std_val_y_plus = zeros(size(t_axis)); %empty array the size of t axis
for i = 1:length(t_axis)
    std_val_y_plus(i) = high_mean+high_std; % vector of upper bound of error
end

std_val_y_minus = zeros(size(t_axis)); %empty array the size of t axis
for i = 1:length(t_axis)
    std_val_y_minus(i) = high_mean-high_std; % vector of lower bound of erro
end


% Plot what you want
figure(1)
set(gcf,'color','white')

% Use for comparing spectra with time
```

```
% semilogy(data(:,1))%(:,length(n)))
% hold on
% semilogy(data(:,10))%(:,length(n)))
% hold on
% semilogy(data(:,25))%(:,length(n)))
% hold on
% semilogy(data(:,50))%(:,length(n)))
% hold on
% semilogy(data(:,75))%(:,length(n)))
% hold on
% semilogy(data(:,100))%(:,length(n)))
%% hold on
%

% Use for plotting all spectra
semilogy(data)
hold on
set(gca,'FontSize',30)
% Formatting
xlim([0 1500])
xlabel('Channel','FontSize',30)
ylabel('Counts','FontSize',30)

figure(2)  % turn on when using the plots above
plot(t_axis,high)
hold on
plot(t_axis,mean_val_y)
hold on
plot(t_axis,std_val_y_plus)
hold on
plot(t_axis,std_val_y_minus)
hold on
ylim([0 max(high)])
legend('data','mean','std1','std1')
xlabel('Time Hours')
ylabel('Integrated Counts')
```